AD-A050 874 OHIO STATE UNIV COLUMBUS ELECTROSCIENCE LAB F/G 20/5
THEORETICAL STUDY OF THE TURBULENCE INDUCED SCINTILLATION OF A --ETC(U)
JAN 78 D D DUNCAN F30602-76-C-0058
UNCLASSIFIED ESL-4232-5 RADC-TR-77-430 NL

1 OF 2
AD A050 874

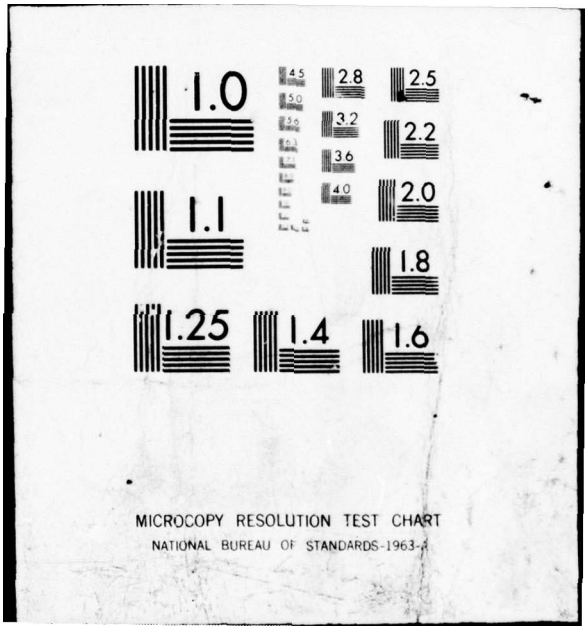
1.0
1.1
1.25
1.4
1.6
1.8
2.0
2.2
2.5
2.8
3.2
3.6
4.0
4.5
5.0
5.6
MICROCOPY RESOLUTION TEST CHART
NATIONAL BUREAU OF STANDARDS-1963-A

RADC-TR-77-430
Interim Report
January 1978

THEORETICAL STUDY OF THE TEMPERATURE-INDUCED SCINTILLATION OF A BEAM LASER BEAM

D.D. Duncan

Ohio State University

Sponsored by
Defense Advanced Research Projects Agency (DoD)
ARPA Order No. 1279

Approved for public release; distribution unlimited.

ROME AIR DEVELOPMENT CENTER
Air Force Systems Command
Griffiss Air Force Base, New York 13441

THEORETICAL STUDY OF THE TURBULENCE-INDUCED SINTILLATION OF A DIRTY LASER BEAM

D. D. Duncan

Contractor: Ohio State University
Contract Number: F30602-76-C-0058
Effective Date of Contract: 1 July 1975
Contract Expiration Date: 30 September 1977
Short Title of Work: Theoretical Study of Turbulence Induced Scintillation of a Dirty Laser Beam
Program Code Number: 6E20
Period of Work Covered: Jan 77 - Sep 77
Principal Investigator: Dr. R.K. Long
Dr. S. Collins
Phone: 614-422-6077
Project Engineer: James W. Cusack
Phone: 315-330-3145

This research was supported by the Defense Advanced Research Projects Agency of the Department of Defense and was monitored by James W. Cusack (OCSE), Griffiss AFB NY 13441 under contract F30602-76-C-0058.

UNCLASSIFIED

SECURITY CLASSIFICATION OF THIS PAGE (When Data Entered)

REPORT DOCUMENTATION PAGE	READ INSTRUCTIONS BEFORE COMPLETING FORM
1. REPORT NUMBER: RADC-TR-77-430	2. GOVT ACCESSION NO.
3. RECIPIENT'S CATALOG NUMBER	
4. TITLE (and Subtitle): THEORETICAL STUDY OF THE TURBULENCE INDUCED SCINTILLATION OF A DIRTY LASER BEAM	5. TYPE OF REPORT & PERIOD COVERED: Interim Report Jan [redacted] - Sep [redacted] 77
6. PERFORMING ORG. REPORT NUMBER: ESL-4232-5	
7. AUTHOR(s): D. D. Duncan	8. CONTRACT OR GRANT NUMBER(s): F30602-76-C-0058
9. PERFORMING ORGANIZATION NAME AND ADDRESS: Ohio State University, Electroscience Laboratory, Columbus OH 43212	10. PROGRAM ELEMENT, PROJECT, TASK AREA & WORK UNIT NUMBERS: P.E. 62301E; 1279; J.O. 12790508; 05
11. CONTROLLING OFFICE NAME AND ADDRESS: Defense Advanced Research Projects Agency, 1400 Wilson Blvd, Arlington VA 22209	12. REPORT DATE: Jan [redacted] 978
	13. NUMBER OF PAGES: 166; 178P.
14. MONITORING AGENCY NAME & ADDRESS (if different from Controlling Office): Rome Air Development Center (OCSE), Griffiss AFB NY 13441	15. SECURITY CLASS. (of this report): UNCLASSIFIED
	15a. DECLASSIFICATION/DOWNGRADING SCHEDULE: N/A

16. DISTRIBUTION STATEMENT (of this Report)

Approved for public release; distribution unlimited.

DDC RECEIVED MAR 8 1978 F

17. DISTRIBUTION STATEMENT (of the abstract entered in Block 20, if different from Report)

Same

18. SUPPLEMENTARY NOTES

RADC Project Engineer: James W. Cusack (OCSE)

The material contained in this report was also used as a dissertation submitted to the Department of Electrical Engineering, The Ohio State University, as partial fulfillment for the degree Doctor of Philosophy.

19. KEY WORDS (Continue on reverse side if necessary and identify by block number)

Turbulence
Laser
Laser Propagation

20. ABSTRACT (Continue on reverse side if necessary and identify by block number)

Within this work ~~we are~~ concerned with predicting the temporal scintillation spectrum of a laser beam which has propagated through the turbulent atmosphere. Use is made of the Extended Huygens-Fresnel principle in deriving a very general but compact mathematical expression for the temporal scintillation spectrum of an unspecified source field with an arbitrary shaped extended receiver aperture. This formula, which is restricted to the weak turbulence regime, is then applied to the analysis of several situations of contemporary

→ next page

DD FORM 1 JAN 73 1473 EDITION OF 1 NOV 65 IS OBSOLETE

UNCLASSIFIED

SECURITY CLASSIFICATION OF THIS PAGE (When Data Entered)

402 251 JOB

interest. Specifically, the analysis is directed toward the description of the effects of such a laser beam which is blemished in a deterministic sense. Spectra obtained under these conditions are shown to display increased sensitivity to the path distribution of the turbulence strength.

ACKNOWLEDGMENTS

I wish to express my gratitude to my adviser Dr. Stuart A. Collins, Jr. for his constant encouragement during the research embodied by this dissertation and his many helpful suggestions and criticisms during the preparation of the manuscript.

The material contained in this report is also used as a dissertation submitted to the Department of Electrical Engineering, The Ohio State University as partial fulfillment for the degree Doctor of Philosophy.

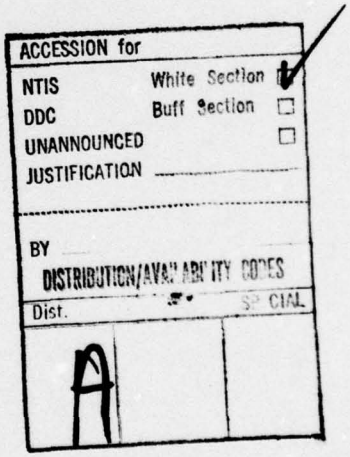

PREFACE

This report, Ohio State University Research Foundation Report Number 4232-5, was prepared by The Ohio State University ElectroScience Laboratory, Department of Electrical Engineering at Columbus, Ohio. Research was conducted under Contract F30602-76-C-0058 (Project PR-A-1639). Mr. James W. Cusack, RADC (OCSE), of Rome Air Development Center, Griffiss Air Force Base, New York, is the Project Engineer.

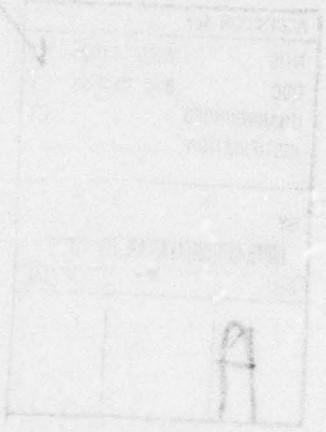

TABLE OF CONTENTS

LIST OF FIGURES

CHAPTER I
INTRODUCTION

A. Purpose of Investigation

Light propagating through the atmosphere undergoes bending due to variations in the index of refraction. When this bending is uniform one witnesses phenomena such as mirages [1] and the apparent flattening of the sun as it approaches the horizon. If the index of reflection is fluctuating randomly the phase and amplitude of the light are perturbed in a random manner. Phase fluctuations give rise to an uncertainty in the location of a radiating body [2]. This behavior is exemplified by the "dancing" or "quivering" of the image of a star as seen through a telescope. Intensity fluctuations, or scintillations [3] as they are commonly called, are typified by the twinkling of stars or distant headlights.

By examining the temporal power spectrum of the scintillations one can discern important properties of the medium through which the light has propagated. With the ready availability of the laser it is therefore natural that we be interested in the temporal scintillation spectrum of a laser beam.

A realizable laser beam may not always have the perfect properties which analytical studies assume. The need therefore arises to determine the effect upon its scintillation spectrum of a laser beam containing a certain amount of deterministic degradation, e.g., a beam partially blocked by dirt specks. We are concerned herein with the temporal scintillation spectrum of just such a "dirty" beam.

Within this work a contemporary technique currently appearing in the literature is employed in deriving a very general but compact mathematical expression for the scintillation spectrum. This expression, which is restricted to the weak turbulence regime, is then applied to the analysis of several situations of great interest. Specifically the analysis is directed toward description of the effects of such phenomena as localized turbulence, off-axis detectors, and the use of a laser beam which is blemished in a deterministic sense. Spectra obtained under these conditions will be shown to provide additional information about the propagation medium.

This study was motivated by a desire to provide theoretical support for experimentally obtained scintillation spectra. As illustrated in Figure 1, these spectra were digitally calculated from data obtained by propagating a laser beam over an approximately one kilometer path between two aircraft flying abreast. The spectra thus generated displayed a number of pecularities and in the course of the effort to put this behavior on a firm theoretical basis a number of heretofor unexplored phenomena were encountered.

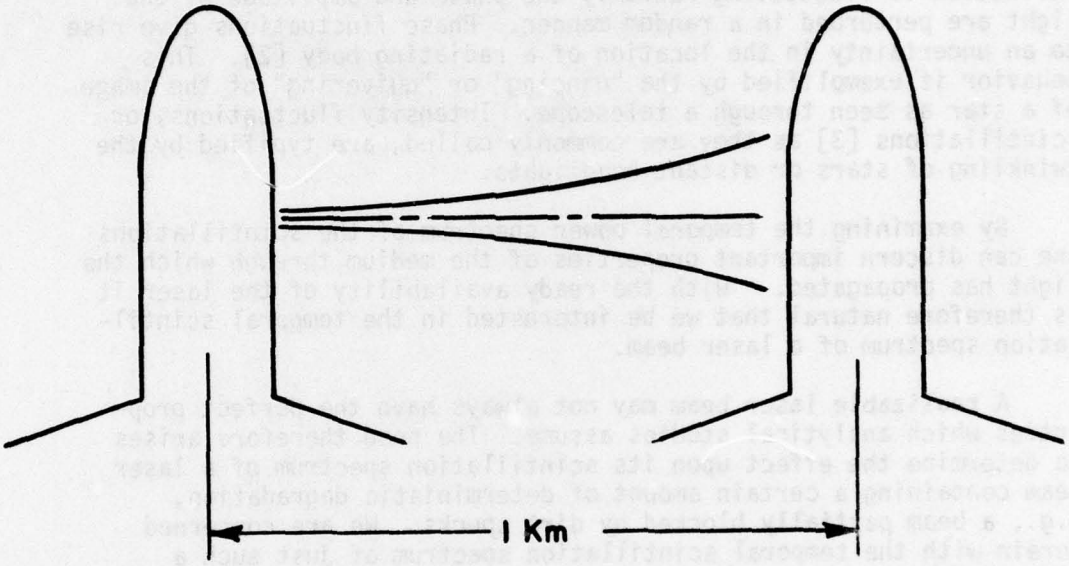

Figure 1--Sketch of experimental situation.

The principal contribution of this effort lies in the development of a simplified formula for the temporal scintillation spectrum and its application to several important configurations which are commonly encountered in practical situations. The problem attacked in this dissertation is therefore a theoretical description of the temporal scintillation spectrum of a "dirty" laser beam.

The general formalism presented here is also applicable to arbitrary transmitter and receiver shapes such as the beam transmitted from an unstable resonator or a Cassegrain telescope receiver or transmitter.

B. Perspective

Whenever an electromagnetic wave is propagated through the atmosphere it is perturbed in a random manner. For radio frequency waves this corruption is due to index of refraction variations caused by humidity fluctuations within the atmosphere. At optical frequencies the index of refraction variations are due primarily to temperature fluctuations. Both humidity and temperature fluctuations are caused directly or indirectly by radiant heating of the earth and convective heating of the atmosphere in conjunction with wind shears. The research effort described herein in aimed primarily at predicting the effects of turbulent index fluctuations at optical frequencies but may be generalized to longer wavelengths.

The refractive index field is composed of randomly arrayed eddies of various sizes and indices of refraction. These eddies have sizes ℓ such that $\ell_o < \ell < L_o$ where ℓ_o and L_o are respectively the inner and outer scales of turbulence. Mechanical energy is injected by wind shears into the large scale sizes which then break into smaller and smaller eddies through the phenomena of vortex stretching[89]. The energy thus cascades into smaller and smaller scale sizes until it is dissipated in the form of heat at scale sizes on the order of the inner scale, ℓ_o.

If one assumes that the turbulent eddies are blown en masse through the wave transverse to the propagation path, then what will be observed at the receiver plane is simply the moving diffraction patterns of eddies of various sizes and locations.

For short propagation paths ($L < \ell_o^2/\lambda$ where λ is the free-space wavelength) the incident wave undergoes perturbations to its phase only. As the path length is increased, amplitude fluctuations are also introduced. When viewed by a square-law detector (e.g., the eye or a photomultiplier) the resultant power (irradiance) fluctuations are commonly referred to as scintillation.

By using a detector (photomultiplier) to measure the variance of the irradiance of a perturbed wavefront it is noticed that to a point, as the path length or turbulance level increases, so does the irradiance variance. However for very strong turbulence and/or long path lengths the variance is seen to peak or saturate [4],[5] and to even decrease slightly [6]. This effect has attracted much attention partly because people intuitively expected the variance to increase without limit.

Within the weak turbulence regime (or for moderate propagation lengths) the effects of index inhomogeneities can be closely approximated by the linear superposition of the interactions of the coherent (unperturbed) wave with turbulent eddies of all sizes at all locations

between transmitter and receiver. This is a single scattering model. Strong turbulence gives rise to multiple scatterings which manifest themselves as the aforementioned saturation phenomenon. We shall be concerned herein principally with the weak turbulence model. However where appropriate modifications will be pointed out which enable generalization to the strong turbulence domain.

The temporal spectrum of the irradiance fluctuations could easily have been measured instead of the variance of irradiance. It is just this power spectrum in which we are interested.

C. Discussion of Previous Work

Since primordial man first turned his gaze toward the night-time sky he has been intrigued by the phenomenon of scintillation. (Recall the nursery rhyme which goes "Twinkle, twinkle, little star ....") It seems natural then, that scintillation be a topic of research from earliest times. Further, it is reasonable that the study of scintillation have its roots in one of the oldest sciences, astronomy [7]. In more recent times scintillation has been an important device for passive remote sensing, for example determining the velocity of the interplanetary solar wind [8,9], the ionospheric drift [10,11] or terrestrial wind [12]. With the advent of the laser, scintillation has become important within the realms of optical communication [13,14] and active remote sensing [15,16,17,18,19].

One of the classical mathematical tools with which scintillation is predicted, is known as the Method of Smooth Perturbations [20]. This technique, popularized by Tatarski [20], hypothesizes an iterative solution (for weak turbulence) to the scalar wave equation for the natural logarithm of the field. A great many authors have employed this method in the study of (among other phenomena) scintillation.

The simplest problem related to scintillation which has been attacked with the Method of Smooth Perturbations is the calculation of the log-amplitude variance. This problem has been solved for plane wave sources [21], spherical wave sources [22,23], and the more complex finite beam (viz. gaussian beam) sources [24,25].

Another topic routinely of interest is the spatial spectrum (or its inverse Fourier transform, the covariance) of the log-amplitude for plane [26], spherical [22], and finite beam wave sources [24].

The next step in complexity is the calculation of temporal spectra of, for example, angle of arrival [27,28,29], phase [30,31,32], phase difference [31,33,34] or irradiance [35,36,37,38,39]. The temporal scintillation spectrum for plane waves was examined by Tatarski [36]. An interesting feature of his development was that it accounted for a finite receiver aperture. However, since the true plane wave is merely

a mathematical abstraction, his analysis is applicable to only a small class of problems [40].

An extension of Tatarski's method to the calculation of the spherical wave temporal scintillation spectrum was provided by Clifford [35]. In his evaluation he developed expressions for the asymptotic behavior of both plane and spherical waves. Solution of the spherical wave problem represented a significant advance in the theory because the spherical wave could be closely approximated in practice, thus allowing experimental verification.

The calculation of the temporal scintillation spectrum of a practically realizable source (the laser) was provided by Ishimaru [39] and later by Mironov, et al [37]. Both authors presented numerically calculated spectra for a variety of laser beam configurations.

The Method of Smooth Perturbations, as it has been used in the past is, however, extremely cumbersome when applied to an extended source. Its use in the analysis of each of the aforementioned problems necessitated solving the wave equation for a particular source field (plane, spherical, gaussian, etc.).

A more modern approach is to not solve the wave equation for the field directly, but rather for the Green's function for the particular propagation path configuration. The receiver plane field is obtained merely by convolving the Green's function with the incident field. This extension of the Green's function technique to propagation within an inhomogeneous medium is commonly referred to as the Extended Huygens-Fresnel Principle [41]. It is perhaps paradoxical that the Green's function technique (for propagation within a homogeneous medium) predates the Method of Smooth Perturbations [42].

The study with which we are concerned employs elements of both the classical (Method of Smooth Perturbations) and the modern (Extended Huygens-Fresnel Principle) techniques. Virtues of each method are exploited to obtain an expression for the temporal scintillation spectrum of an arbitrary source field. This formula is much simpler yet more general than those developed by Tatarski, Clifford, or Ishimaru. In fact their results are special cases of our formula. This study extends the results of Ishimaru and Mironov in that it accounts for an arbitrary extended source and an arbitrarily located extended receiver aperture.

A portion of our analysis deals with the effects of extended receiver apertures and the ensuing "aperture averaging". This topic has also been treated theoretically by Fried, et al [43] and experimentally by Homstad, et al [44] and Dumphy and Kerr [45].

The evaluation of the temporal scintillation spectrum for a gaussian beam with an off-axis detector represents a significant

contribution to the body of knowledge. Previous authors have always dealt with axial detectors.

Finally, use of our formula in the modeling of a dirty laser beam and the subsequent evaluation of the scintillation spectrum provides an important description of a situation which is universally encountered experimentally, but rarely treated even qualitatively. The techniques applied to the modeling of a dirty laser beam could also be applied to the prediction of the scintillation spectrum of a laser with cassegrain optics.

D. Outline of Effort

Chapter II provides the bulk of the background plus the mathematical foundation for the remainder of the research effort. The development relies upon the extension of the familiar Huygens-Fresnel diffraction integral to the problem of propagation within an inhomogeneous medium. Use of the Extended Huygens-Fresnel Integral results in an expression for the temporal scintillation spectrum for an arbitrary source field in terms of the generalized spatio-temporal second order statistical moments of a spherical wave. These moments which are functions of separations within the transmitter plane, the receiver plane, and time are then derived. With some easily justified approximations the expression for the spectrum undergoes tremendous simplification. The final expression, which is very compact, has some very interesting interpretations. A description of the final expression in the context of a phase grating model of the atmosphere completes this chapter.

The formula for the scintillation spectrum derived in Chapter II is applied in Chapter III to the case of a clean gaussian beam source. Results of the analysis are in terms of analytic formulae for the asymptotes of the spectrum under a variety of conditions. Such conditions include the case in which the detector is off-axis to the laser beam, as illustrated in Figure 2, and the case in which the turbulence is localized. In addition to asymptotic results, numerically calculated spectra are presented for typical instances.

In Chapter IV the "dirty" laser beam is studied. The dirty beam is modeled as arising from the propagation of an initially unperturbed laser beam through a window containing an imperfection and thence into the atmosphere. This situation is illustrated in Figure 3. The window imperfection is modeled as an axially located spot which slightly shifts the phase of the incident beam. It is demonstrated that this specific arrangement displays characteristics of a much more general situation. Within the development the phase object is approximated by a truncated series of functions involving Gaussian-Hermite polynomials. These functions are of particular importance because they closely approximate the modes of a laser and because they are exact

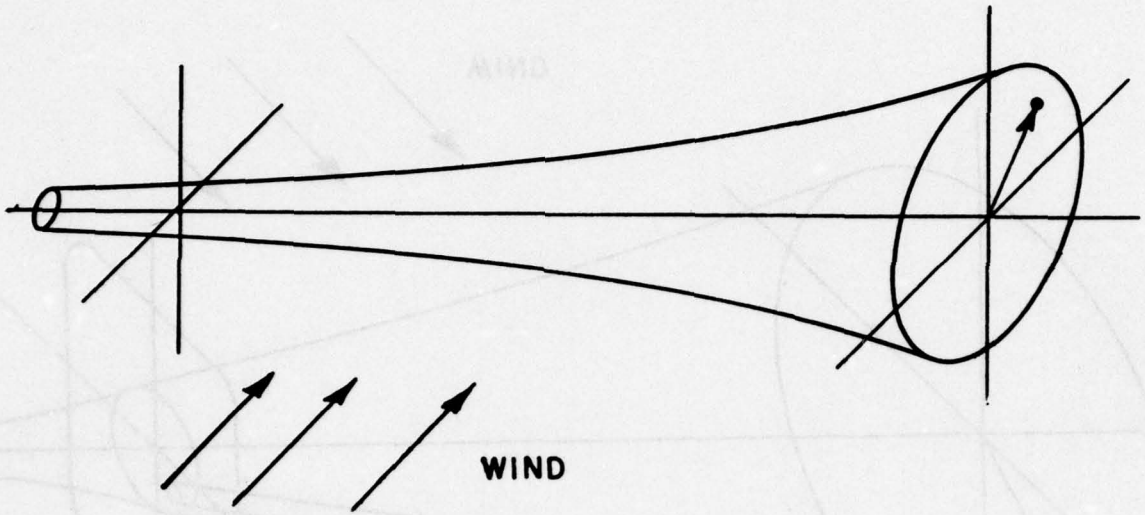

Figure 2--Illustration of off-axis detector.

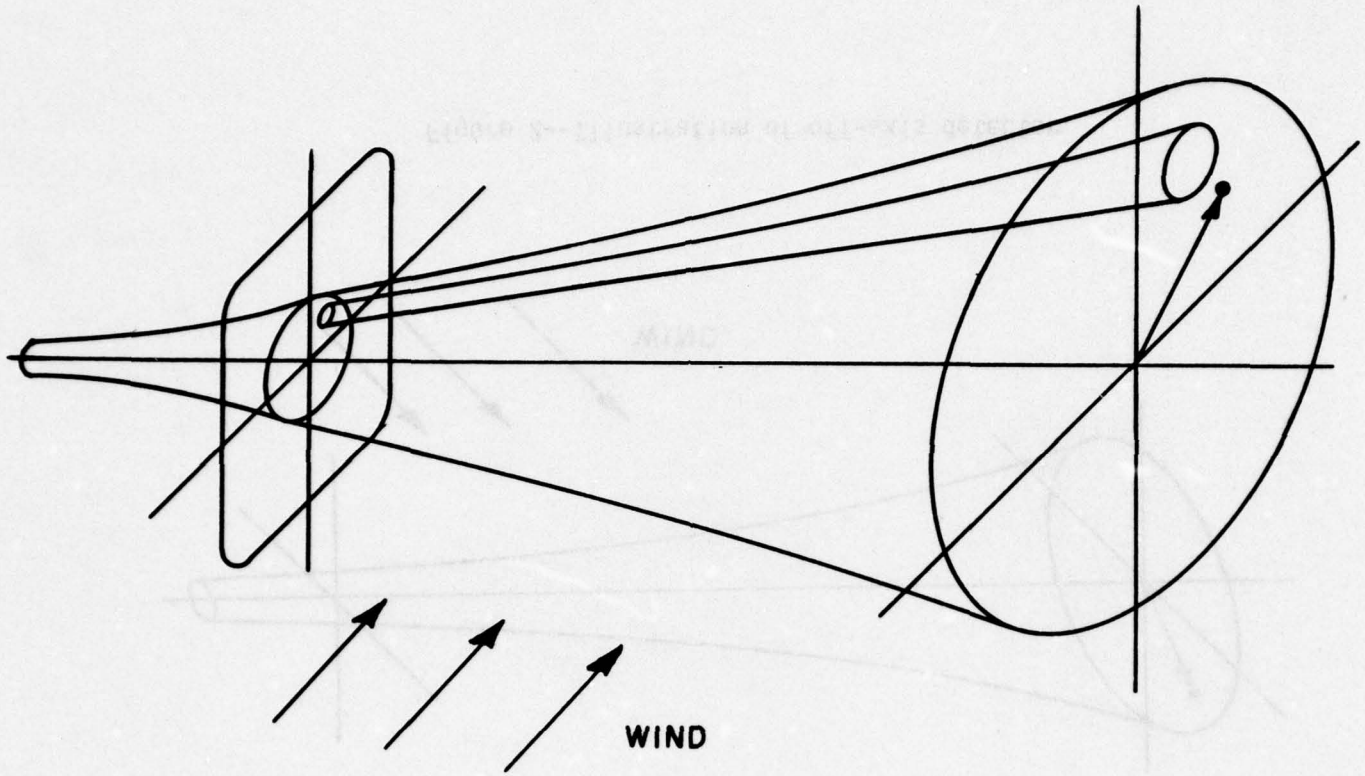

Figure 3--Illustration of dirty beam configuration.

(within the paraxial approximation) eigenfunctions of the free space wave operator. Because the polynomial series is truncated, a procedure is demonstrated which optimizes the approximation.

The expression resulting from the modeling of a dirty laser beam is then numerically evaluated for a variety of situations. As a result of the analysis, the scintillation spectrum is shown to exhibit very interesting and informative low frequency behavior.

The summary and conclusions are contained in Chapter V. Suggestions are provided for future analytical as well as experimental efforts.

CHAPTER II

DERIVATION OF FUNDAMENTAL FORMULA

A. Introduction

This chapter is devoted to the derivation of an expression for the temporal scintillation spectrum of an arbitrary incident field. The final formula obtained is the foundation on which the remainder of the analysis rests.

Within the derivation use is made of the Extended Huygens-Fresnel principle and the weak turbulence approximation. The final result is a very simple and physically interpretable formula for the temporal scintillation spectrum of an arbitrary source field. This formula, which requires knowledge of the free-space receiver-plane field of an unspecified extended source, also accounts for an extended receiver.

In Section B we employ the Extended Huygens-Fresnel Integral to develop an expression for the scintillation spectrum in terms of the second order spatio-temporal statistical moments of spherical waves. These moments, (log-amplitude covariances, phase-log-amplitude cross covariances, and wave structure functions) which are functions of separation in the transmitter plane, separation in the receiver plane, and separation in time, are derived in Section C by use of the method of smooth perturbations.

The results of the two previous sections are combined in Section D. Use is then made (and justified) of the weak turbulence approximation. By rearranging terms of the resulting formula we obtain a series of diffraction integrals which are then performed symbolically to yield the desired expression for the scintillation spectrum.

In Section E the various components of the final formula are interpreted in the context of a phase screen model of the atmospheric turbulence.

Finally Section F consists of a discussion and summary of the chapter.

B. Derivation of General Expression for Scintillation Spectrum

This section is devoted to developing an expression for the temporal scintillation spectrum in terms of the second order statistical moments of a spherical wave. The derivation is based upon use of the Extended Huygens-Fresnel integral and employs standard mathematical procedures currently employed in the literature.

We are interested in the situation in which an arbitrary unperturbed source field is incident (at z=0) upon a region (z>0) containing randomly varying index of refraction inhomogeneities. The field then propagates through the inhomogeneous medium a distance L to a receiver plane in which is located an arbitrary detector. To determine the receiver plane fields we propose to solve the scalar wave equation

$$[\nabla^2 + k^2 n^2(\bar{R})]E(\bar{R}) = 0 \tag{1}$$

where the index of refraction n is a random function of space and k is the free-space wavenumber ($k = 2\pi/\lambda$). By defining a generalized Green's function such that

$$[\nabla^2 + k^2 n^2(\bar{R})]G(\bar{R},\bar{R}') = -4\pi\delta(|\bar{R}-\bar{R}|) \tag{2}$$

it is easily shown (see Appendix A)[41] that the receiver plane field may be expressed approximately as

$$E(\bar{R}') = \frac{-ik}{2\pi} \int G(\bar{r},\bar{R}')E(\bar{r})d\bar{r} \tag{3}$$

where the surface integration is carried out over the plane z=0 and L is the distance between transmitter and receiver planes. In Equation (3) we have denoted the three-dimensional vector by an upper case letter and the two dimensional vector by a lower case letter. We shall attempt to retain this convention throughout the remainder of this work. Using the explicit expression for the generalized Green's function (also discussed in Appendix A) Equation (3) may be written

$$E(\bar{r}_1',t) = \frac{-ik}{2\pi L} \int d\bar{r}_1 \, e^{ikL(\bar{r}_1,\bar{r}_1') + \psi(\bar{r}_1;\bar{r}_1';t)} E(\bar{r}_1) \tag{4}$$

where L is the geometrical (free space) distance between the point $\bar{r}$ in the transmitter plane and the point $\bar{r}'$ in the receiver plane and ψ is a complex phase perturbation to the field of a spherical wave. The variables of interest are illustrated in Figure 4.

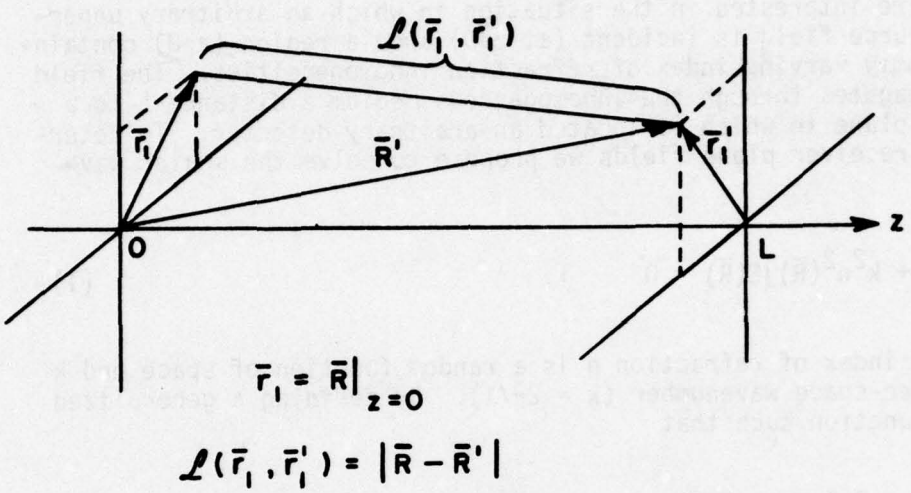

Figure 4--Variables appearing in Huygens-Fresnel formula.

The preceding discussion aimed at solution of the wave equation within an inhomogeneous medium encompasses the method commonly referred to as the Extended Huygens-Fresnel technique. This topic is discussed more fully in Appendix A.

Using Equation (4) we express the irradiance at $\bar{r}'$ as

$$I(\bar{r}_1';t_1) \equiv |E(\bar{r}_1';t_1)|^2 = \left(\frac{k}{2\pi L}\right)^2 \int d\bar{r}_1 \int d\bar{r}_2 \, e^{ik[L(\bar{r}_1,\bar{r}_1')-L(\bar{r}_2,\bar{r}_1')]} \times e^{\psi(\bar{r}_1;\bar{r}_1';t_1) + \psi^*(\bar{r}_2;\bar{r}_1';t_1)} E(\bar{r}_1)E^*(\bar{r}_2) \tag{5}$$

and the total received power as

$$P(t_1) = \int d\bar{r}_1' \; w(\bar{r}_1')I(\bar{r}_1';t_1) \tag{6}$$

where w is the receiver pupil function defined as

$$w(\bar{r}_1') = \begin{cases} 1; & |\bar{r}_1'| \leq D/2 \\ 0; & |\bar{r}_1'| > D/2 \end{cases} \tag{7}$$

and D is the diameter of the receiver aperture. We have assumed the right hand side of Equation (6) to be divided by unity impedance so that the power, P, does indeed have the units of watts. Now under the assumption of temporal (wide sense) stationarity, the temporal scintillation spectrum is given by

$$S_p(\omega) = \int_{-\infty}^{\infty} d\tau \; C_p(\tau)e^{-i\omega\tau} \tag{8}$$

where C is the power covariance,

$$C_p(\tau) = \langle [P(t_1) - \langle P(t_1)\rangle][P(t_2) - \langle P(t_2)\rangle]\rangle \tag{9}$$

$\tau = t_1 - t_2$, and the angular brackets denote the ensemble average.

Equations (6), (8), and (9) yield

$$S_p(\omega) = \int_{-\infty}^{\infty} d\tau \; e^{-i\omega\tau} \int d\bar{r}_1' w(\bar{r}_1') \int d\bar{r}_2' w(\bar{r}_2') \; C_I(\bar{r}_1' - \bar{r}_2';\tau) \tag{10}$$

where C_I is the covariance of irradiance defined as

$$C_I(\bar{r}_1' - \bar{r}_2';\tau) = \langle [I(\bar{r}_1';t_1) - \langle I(\bar{r}_1';t_1)\rangle][I(\bar{r}_2';t_2) - \langle I(\bar{r}_2';t_2)\rangle]\rangle \tag{11-a}$$

or more simply

$$C_I(\bar{r}_1' - \bar{r}_2';\tau) = \langle I(\bar{r}_1';t_1)I(\bar{r}_2';t_2)\rangle - \langle I(\bar{r}_1';t_1)\rangle\langle I(\bar{r}_2';t_2)\rangle \; . \tag{11-b}$$

Note that we have indicated the covariance of irradiance to be simultaneously homogeneous in the receiver plane separation, $\bar{r}_1'-\bar{r}_2'$, and stationary in time, τ. This assumption will be justified later in this chapter.

Use will now be made of Equation (5) to calculate the irradiance correlation and mean irradiance as required in Equation (11-b).

The mean irradiance from Equation (2) is simply

$$\langle I(\bar{r}_1';t_1)\rangle = \left(\frac{k}{2\pi L}\right)^2 \int dr_1 \int dr_2 \; e^{ik[L(\bar{r}_1,\bar{r}_1') - L(\bar{r}_2,\bar{r}_1')]} \times E(\bar{r}_1)E^*(\bar{r}_2)\,\langle e^{\zeta}\rangle \tag{12}$$

where we have defined

$$\zeta = \psi(\bar{r}_1;\bar{r}_1';t_1) + \psi^*(\bar{r}_2;\bar{r}_1';t_1) \quad . \tag{13-a}$$

If we define $\psi = \chi + iS$, where S is the phase and χ is commonly called the log-amplitude then ζ is given by

$$\zeta = \chi(\bar{r}_1;\bar{r}_1';t_1) + iS(\bar{r}_1;\bar{r}_1';t_1) + \chi(\bar{r}_2;\bar{r}_1';t_1) - iS(\bar{r}_2;\bar{r}_1';t_1) \quad . \tag{13-b}$$

The notation in the derivation to follow is greatly simplified by adopting the convention

$$\zeta = (\chi_{111} + \chi_{211}) + i(S_{111} - S_{211}) \tag{13-c}$$

where the subscripts refer to respectively a point, $\bar{r}_1$ or $\bar{r}_2$, in the transmitter plane, a point, $\bar{r}_1'$ or $\bar{r}_2'$, in the receiver plane, and a time, t_1 or t_2.

Under the assumption that the complex phase perturbation is normally distributed [46] we have [47]

$$\langle e^{\zeta}\rangle \; e^{\frac{1}{2}\sigma_\zeta^2 + \mu_\zeta} \tag{14}$$

where σ_ζ^2 and μ_ζ are respectively the variance and mean of ζ. The mean is

$$\mu_\zeta = 2\langle\chi\rangle \quad . \tag{15-a}$$

It is easily demonstrated by conservation of energy arguments [48] that the mean must be the negative of the variance;

$$\mu_\zeta = 2\langle\chi\rangle = -2C_\chi(0;0;0) \quad . \tag{15-b}$$

For an infinite plane wave, relation (15-b) is identically true because the average irradiance at a point in the receiver plane must be independent of turbulence strength (energy must be conserved). For a spherical wave propagating through weak turbulence, energy is not actually diffracted out of the beam but merely instantaneously redistributed. Therefore, for weak turbulence, the mean irradiance of a spherical wave should also be independent of turbulence strength.

The variance of ζ is given by

$$\sigma_\zeta^2 = \langle[(\chi_{111} - \langle\chi\rangle + \chi_{211} - \langle\chi\rangle) + i(S_{111} - S_{211})]^2\rangle$$

$$= 2\,C_\chi(0;0;0) + 2\,C_\chi(\bar{r}_1-\bar{r}_2;0;0) \tag{16-a}$$

$$- i4\langle\chi\rangle\langle(S_{111} - S_{211})\rangle + i2\langle(\chi_{111} + \chi_{211})(S_{111} - S_{211})\rangle$$

$$- D_S(\bar{r}_1-\bar{r}_2;0;0) \tag{16-b}$$

where D_S is the phase structure function defined as

$$D_S(\bar{\rho};\bar{\rho}';\tau) = 2[C_S(0;0;0) - C_S(\bar{\rho};\bar{\rho}';\tau)] \quad , \tag{16-c}$$

and we have assumed simultaneous homogeneity in both the transmitter plane separation, $\bar{\rho}$, and receiver plane separation, $\bar{\rho}'$, and stationarity in the time separation, τ. This assumption of simultaneous homogeneity will be justified in a later section.

The imaginary terms on the right hand side of Equation (16-b) are identically zero. This can be verified by interchanging the points $\bar{r}_1$ and $\bar{r}_2$ in the transmitter plane thus introducing a sign change in these

terms. However by isotropy, this interchange should produce no sign change. Therefore the imaginary terms are zero and Equations (14), (15-b) and (16-b) yield

$$\langle e^{\zeta} \rangle = e^{-\frac{1}{2}D_S(\bar{r}_1-\bar{r}_2;0;0) - \frac{1}{2}D_\chi(\bar{r}_1-\bar{r}_2;0;0)} \tag{17-a}$$

or

$$\langle e^{\zeta} \rangle = e^{-\frac{1}{2}D_W(\bar{r}_1-\bar{r}_2;0;0)} \tag{17-b}$$

where D_W is the "wave" structure function [48] defined simply as the sum of the phase and log-amplitude structure functions.

The mean irradiance term in Equation (11-b) is then finally

$$\langle I(\bar{r}_1';t_1)\rangle\langle I(\bar{r}_2';t_2)\rangle = \left(\frac{k}{2\pi L}\right)^4 \int d\bar{r}_1 \int d\bar{r}_2 \int d\bar{r}_3 \int d\bar{r}_4$$

$$\times E(\bar{r}_1)E^*(\bar{r}_2)E(\bar{r}_3)E^*(\bar{r}_4)\, e^{ik[L(\bar{r}_1,\bar{r}_1')-L(\bar{r}_2,\bar{r}_1')+L(\bar{r}_3,\bar{r}_2')-L(\bar{r}_4,\bar{r}_2')]}$$

$$\times e^{-\frac{1}{2}[D_W(\bar{r}_1-\bar{r}_2;0;0) + D_W(\bar{r}_3-\bar{r}_4;0;0)]} \tag{18}$$

Similarly the correlation of irradiance in Equation (11-b) is given by

$$\langle I(\bar{r}_1';t_1)I(\bar{r}_2';t_2)\rangle = \left(\frac{k}{2\pi L}\right)^4 \int d\bar{r}_1 \int d\bar{r}_2 \int d\bar{r}_3 \int d\bar{r}_4$$

$$\times E(\bar{r}_1)E^*(\bar{r}_2)E(\bar{r}_3)E^*(\bar{r}_4)e^{ik[L(\bar{r}_1,\bar{r}_1')-L(\bar{r}_2,\bar{r}_1')+L(\bar{r}_3,\bar{r}_2')-L(\bar{r}_4,\bar{r}_2')]}$$

$$\times \langle e^{\xi} \rangle \tag{19-a}$$

where

$$\xi \equiv \psi(\bar{r}_1;\bar{r}_1';t_1)+\psi^*(\bar{r}_2;\bar{r}_1';t_1)+\psi(\bar{r}_3;\bar{r}_2';t_2)+\psi^*(\bar{r}_4,\bar{r}_2';t_2) \tag{19-b}$$

By the previously adopted notation we have

$$\xi = (x_{111} + x_{211} + x_{322} + x_{422}) + i(s_{111} - s_{211} + s_{322} - s_{422}) . \tag{20}$$

Reapplication of Equation (14) to calculate the mean of $\exp(\xi)$ requires the calculation of the mean, μ_ξ, and the variance, σ_ξ^2, of ξ.

Again, conservation of energy [48] requires that the mean be equal to the negative of the variance;

$$\mu_\xi = 4\langle x \rangle = -4\, C_x(0;0;0) \tag{21}$$

The variance is

$$\sigma_\xi^2 = f_1 + f_2 + f_3 + f_4 \tag{22-a}$$

where

$$f_1 = \langle (x_{111} - \langle x \rangle + x_{211} - \langle x \rangle + x_{322} - \langle x \rangle + x_{422} - \langle x \rangle)^2 \rangle \tag{22-b}$$

$$f_2 = -i8\, \langle x \rangle \langle (s_{111} - s_{211} + s_{322} - s_{422}) \rangle \tag{22-c}$$

$$f_3 = i2\, \langle (x_{111} + x_{211} + x_{322} + x_{422})(s_{111} - s_{211} + s_{322} - s_{422}) \rangle \tag{22-d}$$

and

$$f_4 = - \langle (s_{111} - s_{211} + s_{322} - s_{422})^2 \rangle \tag{22-e}$$

The term f_1 is easily shown to be

$$f_1 = 4\, C_\chi(0;0;0) + 2\, C_\chi(\bar{r}_1-\bar{r}_2;0;0) + 2\, C_\chi(\bar{r}_3-\bar{r}_4;0;0)$$

$$+ 2\, C_\chi(\bar{r}_1-\bar{r}_3;\bar{r}_1'-\bar{r}_2';t_1-t_2) + 2\, C_\chi(\bar{r}_1-\bar{r}_4;\bar{r}_1'-\bar{r}_2';t_1-t_2)$$

$$+ 2\, C_\chi(\bar{r}_2-\bar{r}_3;\bar{r}_1'-\bar{r}_2';t_1-t_2) + 2\, C_\chi(\bar{r}_2-\bar{r}_4;\bar{r}_1'-\bar{r}_2';t_1-t_2)\ . \quad (23)$$

Term f_2 is identically zero because of stationarity and term f_3 with isotropy arguments similar to those employed previously is given by

$$f_3 = i2[\langle(S_{322} - S_{422})(\chi_{111} + \chi_{211})\rangle + \langle(S_{111} - S_{211})(\chi_{322} + \chi_{422})\rangle] \quad (24\text{-a})$$

$$f_3 = i4[C_{\chi S}(\bar{r}_1-\bar{r}_3;\bar{r}_1'-\bar{r}_2';t_1-t_2) - C_{\chi S}(\bar{r}_2-\bar{r}_4;\bar{r}_1'-\bar{r}_2';t_1-t_2)]\ , \quad (24\text{-b})$$

where $C_{\chi S}$ is the cross-covariance between phase and log-amplitude.

Use of the identity

$$(a-b+c-d)^2 = (a-b)^2 + (c-d)^2 + (a-d)^2 + (b-c)^2 - (a-c)^2 - (b-d)^2 \quad (25)$$

gives for the remaining term in Equation (22-a)

$$f_4 = -[\langle(S_{111} - S_{211})^2\rangle + \langle(S_{322} - S_{422})^2\rangle + \langle(S_{111} - S_{422})^2\rangle + \langle(S_{211} - S_{322})^2\rangle - \langle(S_{111} - S_{322})^2\rangle - \langle(S_{211} - S_{422})^2\rangle] \quad (26\text{-a})$$

or

$$f_4 = -[D_S(\bar{r}_1-\bar{r}_2;0;0) + D_S(\bar{r}_3-\bar{r}_4;0;0) + D_S(\bar{r}_1-\bar{r}_4;\bar{r}_1'-\bar{r}_2';t_1-t_2)$$

$$+ D_S(\bar{r}_2-\bar{r}_3;\bar{r}_1'-\bar{r}_2';t_1-t_2) - D_S(\bar{r}_1-\bar{r}_3;\bar{r}_1'-\bar{r}_2';t_1-t_2)$$

$$- D_S(\bar{r}_2-\bar{r}_4;\bar{r}_1'-\bar{r}_2';t_1-t_2)] \qquad (26\text{-b})$$

Finally, combining Equations (19) through (26) gives

$$\langle e^{\xi}\rangle = \exp\left\{-\frac{1}{2}[D_W(\bar{r}_1-\bar{r}_2;0;0) + D_W(\bar{r}_3-\bar{r}_4;0;0)\right.$$

$$+ D_W(\bar{r}_1-\bar{r}_4;\bar{r}_1'-\bar{r}_2';t_1-t_2) + D_W(\bar{r}_2-\bar{r}_3;\bar{r}_1'-\bar{r}_2';t_1-t_2)$$

$$- D_W(\bar{r}_1-\bar{r}_3;\bar{r}_1'-\bar{r}_2';t_1-t_2) - D_W(\bar{r}_2-\bar{r}_4;\bar{r}_1'-\bar{r}_2';t_1-t_2)] \quad .$$

$$+ 2[C_X(\bar{r}_1-\bar{r}_3;\bar{r}_1'-\bar{r}_2';t_1-t_2) + C_X(\bar{r}_2-\bar{r}_4;\bar{r}_1'-\bar{r}_2';t_1-t_2)$$

$$\left. + i\, C_{XS}(\bar{r}_1-\bar{r}_3;\bar{r}_1'-\bar{r}_2';t_1-t_2) - i\, C_{XS}(\bar{r}_2-\bar{r}_4;\bar{r}_1'-\bar{r}_2';t_1-t_2)]\right\} . \qquad (27)$$

The optical distance term in Equations (18) and (19-a) is

$$ikL \equiv ik[L(\bar{r}_1,\bar{r}_1') - L(\bar{r}_2,\bar{r}_1') + L(\bar{r}_3,\bar{r}_2') - L(\bar{r}_4,\bar{r}_2')] \quad . \qquad (28\text{-a})$$

Referring to Figure 5 it is seen that

$$ikL = ik[(L^2+|\bar{r}_1-\bar{r}_1'|^2)^{\frac{1}{2}} - (L^2+|\bar{r}_2-\bar{r}_1'|^2)^{\frac{1}{2}}$$

$$+ (L^2+|\bar{r}_3-\bar{r}_2'|^2)^{\frac{1}{2}} - (L^2+|\bar{r}_4-\bar{r}_2'|^2)^{\frac{1}{2}}] \quad . \qquad (28\text{-b})$$

Invoking the paraxial ray approximation ($|\bar{r}_i-\bar{r}_j'| \ll L \;\forall\; i,j$) we obtain

$$ikL = \frac{ik}{2L}\,[|\bar{r}_1-\bar{r}_1'|^2 - |\bar{r}_2-\bar{r}_1'|^2 + |\bar{r}_3-\bar{r}_2'|^2 - |\bar{r}_4-\bar{r}_2'|^2] \quad .$$

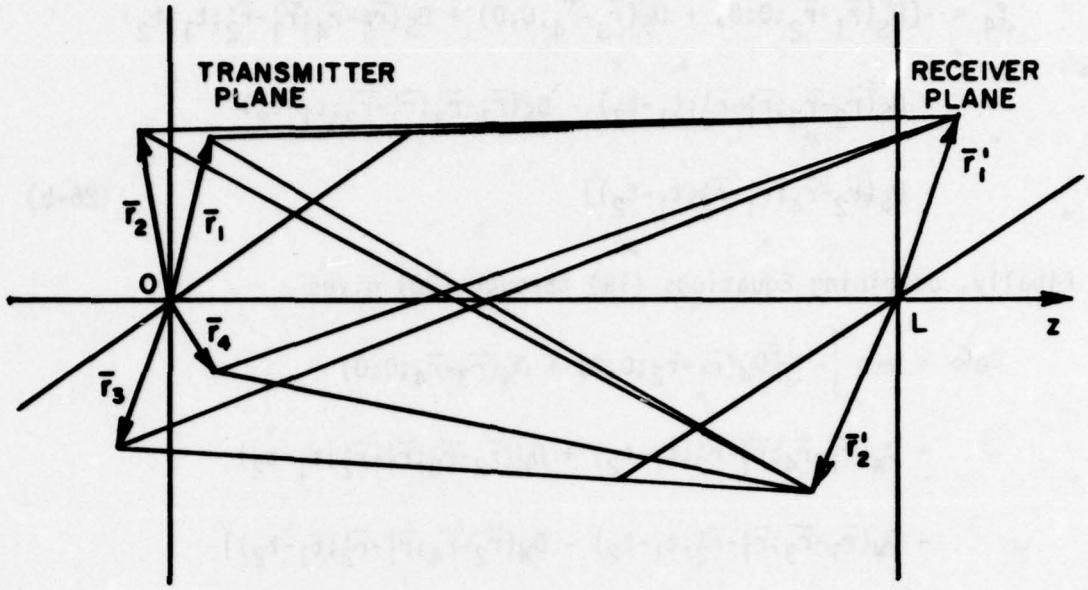

Figure 5--Statistical moment vector arguments.

We now obtain by combining Equations (10), (11), (18), (19-a), (27), and (28-c) the basic expression for the temporal irradiance spectrum;

$$S_p(\omega) = \left(\frac{k}{2\pi L}\right)^4 \int_{-\infty}^{\infty} d\tau\, e^{-i\omega\tau} \int d\bar{r}_1' W(\bar{r}_1') \int d\bar{r}_2' W(\bar{r}_2')$$

$$\times \int d\bar{r}_1 \int d\bar{r}_2 \int d\bar{r}_3 \int d\bar{r}_4\, E(\bar{r}_1)E^*(\bar{r}_2)E(\bar{r}_3)E^*(\bar{r}_4)$$

$$\times e^{\frac{ik}{2L}\left[|\bar{r}_1-\bar{r}_1'|^2 - |\bar{r}_2-\bar{r}_1'|^2 + |\bar{r}_3-\bar{r}_2'|^2 - |\bar{r}_4-\bar{r}_2'|^2\right]}$$

$$\times H(\bar{r}_1,\bar{r}_2,\bar{r}_3,\bar{r}_4;\bar{r}_1',\bar{r}_2';\tau) \qquad (29\text{-a})$$

where

$$H = \exp\left\{-\tfrac{1}{2}[D_W(\bar{r}_1-\bar{r}_2;0;0) + D_W(\bar{r}_3-\bar{r}_4;0;0)\right.$$

$$+ D_W(\bar{r}_1-\bar{r}_4;\bar{r}_1'-\bar{r}_2';\tau) + D_W(\bar{r}_2-\bar{r}_3;\bar{r}_1'-\bar{r}_2';\tau)$$

$$- D_W(\bar{r}_1-\bar{r}_3;\bar{r}_1'-\bar{r}_2';\tau) - D_W(\bar{r}_2-\bar{r}_4;\bar{r}_1'-\bar{r}_2';\tau)]$$

$$+ 2[C_\chi(\bar{r}_1-\bar{r}_3;\bar{r}_1'-\bar{r}_2';\tau) + C_\chi(\bar{r}_2-\bar{r}_4;\bar{r}_1'-\bar{r}_2';\tau)$$

$$\left. + i\, C_{\chi S}(\bar{r}_1-\bar{r}_3;\bar{r}_1'-\bar{r}_2';\tau) - i\, C_{\chi S}(\bar{r}_2-\bar{r}_4;\bar{r}_1'-\bar{r}_2';\tau)]\right\}$$

$$- \exp\left\{-\tfrac{1}{2}[D_W(\bar{r}_1-\bar{r}_2;0;0) + D_W(\bar{r}_3-\bar{r}_4;0;0)]\right\} \quad . \qquad (29\text{-b})$$

At this point it may appear that the spectrum is not real as it should be. This fear may be removed by manipulating the dummy variables in Eqs. (29). Specifically by interchanging $\bar{r}_1$ and $\bar{r}_4$, $\bar{r}_2$ and $\bar{r}_3$; $\bar{r}_1'$ and $\bar{r}_2'$; and setting $\tau=-\tau$ the right hand side of Eq. (29) appears to have been conjugated. However since the left hand side is unchanged, the spectrum S is equal to its complex conjugate, i.e., it is real.

Equations (29) are the final result of this section. The particular form of the transfer function H is important because at least one group of workers [49] has found that for very strong turbulence, the behavior of the H function is dominated by that of the structure functions. That is, the covariances in Equation (29-b) may be neglected. Further, under certain circumstances (on-axis point detector), approximate closed-form expressions for the wave structure functions may be found. For this instance it would be possible to calculate the temporal scintillation spectrum under saturation conditions. This topic seems a fertile area for further research.

We have in this section derived an expression, in terms of the second order moments of a spherical wave, for the temporal scintillation spectrum of an arbitrary field source. Use was made of the Extended Huygens-Fresnel integral which expresses the receiver plane field as the convolution of the transmitter plane field with a Green's function which has been generalized to propagation within an inhomogeneous medium. With standard mathematical procedures and assumptions treated extensively in the literature we arrive at the desired formula expressed in Equations (29).

Finally, approximations were discussed which may enable the use of the final expression to calculate the scintillation spectrum within the saturation regime.

The next section is devoted to a derivation of the statistical moments required by Equation (29).

C. Derivation of Statistical Moments

We now face the task of deriving expressions for the statistical functions required by Equation (29-b) of the previous section. Use will be made of the method of smooth perturbations [2] which is sometimes referred to as the Rytov method [50,51]. Since this method is well known, only the salient features of the derivations are presented within this section. The expressions for the statistical moments which are developed within this section represent generalizations of expressions currently available in the literature.

The method of smooth perturbations relies upon the expression of the field as [2]

$$E = e^{\sum_{n=0}^{\infty} \gamma^n \psi_n} \tag{30-a}$$

where

$$\gamma = \sqrt{\langle [n(\bar{R}) - \langle n(\bar{R}) \rangle]^2 \rangle}$$

is the R.M.S. variation in the index of refraction.

Typically γ is on the order of 10^{-6} [41]. By inserting E from Equation (30-a) in the scalar wave equation and equating like powers of γ one arrives at an infinite series of linear constant coefficient (Recall that the wave equation within an inhomogeneous medium has the variable coefficient $n^2(\bar{R})$.) differential equations which are easily solved by the Green's function technique. The solutions of these differential equations are commonly denoted as ψ_n and are given by

$$\psi_n = \gamma^n \psi_n \quad . \tag{31}$$

Obviously this results in the field being given by

$$E = e^{\sum_{n=0}^{\infty} \psi_n} \quad . \tag{32}$$

Now if we define

$$E = A\, e^{iS} = e^{\ell nA + iS} \tag{33}$$

and denote

$$\psi_n = \ell nA_n + iS_n \tag{34}$$

we see that

$$e^{\ell n(A/A_o)+i(S-S_o)} = e^{\sum_{n=1}^{\infty} \psi_n} \quad . \tag{35}$$

The log-amplitude and phase perturbations which are denoted respectively as

$$\chi = \ell n(A/A_o) \tag{36-a}$$

and

$$S_1 = S - S_o \tag{36-b}$$

are then to first order smallness of γ;

$$\chi = Re\{\psi_1\} \tag{37-a}$$

and

$$S_1 = Im\{\psi_1\} \quad . \tag{37-b}$$

Tatarski [52] gives for the first perturbation to the complex phase

$$\psi_1(\overline{R}') = \frac{k^2}{2\pi} \int_V \frac{e^{ik|\overline{R}-\overline{R}'|}}{|\overline{R}-\overline{R}'|} \frac{E(\overline{R})}{E(\overline{R}')}\, n_1(\overline{R})d\overline{R} \tag{38-a}$$

where

$$n_1(\bar{R}) = n(\bar{R}) - \langle n(\bar{R}) \rangle \qquad (38\text{-b})$$

and the integration is carried out over the scattering volume denoted by $\mathcal{V}$. Figure 6 illustrates the variables used in Equation (38-a).

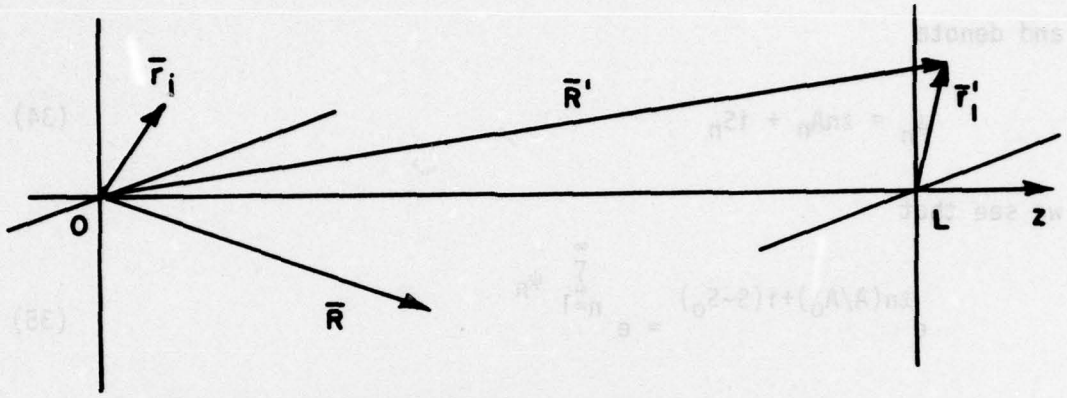

$$\bar{R}' = L\hat{z} + \bar{r}'_i = (x'_i, y'_i, L)$$

$$\bar{r}_i = (x_i, y_i)$$

$$\bar{R} = (x, y, z)$$

Figure 6--Green's function variables.

For the spherical wave fields

$$E(\bar{R}) = \frac{E_o e^{ik|\bar{R}-\bar{r}_i|}}{|\bar{R}-\bar{r}_i|} \text{ and } E(\bar{R}') = \frac{E_o e^{ik|\bar{R}'-\bar{r}_i|}}{|\bar{R}'-\bar{r}_i|} \qquad (39)$$

Equation (38-a) becomes

$$\psi_1(\bar{R}';t) \equiv \psi_1(\bar{r}_1';t) = \frac{k^2}{2\pi} \int_V d\bar{R}\, n_1(\bar{R};t)$$

$$\times \frac{|\bar{R}'-\bar{r}_i|}{|\bar{R}-\bar{r}_i|} \frac{e^{ik[|\bar{R}'-\bar{R}|+|\bar{R}-\bar{r}_i|-|\bar{R}'-\bar{r}_i|]}}{|\bar{R}'-\bar{R}|} \tag{40}$$

where we have indicated explicitly the time dependent behavior of n_1. This time dependence arises because we assume the wind to be blowing the index inhomogeneities across the propagation path.

Utilization of the paraxial approximations

$$|\bar{R}-\bar{r}_i| = z + \frac{(x-x_i)^2+(y-y_i)^2}{2z}$$

$$|\bar{R}'-\bar{r}_i| = L + \frac{(x_1'-x_i)^2+(y_1'-y_i)^2}{2L}$$

$$|\bar{R}'-\bar{R}| = (L-z) + \frac{(x_1'-x)^2+(y_1'-y)^2}{2(L-z)} \tag{41}$$

allows Equation (40) to be written

$$\psi_1(\bar{r}_1';t) = \frac{k^2}{2\pi} \int_0^L dz \left(\frac{L}{z}\right)\left(\frac{1}{L-z}\right) \int_{-\infty}^{\infty} dx \int_{-\infty}^{\infty} dy\, n_1(x,y,z;t)$$

$$\times \exp\left\{ik\left[\frac{(x_1'-x)^2+(y_1'-y)^2}{2(L-z)} + \frac{(x-x_i)^2+(y-y_i)^2}{2z} - \frac{(x_1'-x_i)^2+(y_1'-y_i)^2}{2L}\right]\right\}. \tag{42}$$

In Equation (42) the magnification terms have been approximated by the first term of their Taylor's series expansions:

$$\frac{|\bar{R}'-\bar{r}_i|}{|\bar{R}-\bar{r}_i||\bar{R}'-\bar{R}|} = \frac{L}{z(L-z)} \quad . \tag{43}$$

To examine Equation (42) in the spatial spectral domain we make use of the Fourier-Stieltjes expansions [53]

$$n_1(x,y,z;t) = \iint_{-\infty}^{\infty} e^{i(\kappa_1' x+\kappa_2' y)}\, d\nu(\kappa_1',\kappa_2',z;t) \tag{44-a}$$

$$\psi_1(\bar{r}_1';t) = \iint_{-\infty}^{\infty} e^{i(\kappa_1' x_1'+\kappa_2' y_1')}\, d\Phi(\kappa_1',\kappa_2',L;t) \tag{44-b}$$

so that

$$\iint_{-\infty}^{\infty} e^{i(\kappa_1' x_1'+\kappa_2' y_1')}\, d\Phi(\kappa_1',\kappa_2',L;t) = \frac{k^2}{2\pi}\int_0^L dz \left(\frac{L/z}{L-z}\right)\int_{-\infty}^{\infty} dx \int_{-\infty}^{\infty} dy$$

$$\times \iint_{-\infty}^{\infty} e^{i(\kappa_1' x+\kappa_2' y)}\, d\nu(\kappa_1',\kappa_2',z;t)$$

$$\times \exp\left\{ik\left[\frac{(x_1'-x)^2+(y_1'-y)^2}{2(L-z)} + \frac{(x-x_i)^2+(y-y_i)^2}{2z} - \frac{(x_1'-x_i)^2+(y_1'-y_i)^2}{2L}\right]\right\} . \tag{45}$$

In Appendix B it is demonstrated that inversion of Equation (45) yields for the spatial spectrum of the first perturbation to the complex phase;

$$d\Phi(\kappa_1,\kappa_2,L;t) = ik\int_0^L dz d\nu\left(\frac{L}{z}\kappa_1, \frac{L}{z}\kappa_2, z;t\right)$$

$$x\ \exp\left\{i\left[\frac{(L-z)}{z}\ \bar{r}_i\cdot\bar{\kappa} - \frac{(L-z)}{2k}\frac{L}{z}\kappa^2\right]\right\} \quad , \quad (46)$$

where ν is the spatial spectrum of the index of refraction fluctuations. Since the expansion of Equation (44-b) takes place in the receiver plane, the variables κ_1 and κ_2 correspond to spatial scales within the receiver plane.

Because, by definition, the log-amplitude, χ, is real, it is easily demonstrated [54] that (to the first order smallness in γ)

$$\chi - \langle\chi\rangle \overset{F}{\leftrightarrow} \frac{1}{2}[d\Phi(\kappa_1,\kappa_2,L;t) + d\Phi^*(-\kappa_1,-\kappa_2,L;t)]$$

$$\equiv da(\kappa_1,\kappa_2,L;t) \quad , \quad (47)$$

where F indicates the two dimensional spatial Fourier-Stieltjes transform.

Using the fact that the index of refraction field is real (thus requiring $d\nu(-\bar{\kappa},z;t) = d\nu^*(\bar{\kappa},z;t)$), Equations (46) and (47) give

$$da(\kappa_1,\kappa_2,L;t) = k\int_0^L dz d\nu\left(\frac{L}{z}\kappa_1, \frac{L}{z}\kappa_2, z;t\right) e^{\frac{i(L-z)}{z}\bar{r}_i\cdot\bar{\kappa}}$$

$$\sin\left[\frac{L(L-z)}{2kz}\kappa^2\right]. \quad (48)$$

Similarly, to the first approximation, the phase fluctuation is given by

$$S_1 \overset{F}{\leftrightarrow} \frac{1}{2i}[d\Phi(\kappa_1,\kappa_2,L;t) - d\Phi^*(-\kappa_1,-\kappa_2,L;t)]$$

$$\equiv d\phi(\kappa_1,\kappa_2,L;t) \quad (49)$$

which is easily shown to give

$$d\phi(\kappa_1,\kappa_2,L;t) = k\int_0^L dz d\nu \left(\frac{L}{z}\kappa_1, \frac{L}{z}\kappa_2, z; t\right) e^{\frac{i(L-z)}{z}\bar{r}_i\cdot\bar{\kappa}} \cos\left[\frac{L(L-z)}{2kz}\kappa^2\right]. \quad (50)$$

As indicated in Equations (47) and (49) we have made use of the Fourier-Stieltjes expansions of the log-amplitude and phase;

$$\chi(\bar{r}_i;\bar{r}_1';t) - \langle\chi\rangle = \iint_{-\infty}^{\infty} e^{i(\kappa_1 x_1' + \kappa_2 y_1')} da_i(\kappa_1,\kappa_2,L;t) \quad (51a)$$

and

$$S_1(\bar{r}_i;\bar{r}_1';t) = \iint_{-\infty}^{\infty} e^{i(\kappa_1 x_1' + \kappa_2 y_1')} d\phi_i(\kappa_1,\kappa_2,L;t) \quad (51b)$$

where the subscript i on the spectra denotes the source point $\bar{r}_i$.

Now the time delayed log-amplitude and phase are given by

$$\chi(\bar{r}_j;\bar{r}_2';t+\tau) - \langle\chi\rangle = \iint_{-\infty}^{\infty} e^{i(\kappa_1 x_2' + \kappa_2 y_2')} da_j(\kappa_1,\kappa_2;t+\tau) \quad (52a)$$

and

$$S_1(\bar{r}_j;\bar{r}_2';t+\tau) = \iint_{-\infty}^{\infty} e^{i(\kappa_1 x_2' + \kappa_2 y_2')} d\phi_j(\kappa_1,\kappa_2;t+\tau) \quad (52b)$$

Introduction of Taylor's frozen-turbulence hypothesis [55] which says eddies do not change shape in the time it takes them to blow through the propagation path,

$$n_1(\bar{r},z;t+\tau) = n_1(\bar{r}-\bar{v}\tau,z;t), \quad (53)$$

where $\bar{r} = (x,y)$ and $\bar{v}$ is the component of the wind velocity transverse to the propagation path, results in the spectrum of Equation (52a) being given by

$$da_j(\kappa_1,\kappa_2,L;t+\tau) = k\int_0^L dz dv\left(\frac{L}{z}\kappa_1, \frac{L}{z}\kappa_2, z; t\right) \tag{54}$$

$$\times\, e^{\frac{i(L-z)}{z}\,\bar{\kappa}\cdot\bar{r}_j}\, e^{-i\tau\frac{L}{z}\,\bar{\kappa}\cdot\bar{v}}\, \sin\left[\frac{L(L-z)}{2kz}\,\kappa^2\right].$$

The expression for the phase spectrum is identical except the sin function is replaced by a cos function.

Since subsequent derivations for the desired statistical quantities are all similar, we will treat explicitly only the log-amplitude covariance and state without proof expressions for the phase and phase-log-amplitude covariances and the wave structure functions.

The log-amplitude covariance defined as

$$C_\chi(\bar{r}_i-\bar{r}_j;\bar{r}_1'-\bar{r}_2';\tau) = \tag{55}$$

$$\langle[\chi(\bar{r}_i;\bar{r}_1';t_1) - \langle\chi\rangle][\chi(\bar{r}_j;\bar{r}_2';t_2) - \langle\chi\rangle]\rangle$$

is, from Equations (51a) and (52a),

$$C_\chi(\bar{r}_i-\bar{r}_j;\bar{r}_1'-\bar{r}_2';\tau) = \tag{56}$$

$$\iint_{-\infty}^{\infty} e^{i\bar{\kappa}\cdot\bar{r}_1'} \iint_{-\infty}^{\infty} e^{-i\bar{\kappa}'\cdot\bar{r}_2'} \langle da_i(\kappa_1,\kappa_2,L;t)da_j^*(\kappa_1,\kappa_2,L;t+\tau)\rangle\ .$$

With Equations (48) and (54) the covariance is

$$C_\chi(\bar{r}_i-\bar{r}_j;\bar{r}_1'-\bar{r}_2';\tau) = \iint_{-\infty}^{\infty} e^{i\bar{\kappa}\cdot\bar{r}_1'} \iint_{-\infty}^{\infty} e^{-i\bar{\kappa}'\cdot\bar{r}_2'}$$

$$\times\, k^2\int_0^L dz_1\int_0^L dz_2\, \sin\left[\frac{L(L-z_1)}{2kz_1}\,\kappa^2\right]\sin\left[\frac{L(L-z_2)}{2kz_2}\,\kappa'^2\right] \qquad (57)$$

$$\times \exp\left[\frac{i(L-z_1)}{z_1}\,\bar{r}_i\cdot\bar{\kappa} - \frac{i(L-z_2)}{z_2}\,\bar{r}_j\cdot\bar{\kappa}' + i\tau\,\frac{L}{z_2}\,\bar{\kappa}'\cdot\bar{v}\right]$$

$$\times\langle d\nu\left(\frac{L}{z_1}\,\kappa_1,\ \frac{L}{z_1}\,\kappa_2, z_1; t\right) d\nu^*\left(\frac{L}{z_2}\,\kappa_1',\ \frac{L}{z_2}\,\kappa_2', z_2; t\right)\rangle .$$

The assumption of wide-sense stationarity of the turbulence provides the (statistical) orthogonality of the index spectra expressed as [56]

$$\langle d\nu\left(\frac{L}{z_1}\,\kappa_1,\ \frac{L}{z_1}\,\kappa_2, z_1; t\right) d\nu^*\left(\frac{L}{z_2}\,\kappa_1',\ \frac{L}{z_2}\,\kappa_2', z_2; t\right)\rangle$$

$$= \left(\frac{L}{z_1}\right)^2\left(\frac{L}{z_2}\right)^2 d\kappa_1 d\kappa_2 d\kappa_1' d\kappa_2'\,\delta\left(\frac{L}{z_1}\,\kappa_1 - \frac{L}{z_2}\,\kappa_1'\right)\delta\left(\frac{L}{z_1}\,\kappa_2 - \frac{L}{z_2}\,\kappa_2'\right) \qquad (58)$$

$$\times\, F_n\left(\frac{L}{z_1}\,\kappa_1,\ \frac{L}{z_1}\,\kappa_2,\ |z_1-z_2|\right),$$

where F_n is the two-dimensional power spectrum of the index of refraction field.

Combining Equations (57) and (58), making the changes of variables

$$u_1 = \frac{L}{z_2}\,\kappa_1' \quad \text{and} \quad u_2 = \frac{L}{z_2}\,\kappa_2', \qquad (59)$$

and performing the integrations over u_1 and u_2 results in

$$C_\chi(\bar{r}_i-\bar{r}_j;\bar{r}_1'-\bar{r}_2';\tau) = k^2\iint_{-\infty}^{\infty} d\bar{\kappa} \int_0^L dz_1 \int_0^L dz_2 \tag{60}$$

$$\times F_n(\kappa_1,\kappa_2,|z_1-z_2|) \sin\left[\frac{z_1(L-z_1)}{2kL}\kappa^2\right] \sin\left[\frac{z_2(L-z_2)}{2kL}\kappa^2\right]$$

$$\times \exp i\bar{\kappa}\cdot\left\{\tau\bar{v} + \left(\frac{z_1}{L}\bar{r}_1' - \frac{z_2}{L}\bar{r}_2'\right) + \left[\frac{(L-z_1)}{L}\bar{r}_i - \frac{(L-z_2)}{L}\bar{r}_j\right]\right\},$$

where we have dropped the primes on the spatial frequencies.

Recall that in Equation (46) the spatial frequencies correspond to scale sizes at the receiver. However the changes of variables in Equations (59) produce in Equation (60), spatial frequencies κ corresponding to spatial inhomogenieties within the medium. This is an important distinction for the subsequent manipulation of Equation (60).

We shall now proceed to simplify the expression for the log-amplitude covariance. The method will make use of a sum and difference change of (path integration) variables and several order-of-magnitude arguments.

The kappa integrand of Equation (60) is of the form

$$\int_0^L dz_1 \int_0^L dz_2\, G(\kappa,z_1,z_2), \tag{61}$$

which upon changing to sum and difference coordinates

$$z = \frac{z_1+z_2}{2} \quad , \quad z_1 = z + \rho/2$$

$$\rho = z_1-z_2 \quad , \quad z_2 = z - \rho/2 \tag{62}$$

yields

$$\int_0^L dz_1 \int_0^L dz_2\, G(\kappa,z_1,z_2) = \int_0^{L/2} dz \int_{-2z}^{2z} d\rho\, G(\kappa,z+\rho/2,z-\rho/2)$$

$$+ \int_{L/2}^{L} dz \int_{-2(L-z)}^{2(L-z)} d\rho\, G(\kappa,z+\rho/2,\, z-\rho/2), \tag{63a}$$

where the G function is given by

$$G(\kappa,z+\rho/2,z-\rho/2) = F_n(\kappa_1,\kappa_2,|\rho|)e^{i\tau\bar{\kappa}\cdot\bar{v}}$$

$$\times \sin\left[\frac{(z+\rho/2)(L-z-\rho/2)}{2kL}\,\kappa^2\right]\sin\left[\frac{(z-\rho/2)(L-z+\rho/2)}{2kL}\,\kappa^2\right] \tag{63b}$$

$$\times \exp\left\{\frac{i\bar{\kappa}}{L}\cdot\left[(z+\rho/2)\bar{r}_1'-(z-\rho/2)\bar{r}_2'+(L-z-\rho/2)\bar{r}_i-(L-z+\rho/2)\bar{r}_j\right]\right\}$$

Using the trigonometric identity for the product of two cosines and factoring the exponents gives for the G function

$$G(\kappa,z+\rho/2,z-\rho/2) = F_n(\kappa_1,\kappa_2,|\rho|)$$

$$\times \exp\left\{i\bar{\kappa}\cdot\left[\frac{z}{L}\,(\bar{r}_1'-\bar{r}_2')+\left(1-\frac{z}{L}\right)(\bar{r}_i-\bar{r}_j)+\tau\bar{v}\right]\right\} \tag{64}$$

$$\times \frac{1}{2}\left\{\cos\left[\frac{\rho(L-2z)}{2kL}\,\kappa^2\right]-\cos\left[\frac{z(L-z)}{kL}\,\kappa^2-\frac{(\rho\kappa)^2}{4kL}\right]\right\}$$

$$\times \quad e^{i\frac{\rho}{2L}\,\bar{\kappa}\cdot\left[(\bar{r}_1'+\bar{r}_2')-(\bar{r}_i+\bar{r}_j)\right]}.$$

For an isotropic field, fluctuations separated a distance ρ are correlated only by index of refraction inhomogenieties of size ℓ such that [57]

$$\rho \lesssim \ell \tag{65}$$

Since the dimension ℓ corresponds to a spatial frequency

$$\ell = 2\pi/\kappa,$$

the two dimensional index of refraction spectrum F_n is markedly different from zero only for

$$\rho \lesssim 2\pi/\kappa \tag{66a}$$

or

$$\kappa\rho \lesssim 2\pi. \tag{66b}$$

Within the region of significance of F_n, the argument of the first cos function in Equation (64) is

$$\rho \frac{(L-2z)}{2kL} \kappa^2 \lesssim \frac{1}{2} \lambda(1-2z/L)\kappa \leq \pi \lambda/\ell_o \tag{67}$$

where ℓ_o is the inner scale of turbulence (typically $\ell_o \sim 10^{-3}$-10^{-2}m). Because the wavelength at optical frequencies ($\lambda \sim 10^{-6}$m) is much smaller than the inner scale, we may let

$$\cos\left[\rho \frac{(L-2z)}{2kL} \kappa^2\right] \approx 1. \tag{68}$$

Also within the aforementioned region

$$\frac{\rho}{2L} \bar{\kappa} \cdot [(\bar{r}_1'+\bar{r}_2')-(\bar{r}_i+\bar{r}_j)] \leq \frac{\pi}{L} |(\bar{r}_1'+\bar{r}_2')-(\bar{r}_i+\bar{r}_j)|. \tag{69}$$

If we restrict our attention to lateral distances from the propagation axis much smaller than the range - the paraxial approximation has already required this - we can allow

$$e^{\frac{i\rho}{2L} \bar{\kappa} \cdot [(\bar{r}_1'+\bar{r}_2')-(\bar{r}_i+\bar{r}_j)]} \approx 1 \quad . \tag{70}$$

With the preceding approximations we now obtain for the integrand of Equation (63a),

$$G(\kappa, z+\rho/2, z-\rho/2) = F_n(\kappa_1, \kappa_2, |\rho|) \sin^2\left[\frac{z(L-z)}{2kL} \kappa^2 - \frac{(\kappa\rho)^2}{8kL}\right]$$

$$\times \exp\left\{i\bar{\kappa} \cdot \left[\frac{z}{L} (\bar{r}_1'-\bar{r}_2') + \left(1 - \frac{z}{L}\right)(\bar{r}_i-\bar{r}_j) + \tau\bar{v}\right]\right\} \quad . \tag{71}$$

Finally, the log-amplitude covariance in Equation (60) is given by

$$C_\chi(\bar{r}_i-\bar{r}_j;\bar{r}_1'-\bar{r}_2';\tau) = 2k^2L^2 \iint_{-\infty}^{\infty} d\bar{\kappa} \left\{ \int_0^{1/2} dz \int_0^{2z} d\rho\ G_\chi(\kappa, z+\rho L/2, z-\rho L/2) + \int_{1/2}^{1} dz \int_0^{2(1-z)} d\rho\ G_\chi(\kappa, z+\rho L/2, z-\rho L/2) \right\} , \tag{72-a}$$

where

$$G_\chi = F_n(\kappa_1,\kappa_2,\rho L)\ \sin^2\left[\frac{z(1-z)L}{2k}\kappa^2 - \frac{L(\kappa\rho)^2}{8k}\right]$$

$$\times\ \exp\{i\bar{\kappa}\cdot[z(\bar{r}_1'-\bar{r}_2') + (1-z)(\bar{r}_i-\bar{r}_j) + \tau\bar{v}]\} , \tag{72-b}$$

and we have replaced the z variable of integration by z/L.

It is easily demonstrated, using arguments identical to the preceding, that the phase covariance and phase-log-amplitude cross-covariance are given respectively by

$$C_S(\bar{r}_i-\bar{r}_j;\bar{r}_1'-\bar{r}_2';\tau) = 2k^2L^2 \iint_{-\infty}^{\infty} d\bar{\kappa} \left\{ \int_0^{1/2} dz \int_0^{2z} d\rho\ G_S(\kappa, z+\rho L/2, z-\rho L/2) + \int_{1/2}^{1} dz \int_0^{2(1-z)} d\rho\ G_S(\kappa, z+\rho L/2, z-\rho L/2) \right\} , \tag{73-a}$$

where

$$G_S = F_n(\kappa_1,\kappa_2,\rho L)\ \cos^2\left[\frac{z(1-z)L}{2k}\kappa^2 - \frac{L(\kappa\rho)^2}{8k}\right]$$

$$\times\ \exp\{i\bar{\kappa}\cdot[z(\bar{r}_1'-\bar{r}_2') + (1-z)(\bar{r}_i-\bar{r}_j) + \tau\bar{v}]\} , \tag{73-b}$$

and

$$C_{\chi S}(\bar{r}_i-\bar{r}_j;\bar{r}_1'-\bar{r}_2';\tau) = k^2L^2\iint_{-\infty}^{\infty} d\bar{\kappa}$$

$$\left\{\int_0^{1/2} dz \int_0^{2z} d\rho\ G_{\chi S}(\kappa,z+\rho L/2,z-\rho L/2)\right.$$

$$\left. + \int_{1/2}^{1} dz \int_0^{2(1-z)} d\rho\ G_{\chi S}(\kappa,z+\rho L/2,z-\rho L/2)\right\}, \qquad (74\text{-a})$$

where

$$G_{\chi S} = F_n(\kappa_1,\kappa_2,\rho L)\sin\left[\frac{z(1-z)L}{k}\kappa^2 - \frac{L(\kappa\rho)^2}{4k}\right]$$

$$\times \exp\{i\bar{\kappa}\cdot[z(\bar{r}_1'-\bar{r}_2') + (1-z)(\bar{r}_i-\bar{r}_j) + \tau\bar{v}]\} \quad . \qquad (74\text{-b})$$

The wave structure function defined as

$$D_W(\bar{\rho}_1;\bar{\rho}_2;\tau) = 2[C_\chi(0;0;0) + C_S(0;0;0)$$

$$- C_\chi(\bar{\rho}_1;\bar{\rho}_2;\tau) - C_S(\bar{\rho}_1;\bar{\rho}_2;\tau)] \qquad (75)$$

is from Equations (72) and (73),

$$D_W(\bar{r}_i-\bar{r}_j;\bar{r}_1'-\bar{r}_2';\tau) = 4k^2L^2\iint_{-\infty}^{\infty} d\bar{\kappa}$$

$$\times\left\{\int_0^{1/2} dz \int_0^{2z} d\rho\ G_W(\kappa,z+\rho L/2,z-\rho L/2)\right.$$

$$\left. + \int_{1/2}^{1} dz \int_0^{2(1-z)} d\rho\ G_W(\kappa,z+\rho L/2,z-\rho L/2)\right\}, \qquad (76\text{-a})$$

where

$$G_W = F_n(\kappa_1,\kappa_2,\rho L)$$

$$\times\left\{1 - e^{i\bar{\kappa}\cdot[z(\bar{r}_1'-\bar{r}_2')+(1-z)(\bar{r}_i-\bar{r}_j)+\tau\bar{v}]}\right\} \quad . \qquad (76\text{-b})$$

Equations (72) through (76) constitute the desired results of this section. In deriving these expressions, we have made no assumptions involving the size of the outer scale of turbulence, L_0. The literature abounds with expressions for the log-amplitude and phase covariances and the phase-log-amplitude cross-covariance for zero time lag (τ=0) [58,59] and/or axial receiver plane points ($\bar{r}_1=\bar{r}_2=0$) [60] or transmitter plane points ($\bar{r}_i=\bar{r}_j=0$) [22],[61],[62]. However, all of these derivations make use of the assumption (usually implicit) that the outer scale is much shorter than the range. We shall demonstrate that, for our purposes, no such assumption is necessary.

D. Reduction of Expression for Spectrum

In this section the results of the two preceding sections are combined. Some simplifying assumptions and observations are then made which tremendously reduce the complexity of the expression for the scintillation spectrum.

Our procedure is to first make the weak turbulence approximation (which we quantify) to simplify the expression for the H function of Equation (29-b). Then by employing the expressions derived in the previous section for the required statistical moments and symbolically performing a number of diffraction integrals we arrive at the final expression.

The H function of Equation (29b) is given by

$$H = e^{-(\alpha-\beta)} - e^{-\alpha}, \qquad (77\text{-a})$$

where

$$\alpha = \frac{1}{2}\left[D_W(\bar{r}_1-\bar{r}_2;0;0) + D_W(\bar{r}_3-\bar{r}_4;0;0)\right] \qquad (77\text{-b})$$

and

$$\beta = -\frac{1}{2}\left[D_W(\bar{r}_1-\bar{r}_4;\bar{r}_1'-\bar{r}_2';\tau) + D_W(\bar{r}_2-\bar{r}_3;\bar{r}_1'-\bar{r}_2';\tau)\right.$$

$$-D_W(\bar{r}_1-\bar{r}_3;\bar{r}_1'-\bar{r}_2';\tau) - D_W(\bar{r}_2-\bar{r}_4;\bar{r}_1'-\bar{r}_2';\tau)]$$

$$+ 2[C_\chi(\bar{r}_1-\bar{r}_3;\bar{r}_1'-\bar{r}_2';\tau) + C_\chi(\bar{r}_2-\bar{r}_4;\bar{r}_1'-\bar{r}_2';\tau)$$

$$\left. + iC_{\chi S}(\bar{r}_1-\bar{r}_3;\bar{r}_1'-\bar{r}_2';\tau) - iC_{\chi S}(\bar{r}_2-\bar{r}_4;\bar{r}_1'-\bar{r}_2';\tau)\right] \quad . \qquad (77\text{-}c)$$

Under the weak turbulence approximation we assume that

$$|\alpha|, |\beta| << 1 \qquad (78)$$

so that we need only keep the first two terms of the Taylor's series expansions of $\exp(-\alpha)$ and $\exp(\beta)$;

$$H \approx 1-(\alpha-\beta) - (1-\alpha) = \beta. \qquad (79)$$

In Appendix C we delineate the conditions under which we are justified in making this approximation. For a von Kármán index of refraction spectrum these conditions are

$$\alpha \leq .546\, C_n^2\, k^2 L\left(\rho_{12}^{5/3} + \rho_{34}^{5/3}\right) << 1$$

and

$$\beta \leq .496\, C_n^2\, k^{7/6} L^{11/6} << 1 \quad .$$

where

$$\rho_{ij} \equiv |\bar{r}_i-\bar{r}_j| \quad .$$

From the results of the previous section (Equations (72) through (76)) we see that H (Equation (29)) is given approximately by

$$H = 2k^2L^2 \iint_{-\infty}^{\infty} d\bar{\kappa} \left\{ \int_0^{1/2} dz \int_0^{2z} d\rho + \int_{1/2}^{1} dz \int_0^{2(1-z)} d\rho \right\} F_n(\kappa_1, \kappa_2, \rho L)$$

$$\times \left\{ -1 + e^{i\bar{\kappa}\cdot[z(\bar{r}_1'-\bar{r}_2')+(1-z)(\bar{r}_1-\bar{r}_4)+\tau\bar{v}]} \right.$$

$$-1 + e^{i\bar{\kappa}\cdot[z(\bar{r}_1'-\bar{r}_2')+(1-z)(\bar{r}_2-\bar{r}_3)+\tau\bar{v}]}$$

$$+1 + e^{i\bar{\kappa}\cdot[z(\bar{r}_1'-\bar{r}_2')+(1-z)(\bar{r}_1-\bar{r}_3)+\tau\bar{v}]}$$

$$+1 - e^{i\bar{\kappa}\cdot[z(\bar{r}_1'-\bar{r}_2')+(1-z)(\bar{r}_2-\bar{r}_4)+\tau\bar{v}]} \qquad (80\text{-a})$$

$$+ 2\sin^2(\gamma) \left[e^{i\bar{\kappa}\cdot[z(\bar{r}_1'-\bar{r}_2')+(1-z)(\bar{r}_1-\bar{r}_3)+\tau\bar{v}]} \right.$$

$$\left. + e^{i\bar{\kappa}\cdot[z(\bar{r}_1'-\bar{r}_2')+(1-z)(\bar{r}_2-\bar{r}_4)+\tau\bar{v}]} \right]$$

$$+ i\sin(2\gamma) \left[e^{i\bar{\kappa}\cdot[z(\bar{r}_1'-\bar{r}_2')+(1-z)(\bar{r}_1-\bar{r}_3)+\tau\bar{v}]} \right.$$

$$\left. \left. - e^{i\bar{\kappa}\cdot[z(\bar{r}_1'-\bar{r}_2')+(1-z)(\bar{r}_2-\bar{r}_4)+\tau\bar{v}]} \right] \right\} ,$$

where

$$\gamma = \frac{z(1-z)L}{2k}\kappa^2 - \frac{L(\kappa\rho)^2}{8k} , \qquad (80\text{-b})$$

and we have adopted an operator notation for the ρ and z integrals. By employing the Euler identities for the trigonometric functions it can easily be shown that

$$H = 2k^2L^2 \iint_{-\infty}^{\infty} d\bar{\kappa} \left\{ \int_0^{1/2} dz \int_0^{2z} d\rho + \int_{1/2}^{1} dz \int_0^{2(1-z)} d\rho \right\} F_n(\kappa_1, \kappa_2, \rho L)$$

$$\times e^{i\bar{\kappa}\cdot[z(\bar{r}_1'-\bar{r}_2')+\tau\bar{v}]} \left[e^{i(1-z)\bar{\kappa}\cdot(\bar{r}_1-\bar{r}_4)} + e^{i(1-z)\bar{\kappa}\cdot(\bar{r}_2-\bar{r}_3)} \right.$$

$$\left. - e^{i(1-z)\bar{\kappa}\cdot(\bar{r}_1-\bar{r}_3)-i2\gamma} - e^{i(1-z)\bar{\kappa}\cdot(\bar{r}_2-\bar{r}_4)+i2\gamma} \right] . \qquad (81)$$

This expression can be factored to yield

$$H = 2k^2L^2 \iint_{\infty}^{\infty} d\bar{\kappa} \left\{ \int_0^{1/2} dz \int_0^{2z} d\rho + \int_{1/2}^{1} dz \int_0^{2(1-z)} d\rho \right\} F_n(\kappa_1, \kappa_2, \rho L)$$

$$\times e^{i\bar{\kappa}\cdot[z(\bar{r}_1'-\bar{r}_2')+\tau\bar{v}]}$$

$$\times \left[e^{i(1-z)\bar{\kappa}\cdot\bar{r}_1 - i\gamma} - e^{i(1-z)\bar{\kappa}\cdot\bar{r}_2 + i\gamma} \right]$$

$$\times \left[e^{-i(1-z)\bar{\kappa}\cdot\bar{r}_4 + i\gamma} - e^{-i(1-z)\bar{\kappa}\cdot\bar{r}_3 - i\gamma} \right] \quad . \tag{82}$$

With Equation (82) plus the expression for the spectrum in terms of the H function (Equation (29-a)) we have

$$S_p(\omega) = 2k^2L^2 \int_{-\infty}^{\infty} d\tau\, e^{-i\omega\tau} \int d\bar{r}_1' W(\bar{r}_1') \int d\bar{r}_2' W(\bar{r}_2')$$

$$\times \iint_{-\infty}^{\infty} d\bar{\kappa} \left\{ \int_0^{1/2} dz \int_0^{2z} + \int_{1/2}^{1} dz \int_0^{2(1-z)} d\rho \right\} F_n(\kappa_1, \kappa_2, \rho L)$$

$$\times e^{i\bar{\kappa}\cdot[z(\bar{r}_1'-\bar{r}_2')+\tau\bar{v}]}$$

$$\times \left\{ \left(\frac{k}{2\pi L}\right)^2 \int_{-\infty}^{\infty} d\bar{r}_1 \int_{-\infty}^{\infty} d\bar{r}_2\, E(\bar{r}_1)E^*(\bar{r}_2)\, e^{\frac{ik}{2L}\left[|\bar{r}_1-\bar{r}_1'|^2 - |\bar{r}_2-\bar{r}_1'|^2\right]} \right.$$

$$\left. \times \left[e^{i(1-z)\bar{\kappa}\cdot\bar{r}_1 - i\gamma} - e^{i(1-z)\bar{\kappa}\cdot\bar{r}_2 + i\gamma} \right] \right\}$$

$$\times \left\{ \left(\frac{k}{2\pi L}\right)^2 \int_{-\infty}^{\infty} d\bar{r}_3 \int_{-\infty}^{\infty} d\bar{r}_4\, E(\bar{r}_3)E^*(\bar{r}_4)\, e^{\frac{ik}{2L}\left[|\bar{r}_3-\bar{r}_2'|^2 - |\bar{r}_4-\bar{r}_2'|^2\right]} \right.$$

$$\left. \times \left[e^{-i(1-z)\bar{\kappa}\cdot\bar{r}_4 + i\gamma} - e^{-i(1-z)\bar{\kappa}\cdot\bar{r}_3 - i\gamma} \right] \right\} \quad . \tag{83}$$

If we look only at the $\bar{r}_1, \bar{r}_2$ integrals we observe that they can be written in the form

$$\left(\frac{k}{2\pi L}\right)^2 e^{-i\gamma} \int d\bar{r}_1 E(\bar{r}_1)\, e^{\frac{ik}{2L}\left\{r_1^2 - 2\bar{r}_1 \cdot \left[\bar{r}_1' - \frac{L(1-z)}{k}\bar{\kappa}\right]\right\}}$$

$$\times \int d\bar{r}_2 E^*(\bar{r}_2)\, e^{\frac{-ik}{2L}(r_2^2 - 2\bar{r}_2 \cdot \bar{r}_1')}$$

$$-\left(\frac{k}{2\pi L}\right)^2 e^{i\gamma} \int d\bar{r}_1 E(\bar{r}_1)\, e^{\frac{ik}{2L}(r_1^2 - 2\bar{r}_1 \cdot \bar{r}_1')}$$

$$\times \int d\bar{r}_2 E^*(\bar{r}_2)\, e^{\frac{-ik}{2L}\left\{r_2^2 - 2\bar{r}_2 \cdot \left[\bar{r}_1' + \frac{L(1-z)}{k}\bar{\kappa}\right]\right\}} \quad . \tag{84}$$

Now recall the formula for the Fresnel diffraction integral;

$$E(\bar{r}) = \frac{-ik}{2\pi L} e^{ikL} \int d\bar{r}_s E(\bar{r}_s)\, e^{\frac{ik}{2L}(r_s^2 - 2\bar{r}_s \cdot \bar{r} + r^2)} \quad . \tag{85}$$

Comparing Equations (84) and (85) we observe that the $\bar{r}_1$ and $\bar{r}_2$ integrations can be performed symbolically to give

$$e^{-i\gamma}\left[e^{\frac{-ik}{2L}\left|\bar{r}_1' - \frac{L(1-z)}{k}\bar{\kappa}\right|^2} E\left(\bar{r}_1' - \frac{L(1-z)}{k}\bar{\kappa}\right)\right]$$

$$\times \left[e^{\frac{ik}{2L}r_1'^2} E^*(\bar{r}_1')\right]$$

$$-e^{i\gamma}\left[e^{\frac{-ik}{2L}r_1'^2} E(\bar{r}_1')\right]\left[e^{\frac{ik}{2L}\left|\bar{r}_1' + \frac{L(1-z)}{k}\bar{\kappa}\right|^2}\right.$$

$$\left.\times E^*\left(\bar{r}_1' + \frac{L(1-z)}{k}\bar{\kappa}\right)\right] \quad , \tag{86}$$

where it is to be understood that the fields are the free-space receiver plane fields. It may easily be verified that the r_3 and r_4 integrations yield the conjugate of this expression with the variable $\bar{r}_1'$ replaced by $\bar{r}_2'$. With these simplifications Equation (83) becomes

$$S_p(\omega) = 2k^2L^2 \left\{ \int_0^{1/2} dz \int_0^{2z} d\rho + \int_{1/2}^{1} dz \int_0^{2(1-z)} d\rho \right\} \iint_{-\infty}^{\infty} d\bar{\kappa}$$

$$\times F_n(\kappa_1, \kappa_2, \rho L) \int_{-\infty}^{\infty} d\tau \, e^{-i\tau(\omega - \bar{\kappa}\cdot\bar{v})}$$

$$\times \left| \int d\bar{r}_1' W(\bar{r}_1') e^{iz\bar{\kappa}\cdot\bar{r}_1'} \left[e^{-i\gamma + i(1-z)\bar{\kappa}\cdot\bar{r}_1'} e^{\frac{-i(1-z)^2 L\kappa^2}{2k}} \right.\right.$$

$$\times E\left(\bar{r}_1' - \frac{L(1-z)}{k}\bar{\kappa}\right) E^*(\bar{r}_1')$$

$$\left.\left. - e^{i\gamma + i(1-z)\bar{\kappa}\cdot\bar{r}_1'} e^{\frac{i(1-z)^2 L\kappa^2}{2k}} E(\bar{r}_1') E^*\left(\bar{r}_1' + \frac{L(1-z)}{k}\bar{\kappa}\right) \right] \right|^2 \qquad (87)$$

or

$$S_p(\omega) = 2k^2L^2 \left\{ \int_0^{1/2} dz \int_0^{2z} d\rho + \int_{1/2}^{1} dz \int_0^{2(1-z)} d\rho \right\}$$

$$\times \iint_{-\infty}^{\infty} d\bar{\kappa} \, F_n(\kappa_1, \kappa_2, \rho L) \, [2\pi\delta(\omega - \bar{\kappa}\cdot\bar{v})]$$

$$\times \left| H(z, \rho, \bar{\kappa}, W) - H^*(z, \rho, -\bar{\kappa}, W) \right|^2 , \qquad (88\text{-a})$$

where

$$H(z,\rho,\bar{\kappa},w) =$$

$$e^{\frac{-i(1-z-\rho^2/4)L\kappa^2}{2k}} \int d\bar{r} W(\bar{r}) e^{i\bar{\kappa}\cdot\bar{r}} \; E\left(\bar{r} - \frac{L(1-z)\bar{\kappa}}{k}\right) \; E^*(\bar{r}) \quad . \tag{88-b}$$

In Appendix D we demonstrate that due to the scintillation spectrum's extreme insensitivity to low spatial frequency index of refraction inhomogeneities, very little error is incurred by dropping the ρ dependence of the H function and extending the limits on the ρ integration in Equation (88-a) to infinity to yield

$$S_p(\omega) = 4\pi^2 k^2 L \int_0^1 dz \iint_{-\infty}^{\infty} d\bar{\kappa} \; \Phi_n(\kappa_1,\kappa_2,0)\delta(\omega-\bar{\kappa}\cdot\bar{v})$$

$$x \; |H(z,\bar{\kappa},w) - H^*(z,-\bar{\kappa},w)|^2 \quad , \tag{89-a}$$

where

$$H(z,\bar{\kappa},w) =$$

$$e^{\frac{-i(1-z)L\kappa^2}{2k}} \int d\bar{r} W(\bar{r}) e^{i\bar{\kappa}\cdot\bar{r}} \; E\left(\bar{r} - \frac{L(1-z)\bar{\kappa}}{k}\right) \; E^*(\bar{r}) \; , \tag{89-b}$$

and we have made use of the relationship between the two and three dimensional index of refraction spectra,

$$\int_{-\infty}^{\infty} d\rho \; F_n(\kappa_1,\kappa_2,\rho L) = \frac{\pi}{L} \Phi_n(\kappa_1,\kappa_2,0) \quad . \tag{90}$$

Finally without loss of generality we can assume the wind to be blowing in the x direction,

$$\bar{v} = \hat{x} \; v \quad , \tag{91}$$

so that performing the κ_1 integration in Equation (89) yields

$$S_p(\omega) = (4\pi^2 k^2 L/v) \int_0^1 dz \int_{-\infty}^{\infty} d\kappa \, \Phi_n\left(\frac{\omega}{v}, \kappa, 0\right)$$

$$\times \left| H(z, \bar{\kappa}', w) - H^*(z, -\bar{\kappa}', w) \right|^2 \quad , \tag{92}$$

where

$$\bar{\kappa}' = \left(\frac{\omega}{v}, \kappa\right) \quad ,$$

and we have dropped the subscript on the remaining spatial frequency variable of integration.

Equation (92) is the expressed objective of this chapter. The utility of this formula lies in the fact that it expresses the temporal scintillation spectrum for an arbitrary field and that the expression for the source field enters the formula only in terms of the free-space receiver plane fields. This latter fact plays an important role in the chapters to follow.

In addition to the mathematical simplicity of Equation (92), its various components are easily interpretable in terms of a physical model of the turbulent atmosphere. The H function in particular displays some very interesting behavior which offers insight into the propagation problem. Equation (92) is explored and discussed more fully in the next section.

E. Physical Model

Now we wish to interpret our expression for the temporal scintillation spectrum in the context of a physical model of the atmospheric turbulence. In this model the index of refraction inhomogeneities are envisioned as a series of phase gratings [63] of various orientations and spatial frequencies. The components of Equation (92) will then be shown to describe the behavior of the fields in terms of the properties of these phase gratings.

We wish to interpret Equation (92) of the previous section:

$$S_p(\omega) = (4\pi^2 k^2/v) \int_0^L dz \int_{-\infty}^{\infty} d\kappa \Phi_n\left(\frac{\omega}{v}, \kappa, 0\right)$$

$$\times \left| H(z, \bar{\kappa}', w) - H^*(z, -\bar{\kappa}', w) \right|^2 \tag{93}$$

where

$$H(z,\bar{\kappa}',w) =$$

$$e^{\frac{-i(L-z)\kappa'^2}{2k}} \int d\bar{r} W(\bar{r}) e^{i\bar{\kappa}'\cdot\bar{r}} E\left(\bar{r} - \frac{(L-z)\bar{\kappa}'}{k}\right) E^*(\bar{r}) \quad ,$$

$$\bar{\kappa}' = \left(\frac{\omega}{v}, \kappa\right) \quad , \tag{94}$$

and we have changed the z variable of integration to the product L·z.

As preliminary background to this discussion we introduce the concept of a phase grating as sketched in Figure 7. Illustrated in this figure is an arbitrary wavefront impinging on a phase grating. The phase grating is merely a diffraction grating whose transmission function is periodic in phase rather than amplitude. To the right of this phase grating (which can be thought of as a periodic variation in index of refraction along a plane perpendicular to the direction of propagation) we have depicted only the zeroth order and plus and minus one order diffracted wavefronts. It is easily shown [64] that the angles of the axes of the two diffracted wavefronts with respect to the axis of the undiffracted wavefront are given by

$$\alpha = \lambda/\ell \quad , \tag{95}$$

where λ is the wavelength of the field and ℓ is the period of the grating.

Now consider the situation shown in Figure 8. Here we have a phase grating of period

$$2\pi/\kappa \tag{96}$$

and orientation

$$\bar{\kappa}/|\bar{\kappa}|$$

located in the plane z.

An axial ray striking this phase grating from the left will produce zeroth and plus and minus one order diffracted rays to the right. From the previous discussion the diffraction angles are seen to be

$$\pm \frac{\lambda}{\ell} = \pm \frac{\lambda\kappa}{2\pi} = \pm \frac{\kappa}{k} \tag{97}$$

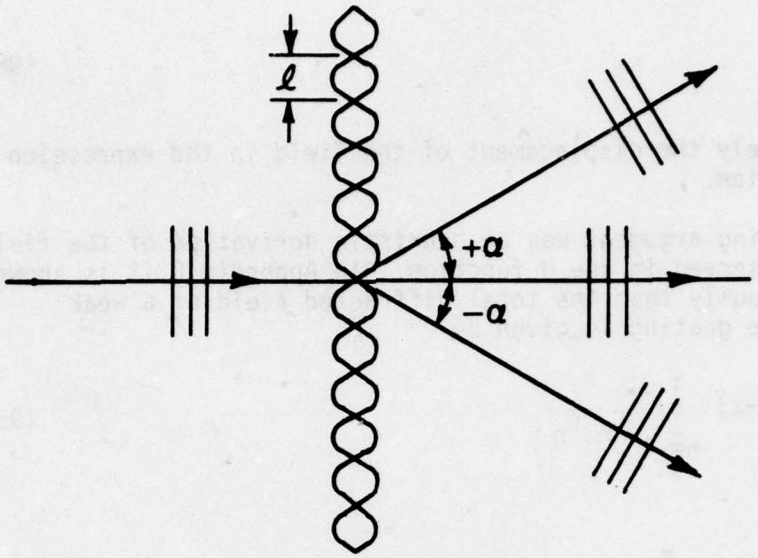

Figure 7--First order diffraction angles of a simple phase grating.

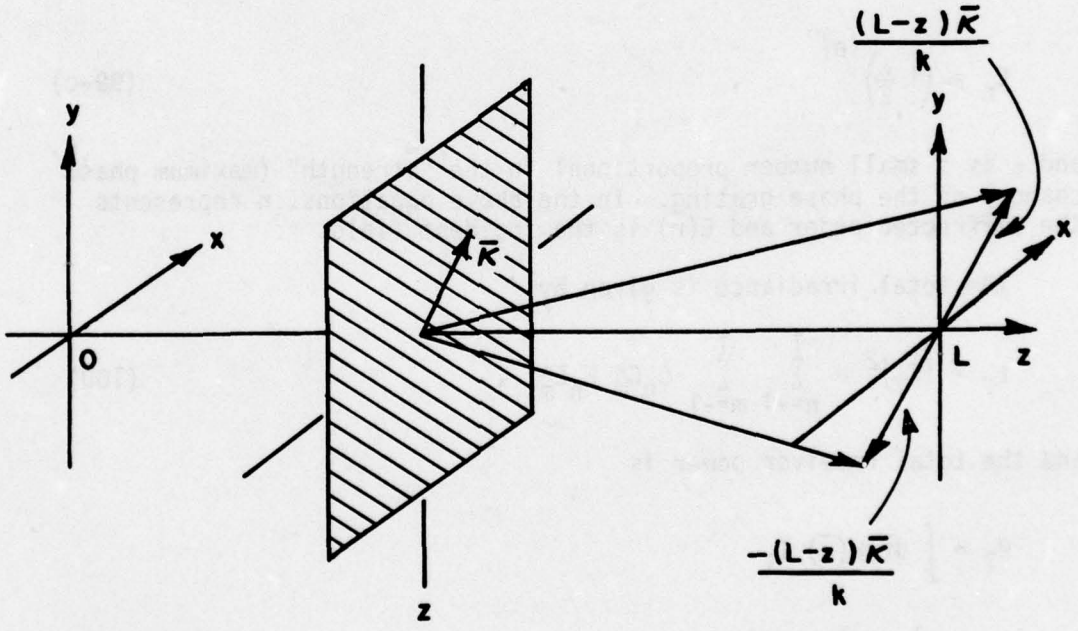

Figure 8--Lateral field displacements due to a phase grating.

and in the plane z=L the displacements from the propagation axis are

$$\pm \frac{(L-z)\kappa}{k} \quad . \tag{98}$$

But this is merely the displacement of the field in the expression for the *H* function.

The foregoing argument was an heuristic derivation of the field translations observed in the *H* function. In Appendix D it is shown much more rigorously that the total diffracted field of a weak sinusoidal phase grating is given by

$$E_T = e^{ik(L-z)} \sum_{n=-1}^{1} C_n E_n \tag{99-a}$$

where

$$E_n = e^{in\bar{\kappa}\cdot\bar{r}} e^{\frac{-in^2(L-z)}{2k}\kappa^2} E\left(\bar{r} - \frac{n(L-z)}{k}\bar{\kappa}\right) \quad , \tag{99-b}$$

$$C_n = \left(i\,\frac{\varepsilon}{2}\right)^{|n|} \quad , \tag{99-c}$$

and ε is a small number proportional to the "strength" (maximum phase change) of the phase grating. In the above equations, n represents the diffracted order and $E(\bar{r})$ is the incident field.

The total irradiance is given by

$$I_T = |E_T|^2 = \sum_{n=-1}^{1} \sum_{m=-1}^{1} C_n C_m^* E_n E_m^* \quad , \tag{100}$$

and the total receiver power is

$$P_T = \int d\bar{r}\, W(\bar{r})\, I_T$$

$$= \sum_{n=-1}^{1} \sum_{m=-1}^{1} C_n C_m^* \int d\bar{r}\, W(\bar{r})\, E_n E_m^* \quad . \tag{101}$$

We retain only the terms in ε^0 and ε^1 (because ε is small) so that Equation (101) gives

$$P_T = \int d\bar{r}\, W(\bar{r})\, E(\bar{r})^2$$

$$+ C_{-1}C_0^* \, e^{\frac{-i(L-z)}{2k}\kappa^2} \int d\bar{r}\, W(\bar{r})\, e^{-i\bar{\kappa}\cdot\bar{r}}\, E\left(\bar{r} + \frac{(L-z)}{k}\bar{\kappa}\right) E^*(\bar{r})$$

$$+ C_{-1}^* C_0 \, e^{\frac{i(L-z)}{2k}\kappa^2} \int d\bar{r}\, W(\bar{r})\, e^{i\bar{\kappa}\cdot\bar{r}}\, E^*\left(\bar{r} + \frac{(L-z)}{k}\bar{\kappa}\right) E(\bar{r})$$

$$+ C_0 C_1^* \, e^{\frac{i(L-z)}{2k}\kappa^2} \int d\bar{r}\, W(\bar{r})\, e^{-i\bar{\kappa}\cdot\bar{r}}\, E^*\left(\bar{r} - \frac{(L-z)}{k}\bar{\kappa}\right) E(\bar{r})$$

$$+ C_0^* C_1 \, e^{\frac{-i(L-z)}{2k}\kappa^2} \int d\bar{r}\, W(\bar{r})\, e^{i\bar{\kappa}\cdot r}\, E\left(\bar{r} - \frac{(L-z)}{k}\bar{\kappa}\right) E^*(\bar{r}) \,. \tag{102}$$

Each of these integrals (with the exception of the first) is merely the *H* function or its complex conjugate. The *H* function is therefore seen to represent the interference between the zeroth order field and the plus or minus one order field.

With the utility of the phase grating model of the turbulence field thus demonstrated, we shall now demonstrate that the general scintillation spectrum formula (Equation (93)) can be derived using this model plus a few previously adopted definitions.

Essentially what we have implied in the preceding development is that the index of refraction field can be expanded in an orthogonal set of (moving) phase screens, the transmission functions of which are given by $\exp(i\varepsilon \cos\bar{\kappa}\cdot\bar{r})$. The problem however, is that the set of cosine functions in itself is not complete [65]. Since the functions sine plus cosine do compose a complete orthogonal set [66], we now wish to apply the preceding technique to the situation in which the "phase" grating transmission function is given by

$$\exp\left(i\varepsilon\, e^{i\bar{\kappa}\cdot\bar{r}}\right) \quad , \tag{103}$$

where ε is a small (generally complex) number. From Appendix E, the resulting receiver plane field is seen to be

$$E_T(z,\bar{\kappa},t) = e^{ik(L-z)} \sum_{n=0}^{1} C_n \, e^{in\bar{\kappa}\cdot\bar{r}} \, e^{\frac{-in^2(L-z)\kappa^2}{2k}} E\left(\bar{r} - \frac{n(L-z)}{k}\bar{\kappa}\right) \quad , \tag{104-a}$$

where

$$C_0 = 1 \quad , \tag{104-b}$$

$$C_1 = i\varepsilon(z,\bar{\kappa},t) \quad , \tag{104-c}$$

and we have indicated explicitly the dependence of the field upon the path variable, z, the spatial frequency, $\bar{\kappa}$, and the time, t. In the strength function, ε, the z dependence denotes the location of the phase grating, the $\bar{\kappa}$ dependence indicates the strength to be a function of spatial frequency, and the time dependence reflects the fact that the phase grating is being blown by the wind across the propagation path.

Following arguments and definitions employed earlier in this section, Equations (94), (102), and (104) give for the receiver plane power

$$P_T(z,\bar{\kappa},t) = P_{DC} - i\varepsilon^*(z,\bar{\kappa},t)H^*(z,\bar{\kappa},w) + i\varepsilon(z,\bar{\kappa},t)H(z,\bar{\kappa},w) \, , \tag{105-a}$$

where

$$P_{DC} \equiv |C_0|^2 \int d\bar{r} \, W(\bar{r})|E(\bar{r})|^2 \tag{105-b}$$

As in Section B of this chapter, we define the scintillation spectrum as the Fourier transform of the power covariance

$$S_p(\omega) = \int_{-\infty}^{\infty} d\tau \, e^{-i\omega\tau} \, C_p(\tau) \quad , \tag{106}$$

where the power covariance is given by

$$C_p(\tau) = \int_0^L dz_1 \int_0^L dz_2 \int d\bar{\kappa} \int d\bar{\kappa}' \, \langle [P_T(z_1,\bar{\kappa},t)-P_{DC}] \times [P_T(z_2,\bar{\kappa}',t+\tau)-P_{DC}]^* \rangle \, . \qquad (107)$$

In this equation we have "summed" the power (density) of Equation (105) over all spatial frequencies and over all phase grating locations between zero and L.

With Equations (105) and (107) the power covariance becomes

$$\begin{aligned} C_p(\tau) = & \int_0^L dz_1 \int_0^L dz_2 \int d\bar{\kappa} \int d\bar{\kappa}' \\ & \times [\langle \varepsilon(z_1,\bar{\kappa},t)\varepsilon^*(z_2,\bar{\kappa}',t+\tau)\rangle H(z_1,\bar{\kappa},w)H^*(z_2,\bar{\kappa}',w) \\ & - \langle \varepsilon(z_1,\bar{\kappa},t)\,(z_2,\bar{\kappa}',t+\tau)\rangle H(z_1,\bar{\kappa},w)H(z_2,\bar{\kappa}',w) \\ & - \langle \varepsilon^*(z_1,\bar{\kappa},t)\varepsilon^*(z_2,\bar{\kappa}',t+\tau)\rangle H^*(z_1,\bar{\kappa},w)H^*(z_2,\bar{\kappa}',w) \\ & + \langle \varepsilon^*(z_1,\bar{\kappa},t)\varepsilon(z_2,\bar{\kappa}',t+\tau)\rangle H^*(z_1,\bar{\kappa},w)H(z_2,\bar{\kappa}',w)] \, . \end{aligned} \qquad (108)$$

We now claim that the correlation function of the phase grating strength is given by [67] (see Equation (58))

$$\langle \varepsilon(z_1,\bar{\kappa},t)\varepsilon^*(z_2,\bar{\kappa}',t+\tau)\rangle = k^2 \, e^{i\tau\bar{\kappa}'\cdot\bar{v}} \, \delta(|\bar{\kappa}-\bar{\kappa}'|) \times F_n(\kappa_1,\kappa_2,|z_1-z_2|) \, , \qquad (109)$$

where F_n is the two dimensional spatial spectrum of the index of refraction field. In this equation the exponential phase term reflects the frozen turbulence approximation and the statistical orthogonality (with respect to spatial frequency) is indicated by the delta function. This orthogonality states that, on the average, only phase grating pairs with equal spatial frequencies and identical orientations contribute to the fluctuations in the received power. Finally, the square of the wavenumber, k, yields the correct units.

We also claim that, for the term in Equation (108) in which neither of the strength functions is conjugated, the correlation function is given by [68]

$$\langle \varepsilon(z_1,\bar{\kappa},t)\varepsilon(z_2,\bar{\kappa}',t+\tau)\rangle = k^2\, e^{-i\tau\bar{\kappa}'\cdot\bar{v}}\ \delta(|\bar{\kappa}+\bar{\kappa}'|) \times F_n(\kappa_1,\kappa_2,|z_1-z_2|) \quad . \tag{110}$$

Combining Equations (108), (109), and (110) and performing the $\bar{\kappa}'$ integrations yields for the power covariance

$$C_p(\tau) = k^2 \int_0^L dz_1 \int_0^L dz_2 \int d\bar{\kappa}\, F_n(\kappa_1,\kappa_2,|z_1-z_2|) \times \left\{ e^{i\tau\bar{\kappa}\cdot\bar{v}} \left[H(z_1,\bar{\kappa},w)H^*(z_2,\bar{\kappa},w)-H(z_1,\bar{\kappa},w)H(z_2,\bar{\kappa},w)\right] - e^{-i\tau\bar{\kappa}\cdot\bar{v}} \left[H^*(z_1,\bar{\kappa},w)H^*(z_2,-\bar{\kappa},w)-H^*(z_1,\bar{\kappa},w)H(z_2,\bar{\kappa},w)\right] \right\} . \tag{111}$$

Assuming isotropic turbulence and making use of the change of variable

$$\bar{\kappa} \leftarrow -\bar{\kappa}$$

gives

$$C_p(\tau) = k^2 \int_0^L dz_1 \int_0^L dz_2 \int d\bar{\kappa}\, F_n(\kappa_1,\kappa_2,|z_1-z_2|) e^{i\tau\bar{\kappa}\cdot\bar{v}} \times \left[H(z_1,\bar{\kappa},w)H^*(z_2,\bar{\kappa},w)-H(z_1,\bar{\kappa},w)H(z_2,-\bar{\kappa},w) - H^*(z_1,-\bar{\kappa},w)H^*(z_2,-\bar{\kappa},w)+H^*(z_1,-\bar{\kappa},w)H(z_2,-\bar{\kappa},w)\right] \quad . \tag{112}$$

Switching to sum and difference coordinates on the range variables

$$z = (z_1+z_2)/2 \quad , \qquad \rho = z_1-z_2$$

(which correspond respectively to the mean position and separation of the phase grating pairs) and using the argument that the index of refraction spectrum, F_n, is very small for

$$\kappa\rho \gtrsim 2\pi$$

(see the discussion in Appendix D) we obtain finally

$$C_p(\tau) = 2\pi k^2 \int_0^L dz \int d\bar{\kappa}\, e^{i\tau\bar{\kappa}\cdot\bar{v}}\, \Phi_n(\kappa_1,\kappa_2,0)$$

$$\times\, |H(z,\bar{\kappa},w)-H^*(z,-\bar{\kappa},w)|^2 \quad . \tag{113}$$

The scintillation spectrum is then given by

$$S_p(\omega) = (4\pi^2k^2/v) \int_0^L dz \int_{-\infty}^{\infty} d\kappa\, \Phi_n\left(\frac{\omega}{v},\kappa,0\right)$$

$$\times\, |H(z,\bar{\kappa}',w)-H^*(z,-\bar{\kappa}',w)|^2 \quad , \tag{114}$$

where

$$\bar{\kappa}' = (\omega/v,\kappa) \ ,$$

and we have assumed the wind to be blowing in the x-direction. Comparison of Equations (93) and (114) shows them to be identical. It is indeed satisfying that with a few reasonable assumptions we have duplicated the results of the much more rigorous development of the preceding sections.

The purpose of this section has been to give a more physical picture of the mechanisms giving rise to temporal scintillation. Salient features of the development contained herein were the expansion of the index of refraction field in a complete orthogonal set of phase screens and the symbolic performance of the diffraction integral to obtain the fields diffracted by the phase screens. By using previously adopted definitions for irradiance, power, and the temporal scintillation spectrum, and making some physically justifiable assumptions, the results of the preceding sections were duplicated. The H function in particular was seen to have an interesting interpretation in the context of a phase grating model of the atmosphere. It represents the power associated with the interaction between the zeroth and plus or minus one order diffracted fields of the phase grating.

This concludes the discussion of the formula for the temporal scintillation spectrum.

F. Summary

In this chapter we have performed the bulk of the mathematical development which is to be applied in subsequent chapters. The objective was to derive a general expression for the temporal scintillation spectrum of an arbitrary source field and an extended receiver. This was accomplished in several stages. Use was made of the Extended Huygens-Fresnel integral to derive a formula for the spectrum in terms of the second order statistical moments of spherical waves. Expressions for these statistical moments (within the weak turbulence regime) were derived by the method of smooth perturbations and applied to this formula. Various simplifications and manipulations finally resulted in an extremely compact yet versatile expression which was then interpreted using a phase grating model of the turbulent atmosphere.

Section B of this chapter was devoted to developing a general expression for the temporal scintillation spectrum of an arbitrary field source. An extension of the familiar Huygens-Fresnel diffraction integral was employed to express the receiver plane field of an arbitrary source in terms of the complex phase perturbations to a spherical wave. The power received at the detector was defined as the surface integral of the irradiance (square modulus) of this field, and the temporal scintillation spectrum as the Fourier transform of the covariance of this power. The resulting formula required knowledge of the covariance of irradiance of spherical waves. Under the assumption that the spherical wave complex phase perturbations were normally distributed, this fourth moment of the field was expressed as a series of second order statistical moments. One interesting aspect of the general result of this section was that the expression for the spectrum retained terms proportional to the cross-covariance of phase and log-amplitude.

Expressions for the required log-amplitude covariance, phase-log-amplitude cross-covariances, and wave structure functions were derived in Section C via the method of smooth perturbations. These derivations relied upon the assumption of local homogeneity of the index of refraction statistics, and the paraxial ray approximation. Temporal behavior of the statistical moments was deduced by making use of the frozen turbulence hypothesis. The results, of this section showed the desired statistical moments to be simultaneously homogeneous in temporal separations and spatial separations within both the transmitter and receiver planes.

The results of Sections B and C were combined in Section D. By using the weak turbulence approximation and making some simple algebraic manipulations, the resulting formula was expressed in terms of a series of diffraction integrals which were performed symbolically to yield the final expression for the spectrum. This formula for the temporal scintillation spectrum of an arbitrary source, was in terms

of integrations over the receiver plane fields, a single spatial frequency variable, and a propagation path variable.

In Section E a model of the atmospheric turbulence was developed in terms of weak phase gratings. Using diffraction theory and some physically justifiable assumptions the results of the much more rigorous development of the preceding sections were duplicated, and the component parts of the formula for the scintillation spectrum were given physical interpretations.

The following chapters are concerned with the application of the results of this chapter to problems of contemporary interest.

CHAPTER III

ANALYSIS OF A CLEAN GAUSSIAN BEAM

A. Introduction

This chapter is concerned with application of the results of Chapter II to calculation of the temporal spectrum of a gaussian beam with an off-axis point detector. The choice of this particular source description is appropriate because the output of most lasers is closely approximated by a gaussian beam. Further, the assumption of an off-axis detector is reasonable if for instance the laser beam is being steered by a servo system. Nominally a tracker would steer the laser beam so that it is centered upon the detector. Since however this may not always be the case [69], the development herein is of obvious importance.

Within this chapter an evaluation of the temporal scintillation spectrum of a gaussian beam in the presence of weak turbulence and with an off-axis detector is presented. Analytic expressions are developed for the asymptotes of the spectrum with axial as well as off-axis point detectors. The orientation of the off-axis detector with respect to wind direction is shown to have important effects within the low frequency portion of the spectrum. For a typical laser beam, computer analyses of the spectrum are provided. Plots are presented of the differential path contributions as well as the spectra for various detector locations. Finally we discuss the extension of the theory presented herein to the treatment of finite receiver apertures and a finite inner scale.

As a result of the analysis it is shown that for an off-axis detector, the low-frequency behavior of the gaussian beam spectrum departs markedly from that of plane and spherical waves. In addition, the differential path contribution for an off-axis detector is peaked toward the transmitter (as it is for a plane wave) even though the receiver plane is well within the far field of the laser beam.

In section B of this chapter use is made of the general formula, derived in Chapter II, in developing an expression for the temporal scintillation spectrum of a gaussian beam with an arbitrarily placed point detector.

An asymptotic evaluation of the gaussian beam scintillation spectrum is given in section C. Analytic expressions for the asymptotic high and low frequency behavior are provided.

Section D contains numerically calculated spectra for several typical beam-detector orientations. In this section we also present plots of the computer-calculated differential path contributions for some typical cases.

Two additional topics, the effect of finite receiver apertures and non-zero inner scales, are discussed in section E.

Section F summarizes the chapter.

B. Development of Expression for Gaussian Beam Spectrum

We now wish to apply the results of Chapter II to derive an expression for the scintillation spectrum of a gaussian beam.

Throughout this section and the remainder of this work we shall assume that a laser beam field is typified by a spherical phase front and a gaussian field amplitude profile [39]

$$E(x,y,z) = E_0(z)\, e^{\left\{\frac{ik(x^2+y^2)}{2R(z)} - \frac{(x^2+y^2)}{w^2(z)}\right\}},$$

where $R(z)$ and $w(z)$ are real functions describing respectively the radius of curvature and the e^{-1} amplitude (or spotsize) of the beam. To simplify notation however we will write the field in terms of a complex radius of curvature

$$E(x,y,z) = E_0(z)\, e^{\frac{-k(x^2+y^2)}{2F(z)}} .$$

Specifically we assume that the gaussian beam field within the receiver plane is

$$E(\bar{r}) = e^{ikL(1+z_0/L)} \frac{\sqrt{kN/2L}}{1+iN(1+z_0/L)}\, e^{\frac{-kN/2L\ r^2}{1+iN(1+z_0/L)}}, \qquad (115a)$$

where the beam waist is located at $z=-z_0$ and N is a Fresnel number defined as

$$N = \frac{\lambda L}{\pi w_0^2}, \qquad (115b)$$

where w_o is the beam waist spotsize. For this field the receiver plane radius of curvature and beam spotsize are respectively

$$R(L) = L\left[\frac{1+N^2(1+z_o/L)}{N^2(1+z_o/L)}\right] \tag{115c}$$

and

$$W(L) = w_o\sqrt{1+N^2(1+z_o/L)^2}. \tag{115d}$$

For a point detector located at $\bar{r}_o$;

$$w(\bar{r}) = \delta(|\bar{r}-\bar{r}_o|) \tag{116}$$

the H function of Chapter II becomes

$$H(z,\bar{\kappa}',w) = \tag{117}$$

$$e^{\frac{-i(1-z)L\kappa'^2}{2k}}\; e^{i\bar{\kappa}'\cdot\bar{r}_o}\,\mathring{E}\left(\bar{r}_o - \frac{L(1-z)}{k}\,\bar{\kappa}'\right)E^*(\bar{r}_o)\ .$$

Use of Equation (115a) for the receiver plane field gives

$$H = e^{\frac{-i(1-z)L\kappa'^2}{2k}}\; e^{i\bar{\kappa}'\cdot\bar{r}_o}\left[\frac{kN/2L}{1+N^2(1+\varepsilon)^2}\right]\; e^{\frac{-(kN/L)r_o^2}{1+N^2(1+\varepsilon)^2}}$$

$$\times\, e^{\frac{-kN/2L}{1+iN(1+\varepsilon)}\left\{\frac{-2L(1-z)}{k}\,\bar{r}_o'\cdot\bar{\kappa}' + \left[\frac{L(1-z)}{k}\right]^2\kappa'^2\right\}}, \tag{118a}$$

where we have defined

$$\varepsilon = z_o/L. \tag{118b}$$

with some straightforward algebra we see that

$$|H(z,\bar{\kappa}',w) - H^*(z,-\bar{\kappa}',w)|^2 =$$

$$\left[\frac{kN/2L}{1+N^2(1+\varepsilon)^2}\right]^2 e^{\frac{-(2kN/L)r_o^2}{1+N^2(1+\varepsilon)^2}} e^{\frac{-N(1-z)^2L/k}{1+N^2(1+\varepsilon)^2}\kappa'^2} \tag{119}$$

$$\times\left\{2\cosh\left[\frac{2N(1-z)}{1+N^2(1+\varepsilon)^2}\,\bar{r}_o\cdot\bar{\kappa}'\right]\right.$$

$$\left.-2\cos\left\{\frac{(1-z)L}{k}\kappa'^2\left[\frac{1+N^2(1+\varepsilon)(z+\varepsilon)}{1+N^2(1+\varepsilon)^2}\right]\right\}\right\} .$$

By employing Equation (92) of Chapter II and the double angle formulae for the trigonometric and hyperbolic functions we then obtain the expression for the gaussian beam scintillation spectrum

$$S_p(\omega) = (16\pi^2k^2L/v)\left[\frac{kN/2L}{1+N^2(1+\varepsilon)^2}\right]^2 e^{\frac{-(2kN/L)r_o^2}{1+N^2(1+\varepsilon)^2}}$$

$$\times\int_0^1 dz\int_{-\infty}^{\infty} d\kappa\Phi_n\left(\frac{\omega}{v},\kappa,0\right) e^{\frac{-N(1-z)^2L/k}{1+N^2(1+\varepsilon)^2}\kappa'^2} \tag{120}$$

$$\times\left\{\sinh^2\left[\frac{N(1-z)}{1+N^2(1+\varepsilon)^2}\,\bar{r}_o\cdot\bar{\kappa}'\right]\right.$$

$$\left.+\sin^2\left\{\frac{(1-z)L}{2k}\kappa'^2\left[\frac{1+N^2(1+\varepsilon)(z+\varepsilon)}{1+N^2(1+\varepsilon)^2}\right]\right\}\right\} ,$$

where $\bar{\kappa}' \equiv \left(\frac{\omega}{v},\kappa\right)$.

For the special case of an on-axis point detector ($\bar{r}_o=0$), Equation (120) reduces to

$$S_p(\omega) = (32\pi^2k^2L/v)\left[\frac{kN/2L}{1+N^2(1+\varepsilon)^2}\right]^2 \int_0^1 dz \int_0^\infty d\kappa\Phi_n\left(\frac{\omega}{v},\kappa,0\right)$$

$$e^{\frac{-N(1-z)^2}{1+N^2(1+\varepsilon)^2}\kappa'^2} \sin^2\left\{\frac{(1-z)L}{2k}\kappa'^2\left[\frac{1+N^2(1+\varepsilon)(z+\varepsilon)}{1+N^2(1+\varepsilon)^2}\right]\right\}. \qquad (121)$$

Equation (121) was derived and evaluated for a variety of Fresnel numbers and beam waist locations by Ishimaru [39]. He however employed the technique of Tatarski [70] in obtaining this expression for the spectrum. It is pleasing that, under certain circumstances, these two techniques (Tatarski's and the Extended Huygen's-Fresnel) should produce exactly the same results.

In the limit as $N\to 0$ (plane wave) and $N\to\infty$ (spherical wave) Equation (120) yields respectively

$$S_p(\omega) \propto \int_0^1 dz \int_0^\infty d\kappa\Phi_n\left(\frac{\omega}{v},\kappa,0\right) \sin^2\left[\frac{(1-z)L}{2k}\kappa'^2\right] \qquad (122a)$$

and

$$S_p(\omega) \propto \int_0^1 dz \int_0^\infty d\kappa\Phi_n\left(\frac{\omega}{n},\kappa,0\right) \sin^2\left[\frac{(1-z)L}{2k}\frac{z+\varepsilon}{1+\varepsilon}\kappa'^2\right] \qquad (122b)$$

Equations (122a) and (122b) which are expressions for the plane and spherical wave scintillation spectra, are treated extensively by Tatarski [36] and Clifford [35].

Throughout the remainder of this work use will be made of the von Kármán form of the three-dimensional index of refraction spatial spectrum [31],

$$\Phi_n(\kappa_1,\kappa_2,\kappa_3) = .033C_n^2\left[\kappa_1^2+\kappa_2^2+\kappa_3^2+\left(\frac{1.077}{L_o}\right)^2\right]^{-11/6} \qquad (123)$$

whereas most previous workers [35], [39], [71] assumed the Kolmogorov (infinite outer scale) model. In addition, Equation (120) can be put in a form more convenient for analysis by non-dimensionalizing the κ integral through the change of variable

$$\kappa' = \sqrt{\lambda L} \quad . \tag{124}$$

The temporal spectrum is then given by

$$S_p(\omega) = .033 C_n^2 16 \pi^2 k^2 L (\sqrt{\lambda L})^{8/3} v^{-1} \left[\frac{kN/2L}{1+N^2(1+\varepsilon)^2} \right]^2 \tag{125a}$$

$$\times e^{\frac{-4\pi N r_o'^2}{1+N^2(1+\varepsilon)^2}} \int_0^1 dz \int_{-\infty}^{\infty} d\kappa' \left[\kappa'^2 + \left(\frac{\omega}{\omega_o}\right)^2 + \left(\frac{1.077}{L_o'}\right)^2 \right]^{-11/6}$$

$$\times e^{\frac{-N(1-z)^2[\kappa'^2+(\omega/\omega_o)^2]}{2\pi[1+N^2(1+\varepsilon)^2]}} \left\{ \sinh^2 \left[\frac{N(1-z)}{1+N^2(1+\varepsilon)^2} \left(x_o' \frac{\omega}{\omega_o} + y_o' \kappa' \right) \right] \right.$$

$$\left. + \sin^2 \left\{ \frac{(1-z)}{4\pi} \left[1 - \frac{N^2(1+\varepsilon)(1-z)}{1+N^2(1+\varepsilon)^2} \right] \left[\kappa'^2 + \left(\frac{\omega}{\omega_o}\right)^2 \right] \right\} \right],$$

where all of the primed variables denote those which have been normalized to the plane wave Fresnel zone:

$$L_o' = L_o / \sqrt{\lambda L} \tag{125b}$$

$$\kappa' = \sqrt{\lambda L} \kappa = 2\pi / (\ell / \sqrt{\lambda L}) \tag{125c}$$

$$r_o' = r_o / \sqrt{\lambda L} \tag{125d}$$

and

$$v / \sqrt{\lambda L} \equiv \omega_o \ . \tag{125e}$$

Since the predominant diffraction pattern size at the receiver is of dimension on the order of the Fresnel zone, $\sqrt{\lambda L}$ [62], the normalization

frequency, ω_o, is seen to be the temporal frequency observed when this scale size is blown through the beam path at velocity v.

We now write Equation (125a) in the form

$$S_p(\omega) = .033C_n^2 4\pi^2 k^2 L(\sqrt{\lambda L})^{8/3} v^{-1} \left[\frac{kN/2L}{1+N^2(1+\varepsilon)^2}\right]^2 \tag{126a}$$

$$\times e^{\frac{-4\pi N r_o'^2}{1+N^2(1+\varepsilon)^2}} [S_1(\omega)+S_2(\omega)],$$

where the functions $S_1(\omega)$ and $S_2(\omega)$ are given by

$$S_1(\omega) = 4\int_0^1 dz \int_{-\infty}^{\infty} d\kappa' \left[\kappa'^2 + \left(\frac{\omega}{\omega_o}\right)^2 + \left(\frac{1.077}{L_o'}\right)^2\right]^{-11/6} \tag{126b}$$

$$\times e^{\frac{-N(1-z)^2\left[\kappa'^2+\left(\frac{\omega}{\omega_o}\right)^2\right]}{2\pi[1+N^2(1+\varepsilon)^2]}} \sinh^2\left\{\frac{N(1-z)}{1+N^2(1+\varepsilon)^2}\left(x_o'\frac{\omega}{\omega_o}+y_o'\kappa'\right)\right\}$$

and

$$S_2(\omega) = 4\int_0^1 dz \int_{-\infty}^{\infty} d\kappa' \left[\kappa'^2 + \left(\frac{\omega}{\omega_o}\right)^2 + \left(\frac{1.077}{L_o'}\right)^2\right]^{-11/6} \tag{126c}$$

$$\times e^{\frac{-N(1-z)^2\left[\kappa'^2+\left(\frac{\omega}{\omega_o}\right)^2\right]}{2\pi[1+N^2(1+\varepsilon)^2]}} \sin^2\left\{\frac{(1-z)}{4\pi}\left[1-\frac{N^2(1+\varepsilon)(1-z)}{1+N^2(1+\varepsilon)^2}\right]\left[\kappa'^2+\left(\frac{\omega}{\omega_o}\right)^2\right]\right\}.$$

The purpose of this division of the spectrum into two components is to isolate the effects due to the detector being off-axis (given by the function $S_1(\omega)$) from the behavior of the spectrum with the on-axis detector (given by the function $S_2(\omega)$). If the spectrum of Equation (126) is normalized to the spherical wave log-amplitude variance [21]

$$\sigma_s^2 = \frac{.099\pi^{7/2}\, 2^{1/3}}{64\Gamma(4/3)(-\cos\frac{11}{12}\pi)} C_n^2 k^{7/6} L^{11/6}, \tag{127}$$

we obtain finally

$$\frac{\omega_o S_p(\omega)}{I^2(0,0,L)\sigma_s^2} = C\, e^{\frac{-4\pi N r_o'^2}{1+N^2(1+\varepsilon)^2}} [S_1(\omega)+S_2(\omega)] \qquad (128a)$$

where I is the on-axis receiver plane irradiance

$$I(0,0,L) = \left| \frac{\sqrt{kN/2L}}{1+iN(1+\varepsilon)} \right|^2, \qquad (128b)$$

and

$$C = \frac{256}{3\pi^{2/3}} \sqrt{2}\, \Gamma(4/3)(-\cos \tfrac{11}{12}\pi) = 48.527. \qquad (128c)$$

This particular normalization is chosen so that the area under the spectrum is normalized to the spherical wave log-amplitude variance;

$$\lim_{\substack{N\to\infty \\ \varepsilon\to 0 \\ L_o\to\infty}} \int_{-\infty}^{\infty} d\, \frac{\omega_o S_p(\omega)}{I^2(0,0,L)\sigma_s^2} = 4 \times 2\pi\omega_o, \qquad (129)$$

where the additional factor of four arises from the difference between the variance of irradiance and the log-amplitude variance,

$$\sigma_I^2 = 4\, \sigma_\chi^2,$$

under the weak turbulence approximation [62]. Equation (129) can be verified by taking the indicated limits of expression (129), changing the κ', ω variables to polar coordinates, performing the angular integration, and employing integration formulae presented by Tatarski [72].

Equation (128a) is in a form convenient for asymptotic and numerical analysis. The asymptotic evaluation for each of the two component spectra (S_1 and S_2) of this expression will be presented in the next section.

C. Asymptotic Evaluation

In this section we develop analytic expressions which describe the asymptotic high and low frequency behavior of the scintillation spectrum of a gaussian beam with an off-axis detector. These formulae are derived assuming an arbitrary beam Fresnel number, N, and an arbitrary detector location, $\underline{r}_0$. Because the spectra $S_1(\omega)$ and $S_2(\omega)$ exhibit diverse behaviors, they are evaluated separately.

Asymptotic Behavior of $S_1(\omega)$

The S_1 spectrum of Equation (128a) arises simply because the detector is off-axis to the gaussian beam. It is identically zero if the detector is axially located. Typical results presented later in this section will show that S_1 makes a significant contribution to the total spectrum only within the low frequency range, i.e., for frequencies such that

$$\frac{\omega}{\omega_0} \lesssim 2\pi. \tag{130}$$

We now wish to make two approximations which will greatly simplify the evaluation of the spectrum S_1. First we approximate the exponential function and then the hyperbolic sine function in Equation (126b). The argument of the exponential function is bounded in its z and N variables in the following manner:

$$\frac{N(1-z)^2}{2\pi[1+N^2(1+\varepsilon)^2]}\left[\kappa'^2+(\omega/\omega_0)^2\right] \lesssim \frac{1}{4\pi}\left[\kappa'^2+(\omega/\omega_0)^2\right]. \tag{131}$$

At the point

$$\kappa' = \sqrt{(\omega/\omega_0)^2 + (1.077/L_0')^2}, \tag{132}$$

beyond which the function

$$\left[\kappa'^2+(\omega/\omega_0)^2+(1.077/L_0')^2\right]^{-11/6} \tag{133}$$

decreases rapidly, we have

$$\frac{1}{4\pi}\left[\kappa'^2+(\omega/\omega_0)^2\right] = \frac{1}{4\pi}\left[2(\omega/\omega_0)^2+\left(\frac{1.077}{L_0'}\right)^2\right] \quad . \tag{134}$$

If we restrict our attention to temporal frequencies such that

$$\frac{\omega}{\omega_o} \lesssim 10\left(\frac{1.077}{L_o'}\right) \tag{135}$$

then

$$\frac{1}{4\pi}\left[2\left(\frac{\omega}{\omega_o}\right)^2 + \left(\frac{1.077}{L_o'}\right)^2\right] \leq \frac{201}{4\pi}\left(\frac{1.077}{L_o'}\right)^2 . \tag{136}$$

Then for

$$\frac{201}{4\pi}\left(\frac{1.077}{L_o'}\right)^2 << 1$$

or

$$\sqrt{\frac{201}{4\pi}}\left(\frac{1.077}{L_o'}\right) < 1$$

or

$$L_o > 1.077\sqrt{\frac{201}{4\pi}}\sqrt{\lambda L} \sim 4\sqrt{\lambda L} \tag{137}$$

we can use the approximation

$$\frac{-N(1-z)^2[\kappa'^2+(\omega/\omega_o)^2]}{e^{2\pi[1+N^2(1+\varepsilon)^2]}} \approx 1. \tag{138}$$

We now must approximate the hyperbolic sine function in Equation (126b). Its argument is bounded as follows:

$$\frac{N(1-z)}{1+N^2(1+\varepsilon)^2}\left(x_o'\frac{\omega}{\omega_o} + y_o'\kappa'\right) \lesssim \frac{1}{2\sqrt{\lambda L}}\left(x_o\frac{\omega}{\omega_o} + y_o\kappa'\right). \tag{139}$$

At the point

$$\kappa' = \sqrt{(\omega/\omega_o)^2 + (1.077/L_o')^2}$$

we find

$$\frac{1}{2\sqrt{\lambda L}}\left(x_o\frac{\omega}{\omega_o}+y_o\kappa'\right)=\frac{1}{2\sqrt{\lambda L}}\left(x_o\frac{\omega}{\omega_o}+y_o\sqrt{(\omega/\omega_o)^2+(1.077/L_o')^2}\right). \tag{140}$$

For temporal frequencies such that

$$\frac{\omega}{\omega_o}\lesssim 10\left(\frac{1.077}{L_o'}\right)$$

the argument of the sinh function is

$$\frac{N(1-z)}{1+N^2(1+\varepsilon)^2}\left(x_o'\frac{\omega}{\omega_o}+y_o'\kappa'\right)\lesssim\frac{5}{\sqrt{\lambda L}}\,\frac{(1.077)\sqrt{\lambda L}}{L_o}\,(x_o+y_o)$$

$$\leq\frac{5(1.077)}{L_o}\,r_o. \tag{141}$$

By requiring

$$\frac{5(1.077)r_o}{L_o}\ll 1$$

or

$$r_o\ll\frac{L_o}{5(1.077)}, \tag{142}$$

we can employ the approximation

$$\sinh^2 X\approx X^2\ . \tag{143}$$

With the foregoing approximations the expression for S_1 in Equation (126b) becomes

$$S_1(\omega)=\frac{4}{3}\left[\frac{N}{1+N^2(1+\varepsilon)^2}\right]^2\int_{-\infty}^{\infty}d\kappa'\left[\kappa'^2+\left(\frac{\omega}{\omega_o}\right)^2+\left(\frac{1.077}{L_o'}\right)^2\right]^{-11/6}$$

$$\times\left(x_o'\frac{\omega}{\omega_o}+y_o'\kappa'\right)^2. \tag{144}$$

By expanding the quadratic term in the integrand of Equation (144) it is seen that the cross term is an odd function of κ' and the integral goes to zero. Therefore Equation (144) is

$$S_1(\omega) = \frac{4}{3}\left[\frac{N}{1+N^2(1+\varepsilon)^2}\right]^2$$

$$\times \left\{\left(x_o' \frac{\omega}{\omega_o}\right)^2 \int_{-\infty}^{\infty} d\kappa' \left[\kappa'^2 + (\omega/\omega_o)^2 + \left(\frac{1.077}{L_o'}\right)^2\right]^{-11/6}\right. \tag{145}$$

$$\left. + (y_o')^2 \int_{-\infty}^{\infty} d\kappa' \, \kappa'^2 \left[\kappa'^2 + (\omega/\omega_o)^2 + \left(\frac{1.077}{L_o'}\right)^2\right]^{-11/6}\right\}.$$

The change of variable

$$u = \kappa'^2 \Big/ \left[\left(\frac{\omega}{\omega_o}\right)^2 + \left(\frac{1.077}{L_o'}\right)^2\right] \tag{146}$$

allows the expression of these integrals in terms of Beta functions [73];

$$S_1(\omega) = \frac{4}{3}\left[\frac{N}{1+N^2(1+\varepsilon)^2}\right]^2 \frac{\sqrt{\pi}\,\Gamma(4/3)}{\Gamma(11/6)}$$

$$\times \left\{(x_o')^2 \left(\frac{\omega}{\omega_o}\right)^2 \left[\left(\frac{\omega}{\omega_o}\right)^2 + \left(\frac{1.077}{L_o'}\right)^2\right]^{-4/3}\right.$$

$$\left. + \frac{3}{2}(y_o')^2 \left[\left(\frac{\omega}{\omega_o}\right)^2 + \left(\frac{1.077}{L_o'}\right)^2\right]^{-1/3}\right\}, \tag{147}$$

where we have used the well known identity relating the gamma (Γ) and beta functions [73].

For the detector and beam axis along a line collinear with the wind, $\bar{r}_o' = (x_o', 0)$, (recall that we assumed the wind to be blowing in the x direction) then Equation (147) predicts

$$S_1 \alpha \begin{cases} (\omega/\omega_o)^2 & ; \ \omega/\omega_o < 1.077/L_o' \\ (\omega/\omega_o)^{-2/3} & ; \ \omega/\omega_o > 1.077/L_o' \end{cases} . \tag{148a}$$

However for the detector and beam axis along a line orthogonal to the wind direction, $\bar{r}_o' = (0, y_o')$,

$$S_1 \alpha \begin{cases} \text{constant} & ; \ \omega/\omega_o < 1.077/L_o' \\ (\omega/\omega_o)^{-2/3} & ; \ \omega/\omega_o > 1.077/L_o' \end{cases} \tag{148b}$$

These asymptotic results are summarized in Figure 9a in which we have defined α_r as

$$\alpha_r = \frac{N}{1+N^2(1+\varepsilon)^2} \tag{149a}$$

and the constant C_1 as

$$C_1 = \frac{\sqrt{\pi}\,\Gamma(4/3)}{\Gamma(11/6).} \tag{149b}$$

Figure 9b shows the resulting numerical values of the asymptotes when

$$\begin{aligned} N &= 2 \times 10^3 \\ \varepsilon &= 0 \\ L_o &= 10 \text{ meters} \\ \sqrt{\lambda L} &= 2.516 \times 10^{-2} \text{ meters} \end{aligned} \tag{150}$$

and the detector is located at

$$\bar{r}_o = (.63, 0) \tag{151a}$$

and

$$\bar{r}_o = (0, .63). \tag{151b}$$

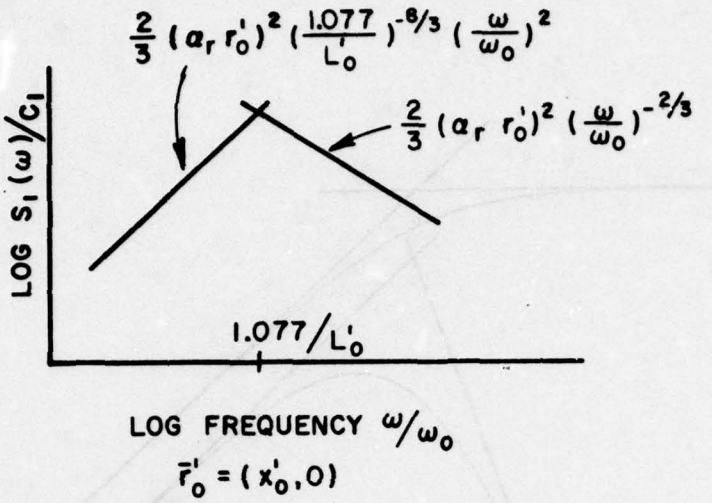

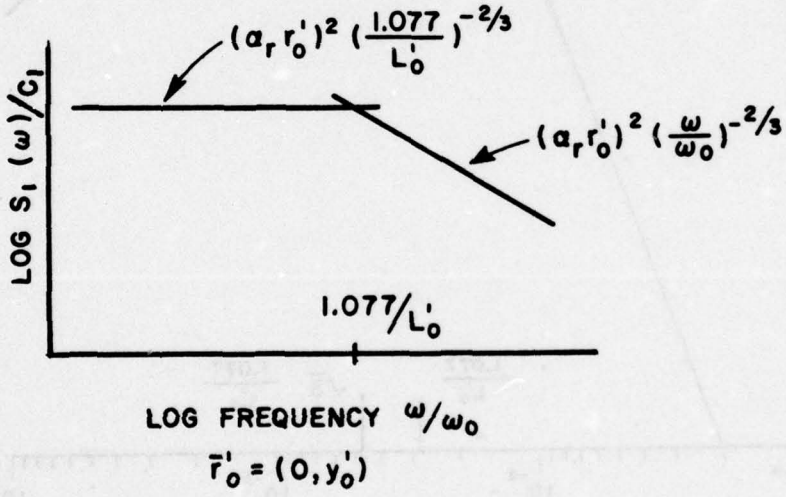

Figure 9a--Asymptotes for S_1 spectrum.

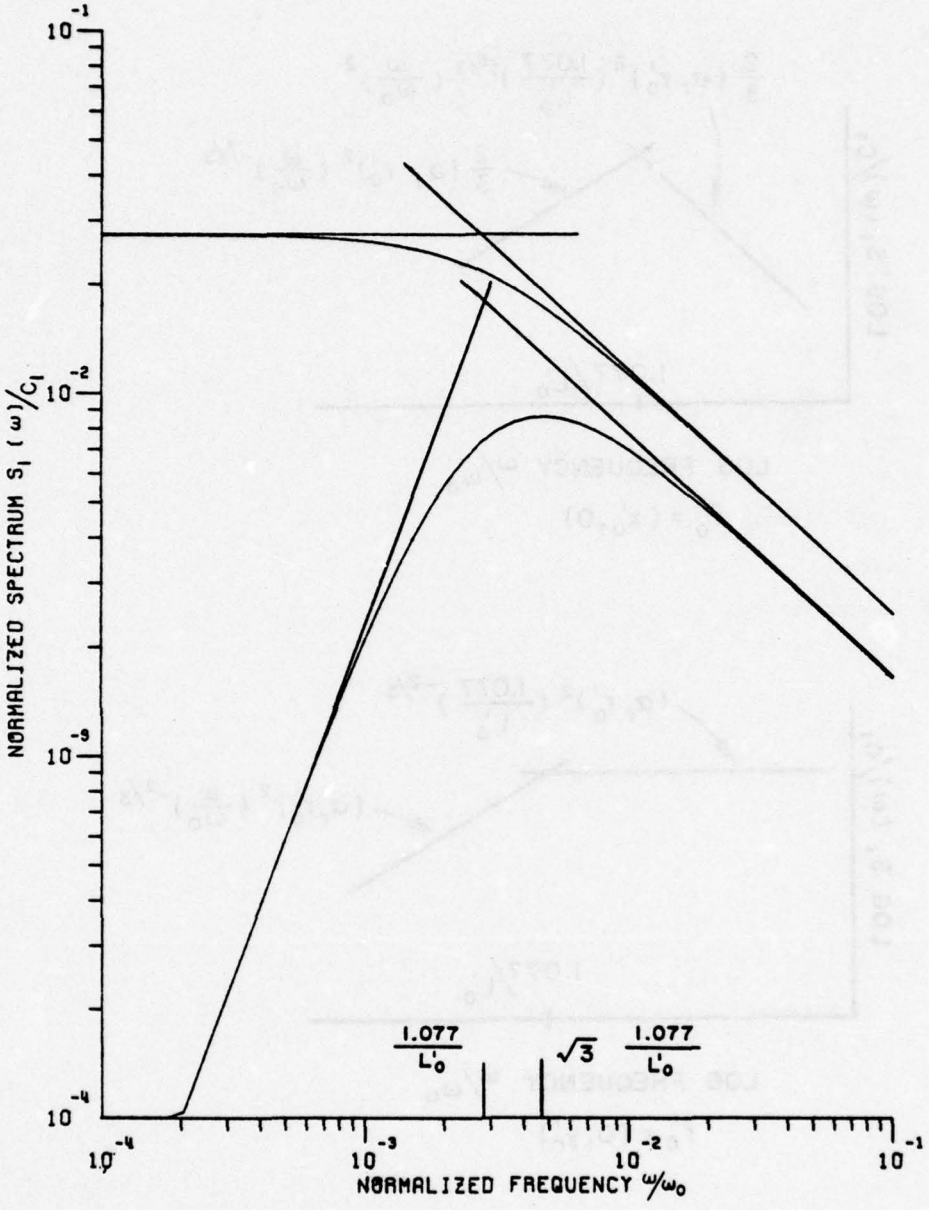

Figure 9b--Typical numerical values of asymptotes of S_1 spectrum.

We can normalize the off-axis distance, r_o, to the receiver plane beam spotsize (Equation (115d)) to obtain for Equations (151)

$$\frac{\bar{r}_o}{w(L)} = (1.00,0) \tag{152a}$$

and

$$\frac{\bar{r}_o}{w(L)} = (0,1.00). \tag{152b}$$

Note that for the case

$$\bar{r}_o = (x_o,0),$$

the peak of the curve occurs at

$$\frac{\omega}{\omega_o} = \sqrt{3}\ \frac{1.077}{L_o'}$$

even though the +2 and -2/3 asymptotes intercept at

$$\frac{\omega}{\omega_o} = \frac{1.077}{L_o'} \quad .$$

This can be verified by differentiating Equation (147) with respect to ω/ω_o.

We now return to our phase grating model of the atmospheric turbulence and sketch, as in Figure 10a, the receiver plane positions of the zeroth and plus and minus one order diffracted beams as functions of the spatial frequencies ω/v and κ. (Recall that the spatial frequency ω/v is associated with the wind direction.) This figure merely illustrates the fact that, for a finite beam, the detector position with respect to the wind direction and the zeroth order beam axis will have an effect upon the scintillation spectrum. Of course for fields of infinite extent, e.g., plane and spherical waves, the detector "position" loses distinction. Indeed, it can easily be seen that the $S_1(\omega)$ spectrum goes to zero as the beam Fresnel number approaches zero or infinity. These limits correspond respectively to plane and spherical waves.

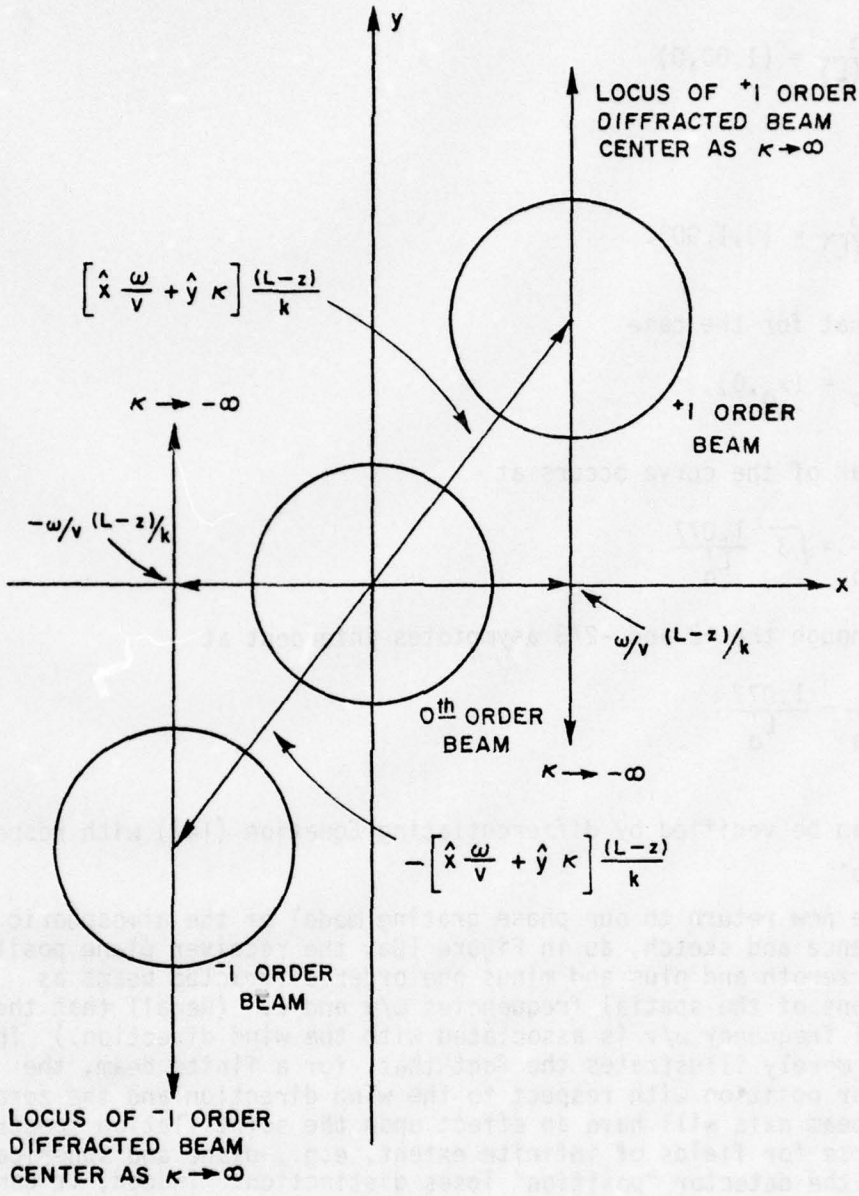

Figure 10a--Diffracted orders of a finite beam.

For the detector off-axis to the zeroth order beam the $0\text{-}^{+}1$ beam interaction and the $^{-}1\text{-}0$ beam interaction contribute unequally to the scintillation spectrum. When the detector is in the 1st or 4th quadrants the contribution to the spectrum is weighted toward the $0\text{-}^{+}1$ beam interaction. Likewise, when the detector is in the 2nd or 3rd quadrants the $^{-}1\text{-}0$ beam interaction predominates.

In Figure 10b we have illustrated the zeroth and $^{+}1$ order beams for a phase screen located at z=0. Also shown in this figure is the beam deflection region for which the index of refraction spectrum, Φ_n, is constant

$$\sqrt{\kappa^2 + (\omega/v)^2}\,\frac{L}{k} \leq \frac{L}{k}\,\frac{1.077}{L_o} \quad .$$

With this figure we wish to illustrate the behavior of the spectrum for the case in which the detector is at either zero or 90 degrees with respect to the x-axis.

For the zero degree case ($\bar{r}_o=(x_o,0)$) the magnitude of the product of the zeroth and $^{+}1$ order beams (in the expression for the H function) increases as ω/v increases simply because the deflected beam's axis moves closer to the detector. In fact, the product is maximum when the deflection is such that

$$\frac{L}{k}\,\frac{\omega}{v} = r_o .$$

However, once the $^{+}1$ order beam is deflected out of the region for which the index of refraction spectrum is constant, the scintillation spectrum will decrease (since Φ_n decreases beyond this point). Therefore the scintillation spectrum will increase up to the point at which

$$\frac{L}{k}\,\frac{\omega}{v} = \frac{L}{k}\,\frac{1.077}{L_o}$$

or

$$\frac{\omega}{\omega_o} = \frac{1.077}{L_o'}$$

and will decrease beyond this point.

For the detector off-axis to the zeroth order beam the $0\text{-}^{+}1$ beam interaction and the $^{-}1\text{-}0$ beam interaction contribute unequally to the scintillation spectrum. When the detector is in the 1st or 4th quadrants the contribution to the spectrum is weighted toward the $0\text{-}^{+}1$ beam interaction. Likewise, when the detector is in the 2nd or 3rd quadrants the $^{-}1\text{-}0$ beam interaction predominates.

In Figure 10b we have illustrated the zeroth and $^{+}1$ order beams for a phase screen located at z=0. Also shown in this figure is the beam deflection region for which the index of refraction spectrum, Φ_n, is constant

$$\sqrt{\kappa^2 + (\omega/v)^2}\,\frac{L}{k} \leq \frac{L}{k}\,\frac{1.077}{L_o} \quad .$$

With this figure we wish to illustrate the behavior of the spectrum for the case in which the detector is at either zero or 90 degrees with respect to the x-axis.

For the zero degree case ($\bar{r}_o=(x_o,0)$) the magnitude of the product of the zeroth and $^{+}1$ order beams (in the expression for the *H* function) increases as ω/v increases simply because the deflected beam's axis moves closer to the detector. In fact, the product is maximum when the deflection is such that

$$\frac{L}{k}\,\frac{\omega}{v} = r_o.$$

However, once the $^{+}1$ order beam is deflected out of the region for which the index of refraction spectrum is constant, the scintillation spectrum will decrease (since Φ_n decreases beyond this point). Therefore the scintillation spectrum will increase up to the point at which

$$\frac{L}{k}\,\frac{\omega}{v} = \frac{L}{k}\,\frac{1.077}{L_o}$$

or

$$\frac{\omega}{\omega_o} = \frac{1.077}{L_o'}$$

and will decrease beyond this point.

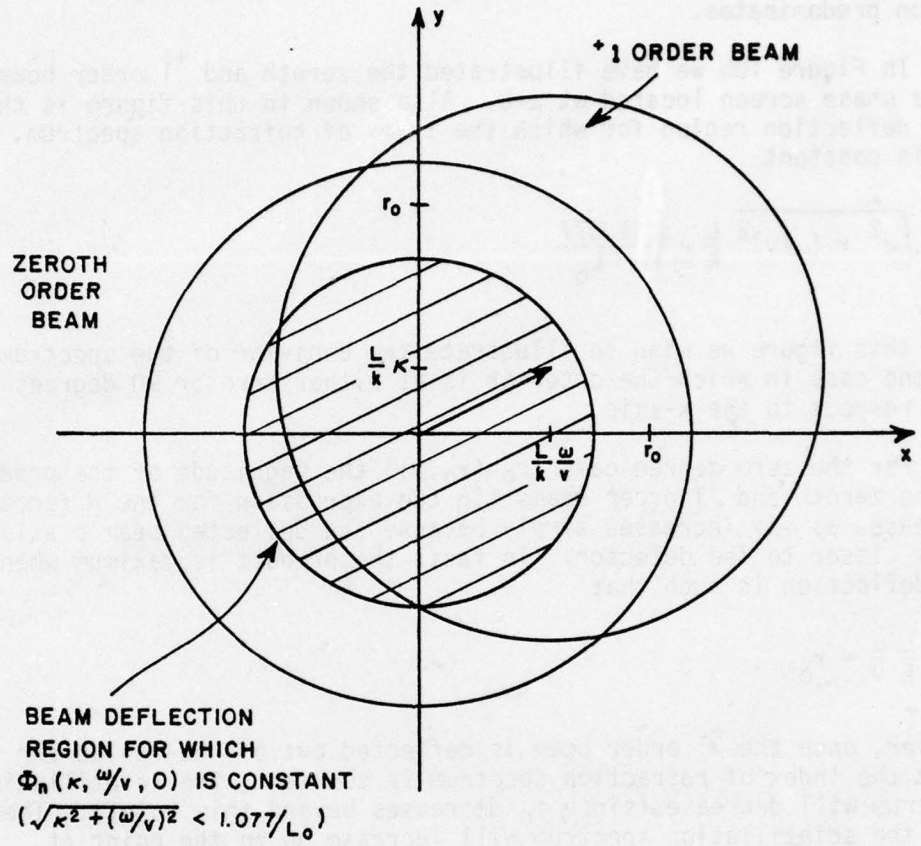

Figure 10b--Zeroth and plus one order diffracted beams.

When the detector is at the 90 degree location ($\bar{r}_o = (0,y_o)$) the κ variable of integration sweeps the deflected beam through all possible orientations with respect to the detector. Hence the scintillation spectrum will remain constant up to the frequency

$$\frac{\omega}{\omega_o} = \frac{1.077}{L_o'}$$

and decrease thereafter.

The purpose of the preceding discussion was to provide a physical interpretation of the effects observed when the detector is off-axis to the beam. Of course if the detector is axially located we should expect to see none of the behavior which has just been described. Qualitatively, the results of this discussion and of the earlier analytic evaluation are identical, thus lending credence to those results.

Asymptotic Behavior of $S_2(\omega)$

The S_2 spectrum of Equation (126c) is simply the spectrum of a gaussian beam with an axially located detector. As such, it determines the behavior of the spectrum of Equation (126a) for an axial detector as well as for the limiting plane and spherical wave cases. We shall be concerned with two basic frequency ranges; high frequencies, such that

$$\frac{\omega}{\omega_o} >> 2\pi,$$

and low frequencies, such that

$$\frac{\omega}{\omega_o} << 2\pi.$$

In addition, within the high frequency region, we are interested in two sub-regions:

$$\frac{N(\omega/\omega_o)^2}{2\pi[1+N^2(1+\varepsilon)^2]} > 1 \quad \text{(sub-region A)}$$

and

$$\frac{N(\omega/\omega_o)^2}{2\pi[1+N^2(1+\varepsilon)^2]} < 1 \quad \text{(sub-region B)}.$$

Within the high frequency region, i.e. frequencies such that

$$\frac{\omega}{\omega_o} >> 2\pi \quad , \tag{153}$$

the $\sin^2$ function is oscillating so rapidly with respect to the other terms in the integrand of Eq. (122c) that we may set

$$\sin^2(\cdots) \approx \frac{1}{2} \quad . \tag{154}$$

The S_2 spectrum is then given by

$$S_2(\omega) = 4 \int_0^\infty d\kappa' \, [\kappa'^2 + (\omega/\omega_o)^2]^{-11/6} \times \int_0^1 du \, e^{-\frac{N[\kappa'^2+(\omega/\omega_o)^2]}{2\pi[1+N^2(1+\varepsilon)^2]} u^2} \tag{155}$$

where we have made use of the change of variable u=1-z. For very high frequencies (high frequency sub-region A) the u integrand is small long before the upper limit of u=1 is approached. Therefore the upper limit may be extended to infinity and the u integration performed in closed form to yield

$$S_2(\omega) = 2\sqrt{\pi} \left[\frac{N/2\pi}{1+N^2(1+\varepsilon)^2}\right]^{-1/2} \int_0^\infty d\kappa' [\kappa'^2 + (\omega/\omega_o)^2]^{-7/3} \quad . \tag{156}$$

The change of variable

$$x = \kappa'^2/(\omega/\omega_o)^2$$

puts Eq. (156) in terms of a Beta function [73] integral which gives for the S_2 spectrum

$$S_2(\omega) = \frac{\sqrt{\pi}\ \Gamma(11/6)}{\Gamma(7/3)} \left[\frac{N/2\pi}{1+N^2(1+\varepsilon)^2}\right]^{-1/2} \left(\frac{\omega}{\omega_o}\right)^{-11/3} . \qquad (157)$$

For the case in which the upper limit on the path integration cannot be extended (high frequency sub-region B)

$$S_2(\omega) = 2\left(\frac{\omega}{\omega_o}\right)^{-8/3} \int_0^1 du\ e^{-bu^2} \int^{\infty} d\kappa\ \kappa^{-1/2}\ (\kappa+1)^{-11/6}\ e^{-bu^2\kappa}\ , \qquad (158)$$

where

$$b = \frac{(N/2\pi)(\omega/\omega_o)^2}{1 + N^2(1+\varepsilon)^2} \qquad (159)$$

and we have used the change of variable

$$\kappa = \kappa'^2/(\omega/\omega_o)^2 .$$

The κ integration is of the form [74]

$$\int_0^{\infty} dt\ t^{2\nu-1}\ (t+1)^{2\mu-1}\ e^{-pt}$$

$$= \Gamma(2\nu)\ p^{-\mu-\nu}\ e^{p/2}\ W_{\mu-\nu,\mu+\nu-\frac{1}{2}}(p)\ , \qquad (160)$$

where W is Whittaker's function [75],[76] which can in turn be expressed as

$$W_{\mu-\nu,\mu-\nu-\frac{1}{2}}(p) = \frac{\Gamma(1-2\mu-2\nu)}{\Gamma(1-2\mu)}\ p^{\mu+\nu}\ e^{-p/2}\ {}_1F_1(2\nu;2\mu+2\nu;p)$$

$$+ \frac{\Gamma(2\mu+2\nu-1)}{\Gamma(2\nu)}\ p^{1-\mu-\nu}\ e^{-p/2}\ {}_1F_1(1-2\mu;2-2\mu-2\nu;p), \qquad (161)$$

where ${}_1F_1$ is Kummer's confluent hypergeometric function [76] defined as

$$ {}_1F_1(x;y;z) = \sum_{n=0}^{\infty} \frac{\Gamma(x+n)}{\Gamma(x)} \frac{\Gamma(y)}{\Gamma(y+n)} \frac{z^n}{n!} \quad . \tag{162} $$

With these formulae Eq. (158) is

$$ S_2(\omega) = 2 \frac{\sqrt{\pi}\,\Gamma(4/3)}{\Gamma(11/6)} \left(\frac{\omega}{\omega_o}\right)^{-8/3} \int_0^1 du\, e^{-bu^2}\, {}_1F_1(\tfrac{1}{2};-\tfrac{1}{3};bu^2) $$

$$ + 2\,\Gamma(-4/3)\left(\frac{\omega}{\omega_o}\right)^{-8/3} \int_0^1 du\, e^{-bu^2} (bu^2)^{4/3}\, {}_1F_1(\tfrac{11}{6};\tfrac{7}{3};bu^2). \tag{163} $$

Employing Eq. (162) and integrating term by term yields finally [77][78]

$$ S_2(\omega) = \left(\frac{\omega}{\omega_o}\right)^{-8/3} \left\{ \frac{\sqrt{\pi}\,\Gamma(4/3)}{\Gamma(11/6)} \sum_{n=0}^{\infty} \frac{(1/2)_n}{(-1/3)_n} \frac{\left[\frac{\alpha_r}{2\pi}\left(\frac{\omega}{\omega_o}\right)^2\right]^n}{n!(n+1/2)} \right. $$

$$ \times\, {}_1F_1\left(n+\tfrac{1}{2};n+\tfrac{3}{2};\, -\frac{\alpha_r}{2\pi}\left(\frac{\omega}{\omega_o}\right)^2\right) $$

$$ \left. + \Gamma(-4/3) \sum_{n=0}^{\infty} \frac{(11/6)_n}{(7/3)_n} \frac{\left[\frac{\alpha_r}{2\pi}\left(\frac{\omega}{\omega_o}\right)^2\right]^{n+4/3}}{n!(n+11/6)} {}_1F_1\left(n+\tfrac{11}{6};n+\tfrac{17}{6};\, \frac{-\alpha_r}{2\pi}\left(\frac{\omega}{\omega_o}\right)^2\right) \right\} , \tag{164} $$

where $(a)_n$ is Pochhammer's symbol defined as

$$ (a)_n = \frac{\Gamma(a+n)}{\Gamma(a)} \, , \tag{165} $$

and α_r is defined as

$$ \alpha_r = \frac{N}{1+N^2(1+\varepsilon)^2} \tag{166} $$

By integrating the hypergeometric functions in Equation (163) term by term we have made the tacit assumption that these series are uniformly convergent [79]. That this is so may be shown by calculating the radius of convergence [80] of

$$ {}_1F_1(a;b;z) = \sum_{n=0}^{\infty} C_n z^n, \tag{167a} $$

where

$$ C_n = \frac{\Gamma(a+n)\Gamma(b)}{\Gamma(b+n)\Gamma(a)} \frac{1}{n!} \quad . \tag{167b} $$

The radius of convergence, R, is given by

$$ \lim_{n\to\infty} \left| \frac{C_{n+1}}{C_n} \right| = \frac{1}{R} \, . \tag{168} $$

For the confluent hypergeometric function

$$ \frac{1}{R} = \lim_{n\to\infty} \left| \frac{(a+n)}{(b+n)(1+n)} \right| = 0, \tag{169} $$

i.e.,

$$ R \to \infty \, . \tag{170} $$

Therefore the (confluent) hypergeometric series is uniformly convergent [81] for all values of the argument z (which is in general, complex), and we are justified in integrating the series term by term.

If we retain only the first few terms of the series in Equation (164) the behavior of S_2 within the high frequency region may be more closely examined;

$$ S_2(\omega) = \frac{2\sqrt{\pi}\Gamma(4/3)}{(11/6)} \left(\frac{\omega}{\omega_o}\right)^{-8/3} \left\{ 1 - \frac{5}{6} \frac{\alpha_r}{2\pi} \left(\frac{\omega}{\omega_o}\right)^2 + \frac{3}{11} \frac{\Gamma(-4/3)\Gamma(11/6)}{\sqrt{\pi}\Gamma(4/3)} \right. $$

$$ \left. \times \left[\frac{\alpha_r}{2\pi} \left(\frac{\omega}{\omega_o}\right)^2 \right]^{4/3} \right\} . \tag{171} $$

The dominant behavior in this frequency range is seen to be the -8/3 power of frequency.

The low frequency behavior of S_2 is now calculated by retracting the approximation of Equation (154), letting

$$\sin^2 x = \frac{1}{2} - \frac{1}{2}\,\mathrm{Re}\{e^{i2x}\} \quad , \tag{172}$$

and employing techniques and formulae similar to the preceding [74,82, 83]. This approach results in the formula

$$S_2(\omega) = 2\sqrt{\pi}\,A^{-8/3}\left\{\frac{1}{2}\,\frac{\Gamma(4/3)}{\Gamma(11/6)}\sum_{n=0}^{\infty}\frac{(1/2)_n}{(-1/3)_n}\,\frac{(\alpha_r A^2/2\pi)^n}{n!}\right.$$

$$\times\ {}_1F_1\!\left(n+\tfrac{1}{2};n+\tfrac{3}{2};-\alpha_r B^2/2\pi\right)\frac{}{n+1/2} + \frac{1}{2}\,\frac{\Gamma(-4/3)}{\sqrt{\pi}}\sum_{n=0}^{\infty}\frac{(11/6)_n}{(7/3)_n}\,\frac{(\alpha_r A^2/2\pi)^{n+4/3}}{n!}$$

$$\times\ \frac{{}_1F_1\!\left(n+\tfrac{11}{6};n+\tfrac{17}{6};-\alpha_r B^2/2\pi\right)}{n+11/6} - \mathrm{Re}\left[\frac{\Gamma(4/3)}{\Gamma(11/6)}\sum_{n=0}^{\infty}\frac{(1/2)_n}{(-1/3)_n}\,\frac{1}{n!}\left(\frac{-iA^2}{2\pi}\right)^n\right.$$

$$\times\ \sum_{m=0}^{\infty}\left(\frac{iB^2}{2\pi}\right)^m \frac{{}_2F_1(-(m+n),m+n+1;m+n+2;-i\alpha)}{m!\,(m+n+1)}$$

$$+\ \frac{\Gamma(-4/3)}{\sqrt{\pi}}\sum_{n=0}^{\infty}\frac{(11/6)_n}{(7/3)_n}\,\frac{1}{n!}\left(\frac{-iA^2}{2\pi}\right)^{n+4/3}\sum_{m=0}^{\infty}\left(\frac{iB^2}{2\pi}\right)^m$$

$$\left.\left.\times\ \frac{{}_2F_1\!\left(-(m+n+\tfrac{4}{3}),m+n+\tfrac{7}{3};m+n+\tfrac{10}{3};-i\alpha\right)}{m!\,(m+n+7/3)}\right]\right\} \quad , \tag{173a}$$

where

$$\alpha = \frac{N}{1-iN(1+\varepsilon)} \tag{173b}$$

$$\alpha_r = \mathrm{Re}\{\alpha\} = \frac{N}{1+N^2(1+\varepsilon)^2} \tag{173c}$$

$$A = \left[\left(\frac{\omega}{\omega_o}\right)^2 + \left(\frac{1.077}{L_o'}\right)^2\right]^{1/2} \tag{173d}$$

$$B = \omega/\omega_o \quad , \tag{173e}$$

and ${}_2F_1$ is Gauss' hypergeometric function [84] defined as

$${}_2F_1(w,x;y;z) = \sum_{n=0}^{\infty} \frac{(w)_n (x)_n}{(y)_n} \frac{z^n}{n!} \tag{174}$$

While we have made no approximations in deriving Eq. (173a), its usefulness is limited to low frequencies because the series do not converge uniformly for N on the order of unity or for high frequencies. If only the first few terms of the equation are retained, we obtain

$$S_2(\omega) = \frac{2\sqrt{\pi}\,\Gamma(4/3)}{\Gamma(11/6)}\left[\frac{27}{22}\left(\frac{1}{4\pi}\right)^{4/3}\frac{\Gamma(11/6)}{\Gamma(7/6)}\begin{pmatrix} F_{1P}(N) \\ F_{1S}(N)\end{pmatrix}\right.$$

$$\left. + F_2(N)\left(A^{-8/3}\,B^4 + 3A^{-2/3}\,B^2 - \frac{27}{8}A^{4/3}\right)\right] \quad , \tag{175a}$$

where the function

$$F_{1P}(N) = \alpha_r^{4/3} + \frac{11}{14}\left[1 - \frac{14}{15}(\alpha_i + \sqrt{3}\,\alpha_r)\right.$$

$$\left. + \frac{14}{9\cdot 13}\,(\alpha_i^2 - \alpha_r^2 + 2\sqrt{3}\,\alpha_r\alpha_i)\right] \tag{175b}$$

gives the correct plane wave D.C. level as $N \to 0$, and the function

$$F_{1S}(N) = \alpha_r^{4/3} + \frac{\sqrt{\pi}\Gamma(4/3)}{3\Gamma(11/b)2^{5/3}} \tag{175c}$$

goes to the spherical wave D.C. level as $N \to \infty$. Also in Equations (175) we have defined

$$F_2(N) = \frac{1}{2}\left(\frac{1}{2\pi}\right)^2 \frac{\Gamma(4/3)}{\Gamma(11/6)}\left(\frac{1}{3} - \frac{1}{2}\alpha_i + \frac{1}{5}\alpha_i^2\right) \tag{175d}$$

and

$$\alpha_i = \mathrm{Im}\{\alpha\} \quad . \tag{175e}$$

To within a multiplicative constant (due to the normalization used herein) Equation (175a) can be shown to yield the limiting plane and spherical wave ($N \to 0, N \to \infty$) behavior as quoted by Reinhardt and Collins [31].

As an indication of its plane and spherical wave limits we have displayed in Figure 11 the D.C. level of S_2 normalized to the spherical wave D.C. level, as a function of the Fresnel number N. Although Figure 11 indicates a lack of agreement between expressions (175b) and (175c) within the region $N \sim 1$, the figure is indicative of the conditions under which the gaussian beam may (for the purposes of observing scintillation spectra) be considered to be in the near or far fields.

Final results of the asymptotic evaluation of the spectrum S_2 are presented in Figure 12a. The breakpoint between the zero slope D.C. level and the -8/3 slope, which is commonly referred to as the Fresnel breakpoint, will move slightly as the Fresnel number N of the gaussian beam varies between zero and infinity. However, owing to the steepness of the cutoff (-8/3), the Fresnel breakpoint will always (for weak turbulence) be on the order of 2π. The Fresnel breakpoint can be interpreted as denoting the temporal coherence length (in the presence of the turbulence) for the source employed. At this breakpoint (at least for plane and spherical waves)

$$\frac{\omega}{\omega_0} \sim 2\pi$$

or

$$f \sim \frac{v}{\sqrt{\lambda L}} \quad .$$

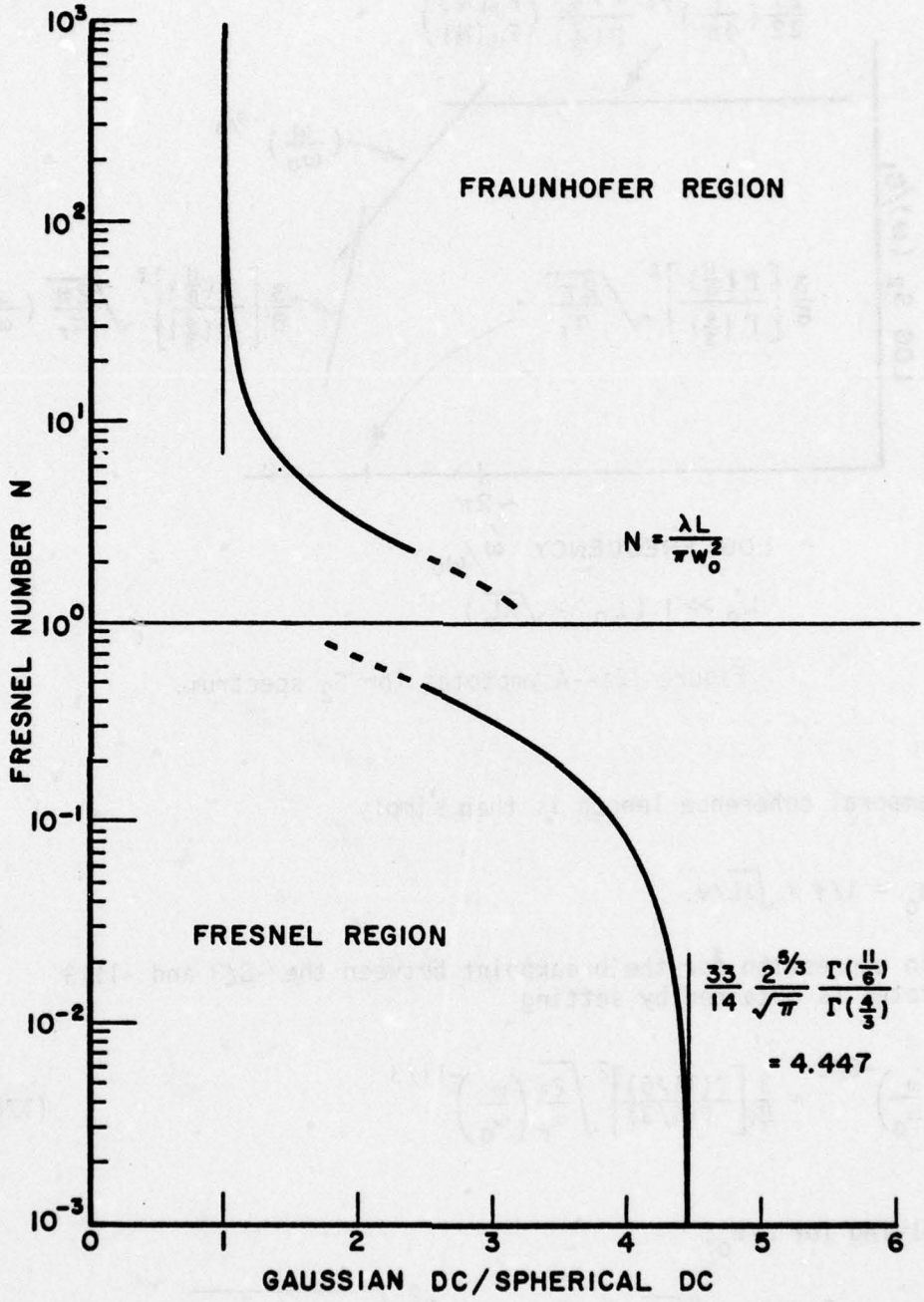

Figure 11--Variation with Fresnel number of the S_2 spectrum D.C. level.

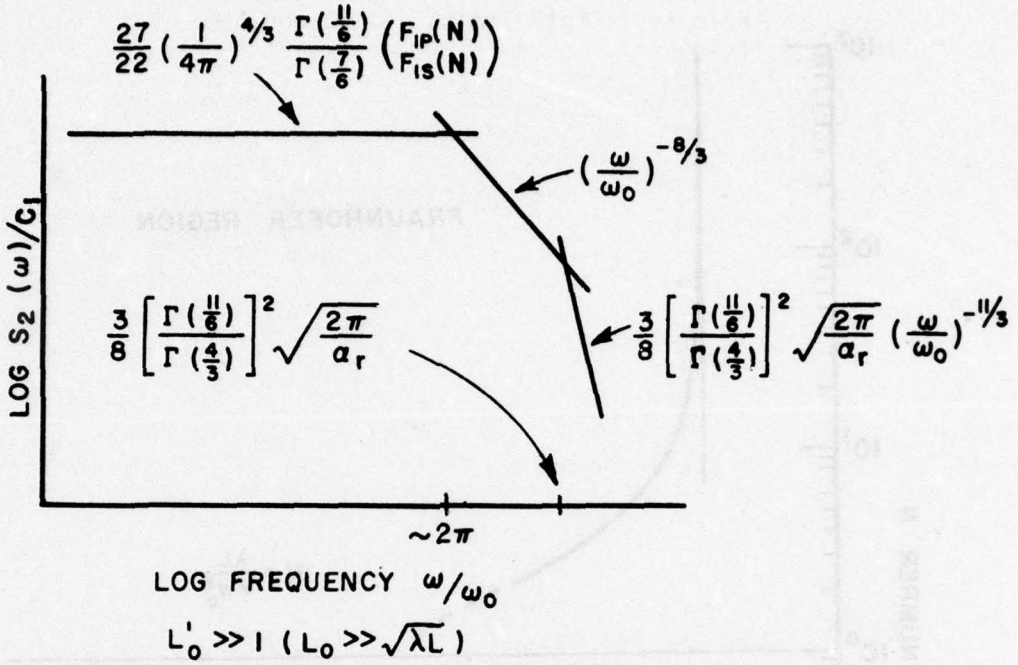

Figure 12a--Asymptotes for S_2 spectrum.

The temporal coherence length is then simply

$$t_0 = 1/f = \sqrt{\lambda L}/v.$$

An expression for the breakpoint between the -8/3 and -11/3 asymptotes is obtained by setting

$$\left(\frac{\omega}{\omega_0}\right)^{-8/3} = \frac{3}{8}\left[\frac{\Gamma(11/6)}{\Gamma(4/3)}\right]^2\sqrt{\frac{2\pi}{\alpha_r}}\left(\frac{\omega}{\omega_0}\right)^{-11/3} \tag{176a}$$

and solving for ω/ω_0;

$$\frac{\omega}{\omega_0} = \frac{3}{8}\left[\frac{\Gamma(11/6)}{\Gamma(4/3)}\right]^2\sqrt{\frac{2\pi}{\alpha_r}} = \frac{3}{8}\left[\frac{\Gamma(11/6)}{\Gamma(4/3)}\right]^2\sqrt{\frac{2\pi[1+N^2(1+\varepsilon)^2]}{N}} \quad . \tag{176b}$$

This breakpoint frequency is minimum for the collimated laser beam $N \sim 1$, and goes to infinity in both limits as $N \to 0$ and $N \to \infty$. From Equations (115d) and (149a) this point is seen to be at

$$\frac{\omega}{\omega_o} = \sqrt{2\pi}\,\frac{3}{8}\left[\frac{\Gamma(11/6)}{\Gamma(4/3)}\right]^2 \frac{W(L)}{\sqrt{\lambda L}} \quad ,$$

or at

$$\omega \approx \frac{V}{\sqrt{\lambda L}} \quad \frac{2W(L)}{\sqrt{\lambda L}}$$

where $W(L)$ is the receiver plane beam spotsize. The frequency of the break point is increased (decreased) as the number of Fresnel zone size patterns contained within an area the size of the receiver plane beam spotsize increases (decreases). Thus the term

$$2W(L)/\sqrt{\lambda L}$$

constitutes a beam size factor.

Figure 12b presents numerical values for the asymptotes when

$$N = 2 \times 10^3$$

$$\varepsilon = 0 \qquad (177)$$

$$L_o = 10 \text{ meters}$$

and

$$\sqrt{\lambda L} = 2.516 \times 10^{-2} \text{ meters},$$

plotted from Equations (157), (171), and (175).

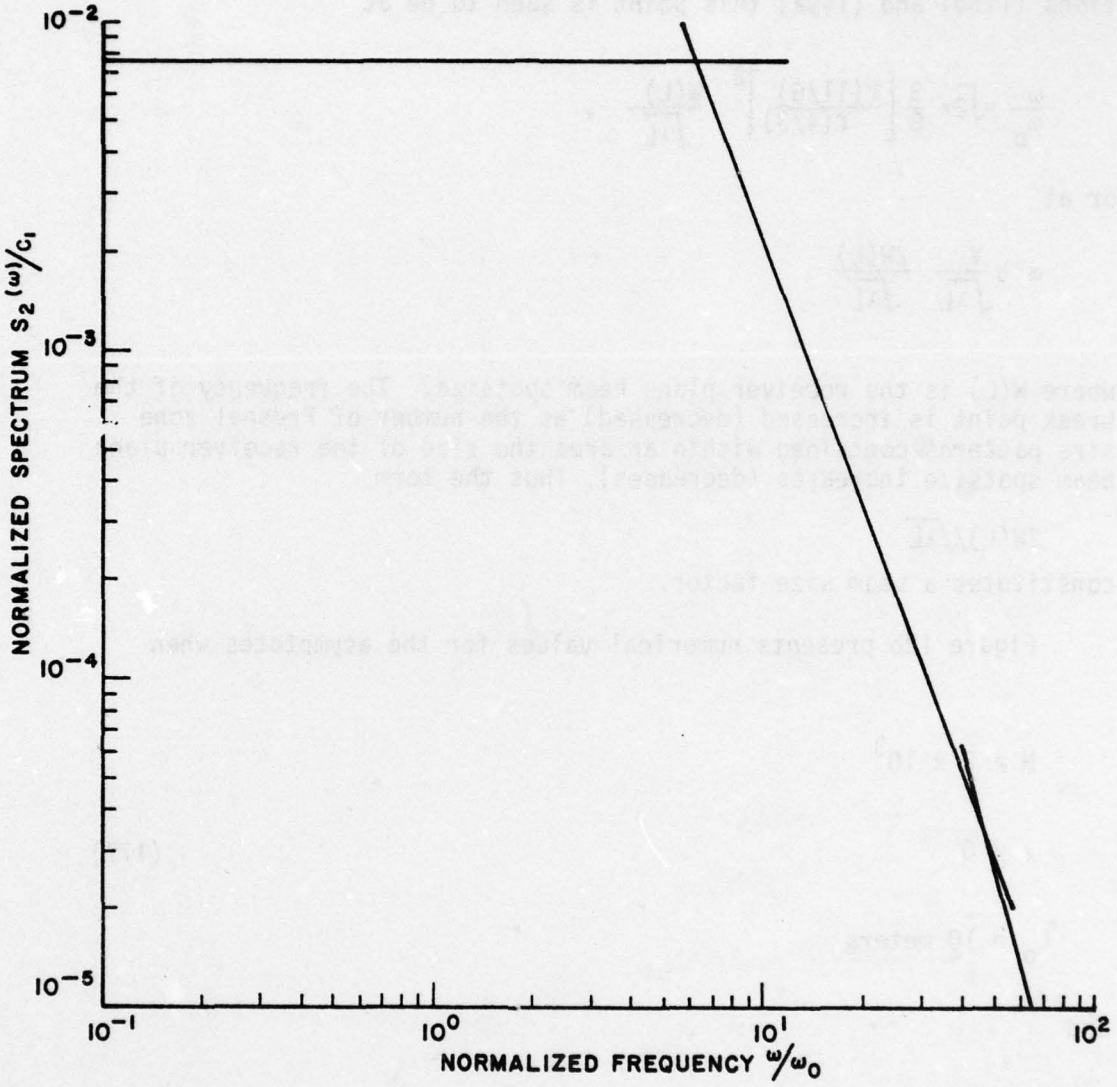

Figure 12b--Typical numerical values of asymptotes of S_2 spectrum.

AD-A050 874 OHIO STATE UNIV COLUMBUS ELECTROSCIENCE LAB F/G 20/5
THEORETICAL STUDY OF THE TURBULENCE INDUCED SCINTILLATION OF A --ETC(U)
JAN 78 D D DUNCAN F30602-76-C-0058
UNCLASSIFIED ESL-4232-5 RADC-TR-77-430 NL

2 OF 2
AD
A050 874

END
DATE
FILMED
4-78
DDC

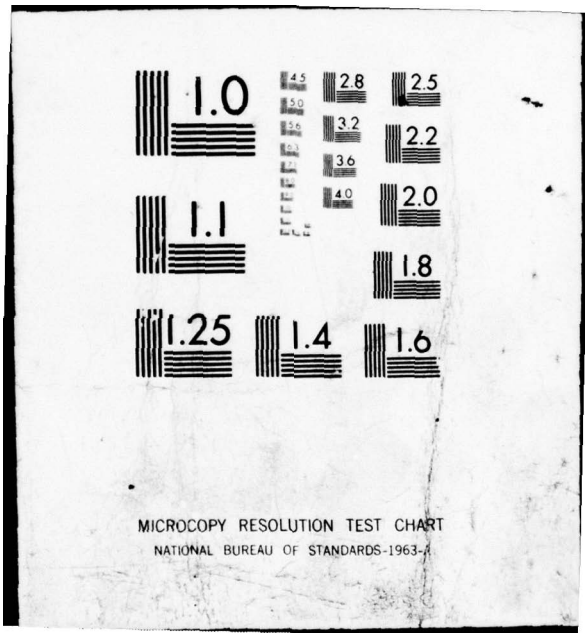
1.0
1.1
1.25
1.4
1.6
1.8
2.0
2.2
2.5
2.8
3.2
3.6
4.0
4.5
5.0
5.6
MICROCOPY RESOLUTION TEST CHART
NATIONAL BUREAU OF STANDARDS-1963-A

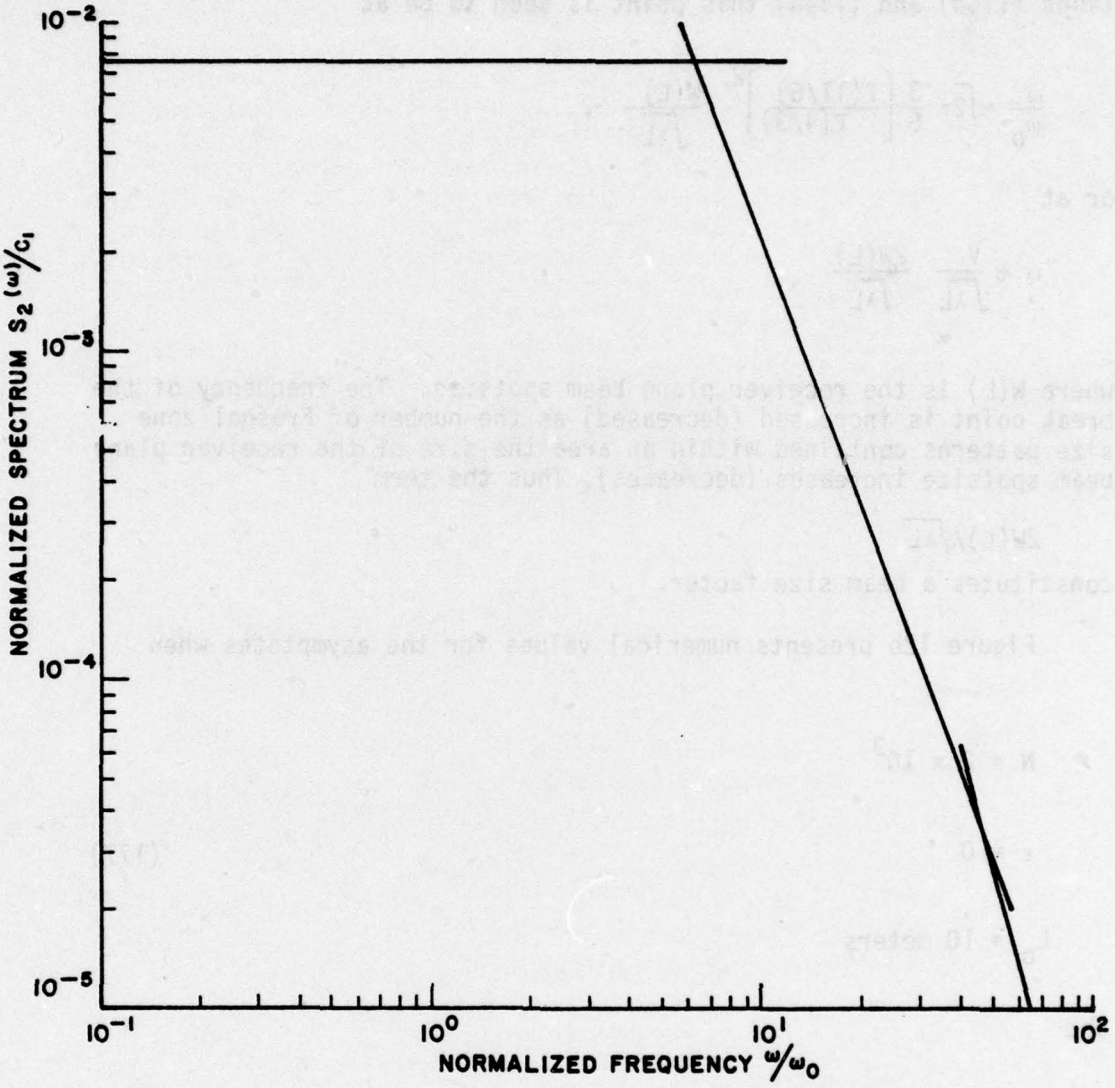

Figure 12b--Typical numerical values of asymptotes of S_2 spectrum.

As a final result of the preceding asymptotic evaluation we present in Figure 13 a composite of the S_1 and S_2 spectra. The slopes and breakpoints have been given earlier. In Figure 13 the departure from a flat spectrum for frequencies below the Fresnel breakpoint is a result of the detector being off-axis. Previous authors [37],[39] who always assumed an axially located detector predicted no such behavior. Other authors [85],[86] assumed that low spatial frequency turbulence or system noise (for the case in which the beam is being pointed by a servo-system) gives rise to beam wander, which is equivalent to saying that r_0 is a random variable. However these workers were not concerned with the resulting effect upon the temporal scintillation spectra.

This concludes the discussion of the asymptotic evaluation of the gaussian beam scintillation spectrum.

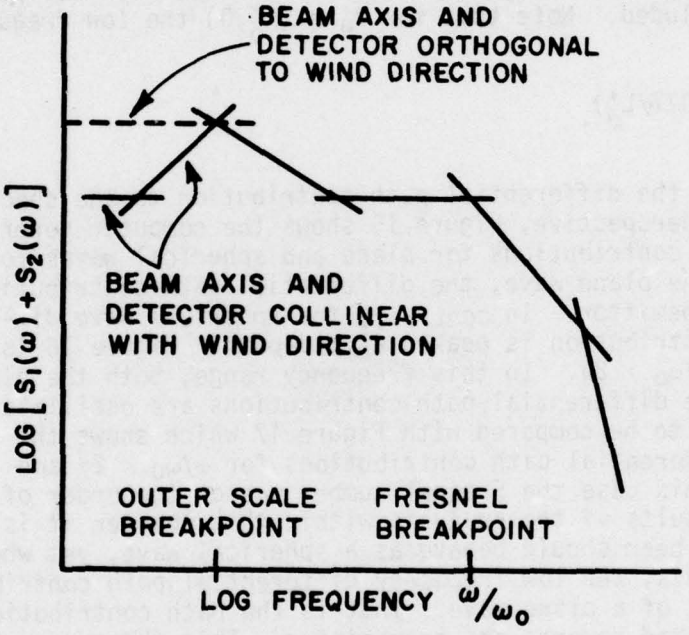

Figure 13--Asymptotes of gaussian beam spectrum.

D. Numerical Evaluation

This section is concerned with a numerical evaluation of Equation (126) for the temporal scintillation spectrum. The computer programs were written in Fortran IV and employed Gaussian quadrature integration techniques. Listings of these programs plus brief descrip-

tions are contained in Appendix G. In addition to the numerically calculated spectra, we also present computer generated plots of the normalized differential path contribution to the spectra, defined as

$$\left[\frac{\omega_o S_p(\omega)}{I^2(0,0,L)\sigma_s^2}\right]^{-1} \frac{d}{dz}\left[\frac{\omega_o S_p(\omega)}{I^2(0,0,L)\sigma_s^2}\right] . \tag{178}$$

Presented in Figure 14 are the computer calculated spectra of a clean gaussian beam for various cases. Note the similarity between these curves and the curves in Figures 12a and 13. The decrease in the magnitude of the spectra for the off-axis cases is due simply to the decreased intensity of the beam at these points. This figure shows the spectrum resulting from a laser beam with Fresnel number $N \sim 2 \times 10^3$. Curves resulting from axial as well as off-axis point detectors are included. Note that for $\bar{r}_o' = (x_o', 0)$ the low frequency peak is at

$$\omega/\omega_o = \sqrt{3}\ (1.077/L_o') .$$

Now consider the differential path contribution to the spectrum. To put things in perspective, Figure 15 shows the computer generated differential path contributions for plane and spherical waves for $\omega/\omega_o < 2\pi$. For the plane wave, the differential path contribution is peaked at the transmitter. In contrast, the spherical wave differential path contribution is peaked at mid-path. Figure 16 is the same except for $\omega/\omega_o > 2\pi$. In this frequency range, both the plane and spherical wave differential path contributions are oscillatory. These figures are to be compared with Figure 17 which shows the gaussian beam differential path contributions for $\omega/\omega_o < 2\pi$ and $\omega/\omega_o > 2\pi$. For this case the Fresnel number was on the order of 2×10^3. From the results of the analysis within this chapter it is seen that the gaussian beam should behave as a spherical wave, yet when the detector is off axis, the low frequency differential path contribution appears to be that of a plane wave. That is the path contribution is more heavily weighted towards the transmitter. This phenomenon has important implications in situations where laser beams are propagated between aircraft. For an off-axis detector the scintillation spectrum will become sensitive to the outer scale of any turbulence localized in the vicinity of the transmitting aircraft's fuselage. For sufficiently short outer scales (typically $\lesssim$ 1 meter) [87] the Fresnel breakpoint at $\omega/\omega_o \sim 2\pi$ may easily be obscured.

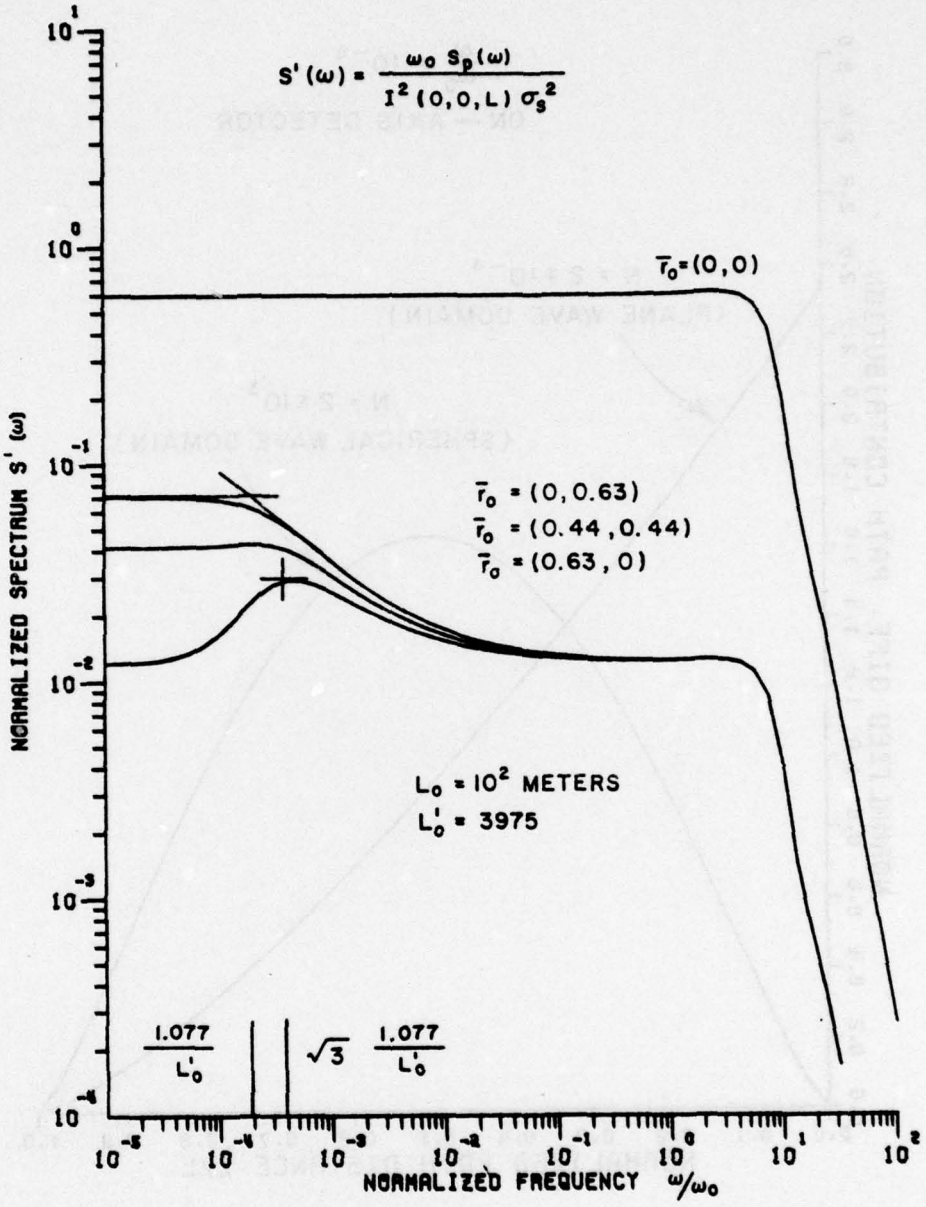

Figure 14--Typical gaussian beam spectra for axial and off-axis detectors.

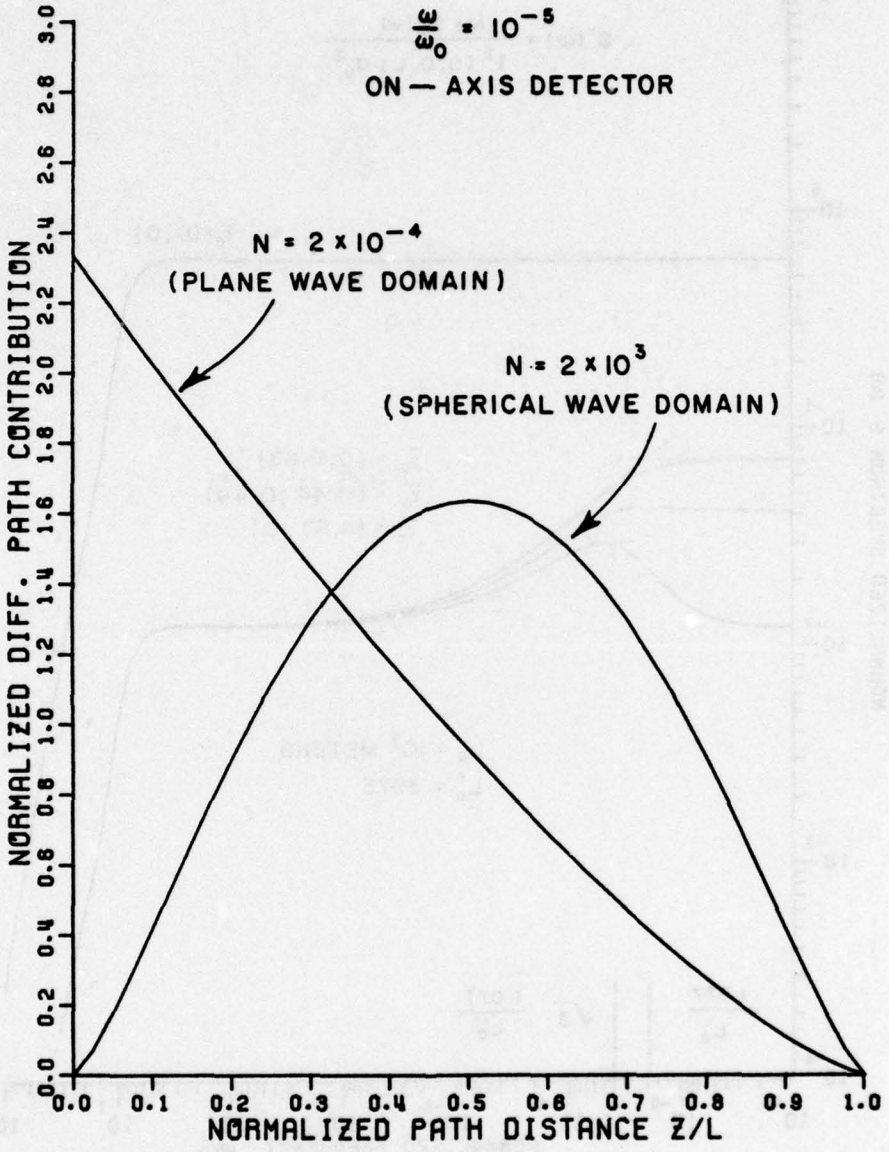

Figure 15--Low frequency differential path contribution for plane and spherical waves.

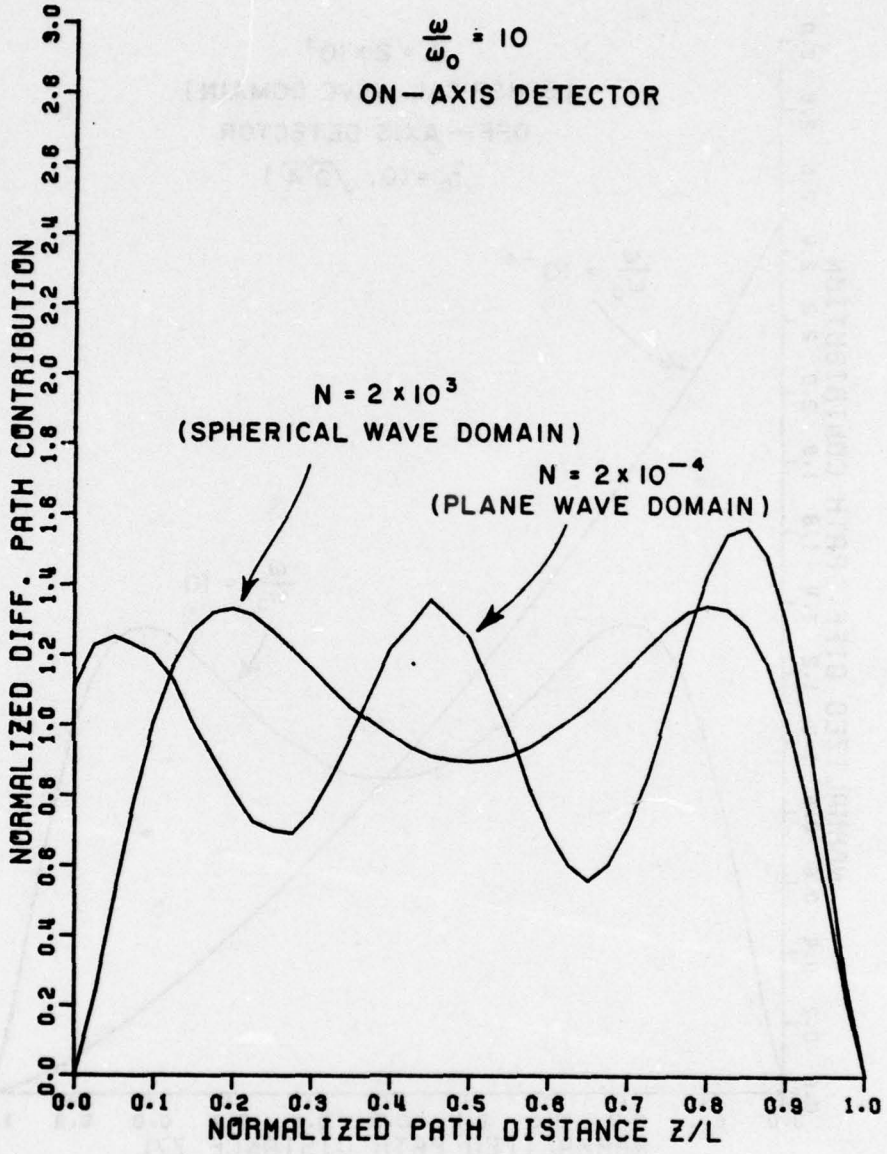

Figure 16--High frequency differential path contribution for plane and spherical waves.

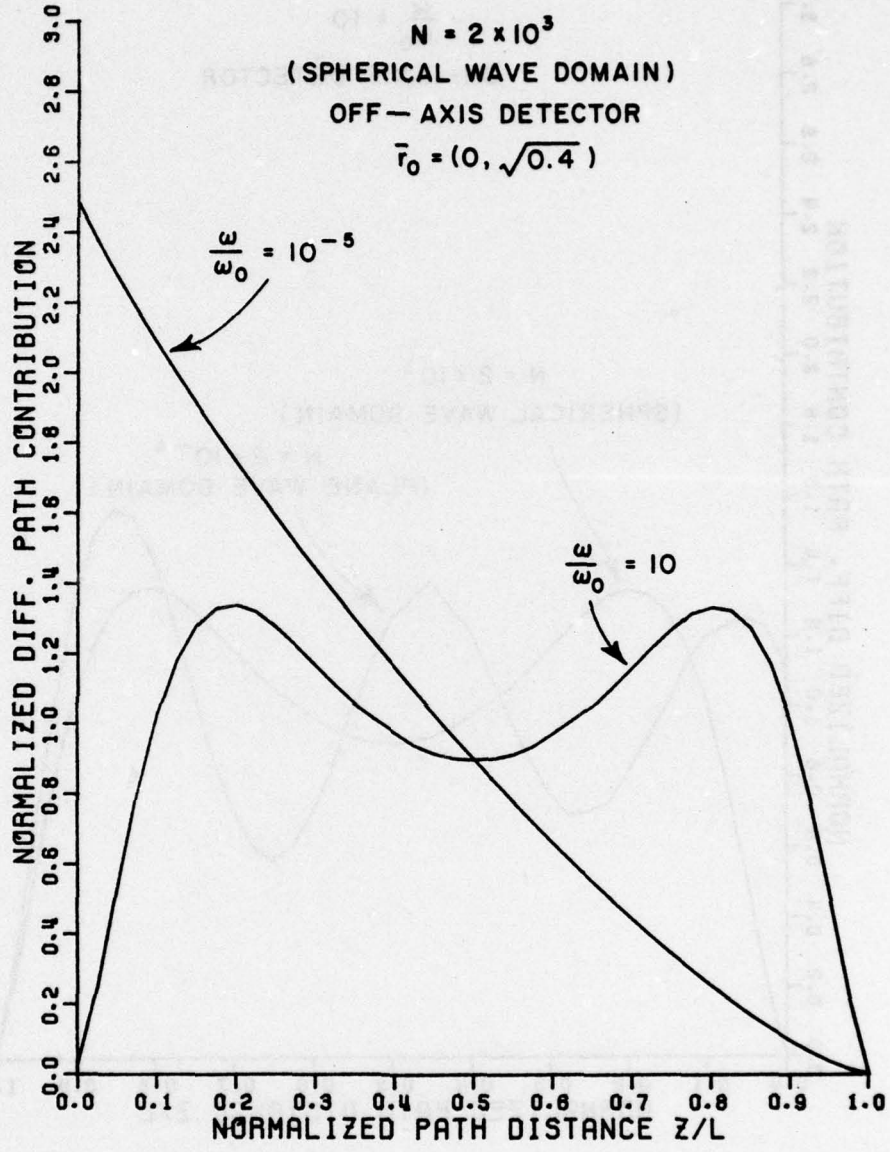

Figure 17--Differential path contribution for gaussian beam with off-axis detector.

This concludes the analysis for a clean gaussian beam with a point receiver. In the next section we will extend the results of this and the previous section to include the effects of finite detector apertures and a finite inner scale.

E. Additional Topics

We now wish to extend the results of Section C to account for two phenomena not previously mentioned, namely the effects upon the scintillation spectrum of finite detector apertures and a finite inner scale. The former effect is of interest because all physically realizable detectors have a finite aperture. The assumption in Section D of a point detector was merely a device used to simplify the mathematics. However, we will demonstrate that, under certain conditions, this is a reasonable approximation to reality. Inclusion of a finite inner scale in the model of the index field reflects the fact that the kinetic energy of very small scale index inhomogeneities is dissipated in the form of heat rather than being passed on to ever-decreasing scale sizes. From the discussion of phase gratings in Chapter II, it is seen that the existence of a finite inner scale requires that (for weak turbulence) the angle of the bending experienced by light rays passing through the turbulent atmosphere be bounded by

$$\alpha_{max} = \lambda/\ell_o,$$

where λ is the wavelength and ℓ_o is the inner scale of turbulence.

In Eq. (123) of Section C we could have easily included an inner scale cut-off in the expression for the power spectrum of the index fluctuations [71];

$$\Phi_n(\kappa_1,\kappa_2,\kappa_3) = 0.033\, C_n^2[\kappa^2 + (1.077/L_o)^2]^{-11/6}\, e^{-(\kappa/\kappa_m)^2}, \quad (179)$$

where

$$\kappa^2 = \kappa_1^2 + \kappa_2^2 + \kappa_3^2,$$

$$\kappa_m \ell_o = [0.033\pi\Gamma(5/3)]^{-3/4} = 5.92,$$

and ℓ_o is the inner scale of turbulence.

Inclusion of this inner scale dependence results in an additional term in the integrand of Eq. (125) of the form

$$\exp \frac{-[\kappa'^2+(\omega/\omega_0)^2]}{(\sqrt{\lambda L}\kappa_m)^2} \tag{180}$$

Inspection of this term shows that the inner scale will produce a gaussian roll-off of the scintillation spectrum in the vicinity of

$$\frac{\omega}{\omega_0} \approx \frac{92\sqrt{\lambda L}}{\ell_0} \tag{181}$$

For a Fresnel length on the order of the inner scale ($\ell_0 \sim 10^{-2}$-10^{-3}m) this effect could easily dominate the high frequency behavior of the scintillation spectrum. If for example the range, L, is one kilometer, the source is a helium-neon laser (λ=.6328x10^{-6}m) and the inner scale, ℓ_0, is one millimeter then the scintillation spectrum will exhibit an inner scale effect for

$$\frac{\omega}{\omega_0} \gtrsim 150 >> 2\pi.$$

Or for a velocity, v, of 150 meters/sec., inner scale effects would begin at

$$f \sim v/\ell_0 = 150 \text{ KHz}.$$

Finite aperture effects are determined by defining the receiver aperture as

$$W(\bar{r}) = \begin{cases} 1 \; ; & |\bar{r}| \leq D/2 \\ 0 \; ; & |\bar{r}| > D/2 \end{cases} \tag{182}$$

where D is the diameter of the photosensitive area of the detector. For a spherical wave (chosen because the integrations are easily performed in closed form) the *H* function is given by (see Equation (89b)

$$H(z,\bar{\kappa}',W) = |E_0|^2 \, e^{-iz\frac{(1-z)L\kappa'^2}{2k}} \int d\bar{r}\, W(\bar{r})\, e^{iz\bar{\kappa}'\cdot\bar{r}}$$

$$= |E_0|^2 \, e^{-\frac{iz(1-z)L\kappa'^2}{2k}} \int_0^{D/2} d\rho\, \rho \int_0^{2\pi} d\phi\, e^{iz\kappa'\rho\cos(\phi-\theta)} \qquad (183)$$

or finally

$$H(z,\bar{\kappa}',W) = \pi\left(\frac{D}{2}\right)^2 |E_0|^2 \left[\frac{2J_1\left(z\,\frac{D}{2}\,\kappa'\right)}{\left(z\,\frac{D}{2}\,\kappa'\right)}\right] e^{-\frac{i\,z(1-z)L\kappa'^2}{2k}} \quad . \qquad (184)$$

The scintillation spectrum, from Eq. (92), is then

$$S_p(\omega) \propto \int_0^1 dz \int_0^\infty d\kappa\, [\kappa^2+(\omega/\omega_0)^2+(1.077/L_0')^2]^{-11/6}$$

$$\times \sin^2\left\{\frac{z(1-z)}{4\pi}\,[\kappa^2+(\omega/\omega_0)^2]\right\}\left[\frac{2J_1\left(z\,\frac{D}{2}'\sqrt{\kappa^2+(\omega/\omega_0)^2}\right)}{z\,\frac{D}{2}'\sqrt{\kappa^2+(\omega/\omega_0)^2}}\right]^2 \quad . \qquad (185)$$

Within the high frequency region we can approximate the $\sin^2$ function by 1/2, extend the z integration to infinity[88], and perform the κ integration to obtain

$$S_p(\omega) \propto \frac{1}{D}\left(\frac{\omega}{\omega_0}\right)^{-11/3} \quad . \qquad (186)$$

Similar results are to be expected for plane or gaussian beam waves. The onset of this so called aperture averaging phenomenon may be determined by equating the formulae for the -8/3 asymptote (derived under the assumption of a point detector) and the -11/3 asymptote for a finite aperture.

This aperture averaging region can also be discerned by physical arguments. At the receiver we observe a series of diffraction patterns of various sizes, ℓ, flowing in the direction of the wind at velocity v. The associated temporal frequency at the output of the detector will therefore be

$$f = v/\ell$$

or

$$\frac{\omega}{\omega_o} = \frac{2\pi}{\ell/\sqrt{\lambda L}} \quad . \tag{187}$$

However for an aperture, D, larger than the dimension ℓ, the detector will integrate over these diffraction patterns [62] thus attenuating the effects of this scale size. Aperture averaging would then occur for frequencies such that

$$\frac{\omega}{\omega_o} \gtrsim \frac{2\pi}{D/\sqrt{\lambda L}} \quad . \tag{188}$$

Therefore aperture averaging should be of little concern if we require that the aperture diameter be much smaller than the Fresnel zone;

$$D << \sqrt{\lambda L} \ .$$

As an example, for a one kilometer range, a HeNe source, and a one centimeter receiver aperture, one would expect to observe aperture averaging for

$$\frac{\omega}{\omega_o} \gtrsim 16 \ .$$

Alternatively, for a velocity of 150 meters/sec., aperture averaging would occur for frequencies

$$f \gtrsim v/D = 15 \text{ KHz}.$$

On the basis of arguments presented in this section it is seen that if we require

$$\ell_o, D << \sqrt{\lambda L} \ , \tag{189}$$

then the inner scale effects and aperture averaging effects should be of little concern in the determination of the scintillation spectrum. This concludes the analysis of the temporal scintillation spectrum of a clean gaussian beam.

F. Summary and Conclusions

Within this chapter we have presented an evaluation of the temporal scintillation spectrum of a clean gaussian beam for the case in which the detector is off-axis to the beam. The off-axis detector problem has not been previously treated in the literature. The general formula for the spectrum derived in Chapter II, was employed in conjunction with a particular model of the index of refraction spatial spectrum, plus the assumption of an off-axis point detector, in deriving an expression which was then evaluated asymptotically and numerically. As a result of the analysis it was shown that the fact that the detector was off axis produces some interesting outer scale-dependent behavior for frequencies below the Fresnel breakpoint. In addition, this low frequency behavior was shown to be dependent upon the location of the detector with respect to the beam axis and wind direction.

Section B was concerned with setting-up the problem. The von-Karman model of the index spectrum together with a gaussian beam source field were used in the expression for the spectrum derived in Chapter II. The assumption of a point detector enabled performance of the integration for the H function of Chapter II. The final expression for the scintillation spectrum was demonstrated to reduce to that which was derived by other authors when the detector was axially located, as well as to the expressions for the plane and spherical wave scintillation spectra when the beam Fresnel number was allowed to go to zero and infinity respectively.

In Section C the expression for the spectrum was evaluated. The first portion of the section was devoted to developing analytic expressions for the spectrum of a gaussian beam with arbitrary Fresnel number. Expressions for the spectrum in terms of hypergeometric functions were developed and asymptotic behavior (for high and low frequencies) was determined by retaining only the first few terms of the series expressions for these functions. Under certain conditions it was found possible to determine closed form expressions for the spectrum asymptotes.

Section D was devoted to a computer evaluation of the spectrum for a particular beam Fresnel number, and a variety of detector locations. In addition, differential path contribution plots were presented for plane and spherical waves, and for gaussian beams with off-axis point detectors.

As a result of this section it was shown that for the detector and beam axis along a line collinear with the wind direction, the scintillation spectrum displayed a peak at $\omega/\omega_0 = \sqrt{3}(1.077/L_0')$ with a +2 power law for frequencies below and a -2/3 power law for frequencies above this point. For the detector and beam axis along a line perpendicular to the wind direction the spectrum showed a breakpoint at $\omega/\omega_0 = 1.077/L_0'$ with a -2/3 power law for frequencies above this point.

The differential path contribution plots showed that despite the fact that a gaussian beam may be well within the Fraunhofer zone ($N > 1$), the off-axis detector causes the path contribution to be peaked at the transmitter (as it is for a plane wave) rather than at midpath (as it is for a spherical wave). This effect has important implications (as will be demonstrated in the next chapter) for cases in which the turbulence strength is non-uniform along the propagation path.

In Section E the analysis was extended to describe finite inner scale and finite aperture effects. Through mathematical and physical arguments it was demonstrated that if the inner scale and the aperture diameter are much smaller than the plane wave Fresnel zone ($\sqrt{\lambda L}$) then their effects can be ignored.

Throughout this chapter the off-axis distance and orientation of the detector have been assumed to be deterministic. For the case in which the laser beam is being steered by a servo system however, these variables could easily be considered random. By assuming appropriate statistical distributions for these variables it would then be possible to determine the effects upon the scintillation spectrum of servo tracking error or noise.

CHAPTER IV

THE DIRTY GAUSSIAN BEAM

A. Introduction

The purpose of this chapter is to develop a model of a dirty, i.e., spatially corrupted laser beam, and to determine the effect upon its scintillation spectrum of the laser beam being dirty. This objective is pertinent because laser beams sometimes do not have the perfect spatial properties which most analytical studies presume. Even if the beam does have good spatial quality, many situations require it to be passed through a window, for example on an aircraft. This unavoidably introduces a certain amount of deterministic spatial noise into the phase and/or amplitude of the beam.

The configuration chosen for analysis within this chapter is that of a clean gaussian beam shining through a window whose transmission function is assumed to be unity except within a small axially located spot where the phase of the incident beam is shifted slightly. This model is appropriate for the situation in which the laser beam is transmitted through a window on which there is an oil spot or an imperfection.

Instead of calculating the actual receiver plane fields due to such a configuration, (as required by the general formula for the scintillation spectrum which was derived in Chapter II) the field immediately past the window is expanded in a two dimensional series of functions involving Gauss-Hermite polynomials. The particular formulation used enables the receiver plane fields to be written down immediately without having to resort to performing the diffraction integrals. Since the size and phase of the spot are chosen a priori, and we wish to use as few terms of the polynomial expansion as possible, an optimization procedure for approximating the fields behind the window is presented.

The integral expression for the scintillation spectrum resulting from our formulation of the dirty beam problem is evaluated numerically and the results presented as a series of plots. As a result of the analysis the dirty beam's scintillation spectrum is shown to be sensitive to turbulence localized in the vicinity of the transmitter. This sensitivity gives rise to low frequency behavior similar to that demonstrated in Chapter III.

In Section B the dirty beam representation is formulated. The dirty beam is modeled as a clean gaussian beam which has been transmitted through a window having a unity transmission function except

for a small axially located spot where the transmission function is complex. The fields to the immediate right of the window are expanded in a complete orthonormal free-space eigenmode set [90,91]. These functions which closely describe the modes of an optical resonator (i.e., a spherical mirror laser) are exact eigenfunctions (within the paraxial approximation) of the free-space wave operator. Therefore an arbitrary field may be expanded in some plane in terms of these functions. The functions then can propagate independently to any other plane and be reassembled with the known weights to determine the actual field. This property of the Gauss-Hermite polynomial expansion is employed in the evaluation of the general expression developed in Chapter II.

By use of Babinet's principle [92] the dirty spot is essentially expanded in terms of a truncated series of laser modes. Since this series is truncated, we present a procedure for optimizing the approximation.

A particular case of the dirty beam problem is treated in Section C. The required integrations are carried out numerically for a variety of detector locations and turbulence strength distributions and the results presented in the form of several plots of spectra.

Section D contains a summary and conclusions.

B. Development of Model

This section is concerned with the formulation of a model of the dirty beam and an optimization procedure for approximating it in terms of eigenmodes of the free space wave operator.

We shall first demonstrate the use of this particular eigenmode expansion as a means of expressing an arbitrary field. The specification of a general field in terms of the Gaussian-Hermite polynomial functions is written as [91]

$$E(x,y,z) = \sum_{m=0}^{\infty} \sum_{n=0}^{\infty} \alpha_{mn} f_m(x,z+z_o) f_n(y,z+z_o) \qquad (190\text{-a})$$

where the f functions are defined as

$$f_m(x,z+z_o) = \left(\frac{2}{\pi}\frac{kN}{2L}\right)^{\frac{1}{4}} \left(\frac{1}{2^m m!}\right)^{\frac{1}{2}} [1-iN(z+z_o)/L]^{m/2}$$

$$\times [1+iN(z+z_o)/L]^{-(m+1)/2} H_m(\sqrt{2\alpha_r(z+z_o)}\, x)\, e^{-\alpha(z+z_o)x^2}, \qquad (190\text{-b})$$

$$\alpha(z+z_0) = \frac{kN/2L}{1+iN(z+z_0)/L} \quad ,$$

$$\alpha_r(z+z_0) \equiv \mathrm{Re}\{\alpha(z+z_0)\} \quad , \qquad (190\text{-c})$$

H_m is the m^{th} order Hermite polynomial [93], N is the beam Fresnel number defined in Equation (115b), and the beam waist is located at $z=-z_0$. Making use of the orthonormality [94] of the mode functions

$$\int_{-\infty}^{\infty} dx\ f_K(x,z+z_0)\ f_L^*(x,z+z_0) = \delta_{KL} \qquad (191)$$

gives the expansion coefficients

$$\alpha_{mn} = \iint_{-\infty}^{\infty} dxdy\ E(x,y,z)\ f_m^*(x,z+z_0)\ f_n^*(y,z+z_0) \quad . \qquad (192)$$

The field of a spherical mirror laser operating in the lowest order transverse spatial mode nominally consists of only the zero-zero eigenmode. If we arbitrarily assume

$$\alpha_{mn} = \begin{cases} \sqrt{\frac{\pi}{2}} ; & m,n=0 \\ 0 ; & m,n\neq 0 \end{cases} \qquad (193)$$

then the field is simply

$$E(x,y,z) = \frac{\sqrt{kN/2L}}{1+iN(z+z_0)/L}\ e^{-\frac{kN/2L}{1+iN(z+z_0)/L}(x^2+y^2)} \quad . \qquad (194)$$

With the exception of the trivial phase factor $\exp[ik(z+z_0)]$, Equation (194) is recognized as the expression for the field used in Chapter III (Equation (115a)). Throughout the remainder of this chapter we assume that the unperturbed laser beam is described by Equation (194).

We now proceed in the development of a particular model for the dirty laser beam.

With reference to Figure 18, we define a circular region at the z=0 plane (the plane of the dirty window) within which the field of Equation (194) is corrupted.

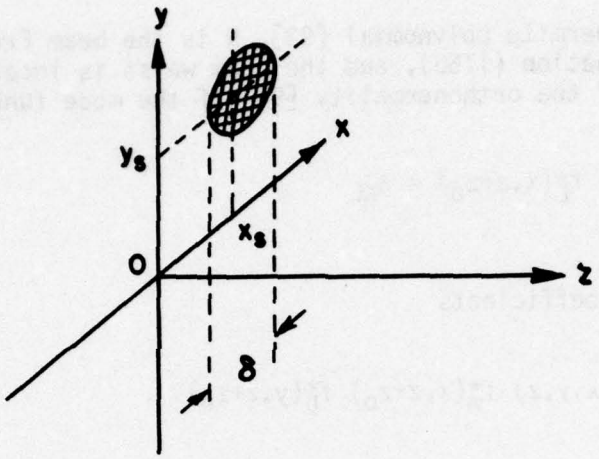

Figure 18--Illustration of phase obstacle.

To the immediate right of the z=0 plane the field is

$$E(x,y,0^+)D_\delta(x-x_s,y-y_s) \tag{195-a}$$

where the window transmission function, D_δ, is given by

$$D_\delta(x-x_s,y-y_s) = \begin{cases} A\, e^{i\mu} & ;\sqrt{(x-x_s)^2+(y-y_s)^2} \leq \delta/2 \\ 1 & ; \text{elsewhere} \end{cases}, \tag{195-b}$$

δ is the diameter of the circular region and the field is given by Equation (194). Equivalently by use of Babinet's principle we may express the field within this plane as

$$E(x,y,0^+) - [1-D_\delta(x-x_s,y-y_s)]E(x,y,0^+) \tag{196}$$

or by defining a new variable, D'_δ,

$$E(x,y,0^+) - D'_\delta(x-x_s,y-y_s)E(x,y,0^+) \quad . \tag{197}$$

In the material to follow, we shall define the complementary field as

$$E^C(x,y,0^+) = D'_\delta(x-x_s,y-y_s)E(x,y,0^+) \tag{198-a}$$

where

$$D'_\delta = \begin{cases} 1-A\, e^{i\mu} & ; \sqrt{(x-x_s)^2+(y-y_s)^2} \leq \delta/2 \\ 0 & ; \text{elsewhere} \end{cases} \quad . \tag{198-b}$$

As an example consider the case in which A=0. Then the complementary field is

$$E^C(x,y,0^+) = \begin{cases} E(x,y,0^+) & ; \sqrt{(x-x_s)^2+(y-y_s)^2} \leq \delta/2 \\ 0 & ; \text{elsewhere} \end{cases} \quad . \tag{199}$$

Within the region to the immediate right of the disc, the complementary field exactly cancels the incident field.

The eigenmode expansion will now be applied to the complementary field:

$$E^C(x,y,z) = \sum_{m=0}^{\infty} \sum_{n=0}^{\infty} \gamma_{mn}\, g_m(x,z+z_1) g_n(y,z+z_1) \quad , \tag{200-a}$$

where the mode functions are given by

$$g_m(x,z+z_1) = \left(\frac{2}{\pi}\frac{kM}{2L}\right)^{\frac{1}{4}} \left(\frac{1}{2^m m!}\right)^{\frac{1}{2}} [1-iM(z+z_1)/L]^{m/2}$$

$$\times\, [1+iM(z+z_1)/L]^{-(m+1)/2}\, H_m(\sqrt{2\beta_r(z+z_1)}\,x)\, e^{-\beta(z+z_1)x^2} \quad , \tag{200-b}$$

$$\beta(z+z_1) = \frac{kM/2L}{1+iM(z+z_1)/L} \quad ,$$

$$\beta_r(z+z_1) \equiv \mathrm{Re}\{\beta(z+z_1)\} \quad , \qquad (200\text{-c})$$

M is the Fresnel number of the complementary beam defined as

$$M = \frac{\lambda L}{\pi W_1^2} \quad , \qquad (200\text{-d})$$

and W_1 is the spotsize of the beam waist which is located at $z=-z_1$.

In Appendix F we approximate the complementary field by the zero-zero term of its eigenmode expansion. This approximation is optimized by minimizing the integral square difference between the actual complementary field and its truncated series approximation.

Also in Appendix F we justify the claim that without loss of generality we can assume the phase obstacle to be axially located within the incident (main) beam. This is subject to the conditions that the detector be near the center of the main beam ($r_o << W(L)$) and that the receiver be in the far field of the main beam.

As shown in this appendix the complementary beam mode expansion coefficient, γ_{oo}, is given by

$$\gamma_{oo} = \pi\sqrt{\frac{2}{\pi}}\, W_o W_1 (1-A\, e^{i\mu})\, \frac{\alpha(z_o)\beta^*(z_1)}{\alpha(z_o)+\beta^*(z_1)}$$

$$\times \left\{1 - e^{-[\alpha(z_o)+\beta^*(z_1)](\delta/2)^2}\right\} \qquad (201\text{-a})$$

and the complementary beam Fresnel number and beam waist location are given by the solution of the simultaneous equations

$$\mathrm{Im}\{\alpha(z_o)\} = \mathrm{Im}\{\beta(z_1)\} \qquad (201\text{-b})$$

and

$$x = \frac{1}{y}\,\ell n\left[1-2xy\left(\frac{1+x}{1-x}\right)\right] - 1 \qquad (201\text{-c})$$

where

$$x = \frac{\beta_r(z_1)}{\alpha_r(z_0)} \tag{201-d}$$

and

$$y = \alpha_r(z_0)\left(\frac{\delta}{2}\right)^2 \quad . \tag{201-e}$$

With the complementary beam thus completely specified, we may proceed, in the manner of the development of Chapter III, to calculate the *H* function. The exception is that the expression for the field in Equation (89-b) is replaced by

$$E(x,y,L) - E_L^C(x,y,L) \quad . \tag{202-a}$$

In our case L=0, and the total field assumes the form of the difference of two gaussian beams:

$$E(x,y,L) - E_0^C(x,y,L) =$$

$$W_0\alpha(L+z_0)e^{-\alpha(L+z_0)(x^2+y^2)} - W_1\beta(L+z_1)e^{-\beta(L+z_1)(x^2+y^2)}$$

$$\times\ 2W_0W_1\ \frac{\alpha(z_0)\beta^*(z_1)}{\alpha(z_0)+\beta^*(z_1)}\ (1-Ae^{i\mu})\left\{1-e^{-[\alpha(z_0)+\beta^*(z_1)](\delta/2)^2}\right\} \quad . \tag{202-b}$$

This completes the discussion of the modeling of the dirty beam and the optimization of the field expansion. These results will be applied in the next section to the calculation of the scintillation spectrum of a particular dirty beam.

C. Evaluation

The modeling of the previous section was applied in the calculation of the scintillation spectrum for a particular configuration; that of a laser beam with a central phase perturbation. The spectrum resulting from this field configuration was calculated for three turbulence models; homogeneous turbulence with a large outer scale, localized turbulence with a small outer scale, and a combination of these two. The detector was assumed to be off-axis.

We evaluated the spectrum resulting from the situation in which a laser beam with waist spotsize (W_0) of 20.6×10^{-6} meter was directed through a dirty window toward a receiver approximately one kilometer distant. The beam waist was located one meter inside the window, and the beam was assumed to have propagated in free space until it passed through the window into the turbulent atmosphere. The phase and diameter of the spot on the window were chosen so that its receiver plane diffraction pattern consisted of a dark spot approximately one meter in diameter. These parameters were respectively μ=5.336 radians and δ=.917 $\times 10^{-3}$ meter. The values of these variables were deduced by numerically calculating the receiver plane diffraction patterns of obstacles of various phases and diameters. Although this procedure supplied the receiver plane fields as required by the general formula for the scintillation spectrum, the computations were lengthy and time consuming. Therefore we resorted to the approximation of the complementary field as outlined in the previous section.

The routine of the previous section gave, for the complementary beam, a waist spotsize, W_1, of 3.146×10^{-4} meter and a beam waist location, $-z_1$, of -.408 meter. For the Helium-Neon laser (λ=.6328 $\times 10^{-6}$ meter) the complementary and main beam Fresnel numbers were respectively 2.04×10^3 and 4.75×10^5, and the receiver plane spotsizes were $W_1(L)$ = .64 meter and $W_0(L)$ = 9.79 meters. The parameters of interest are illustrated in Figure 19.

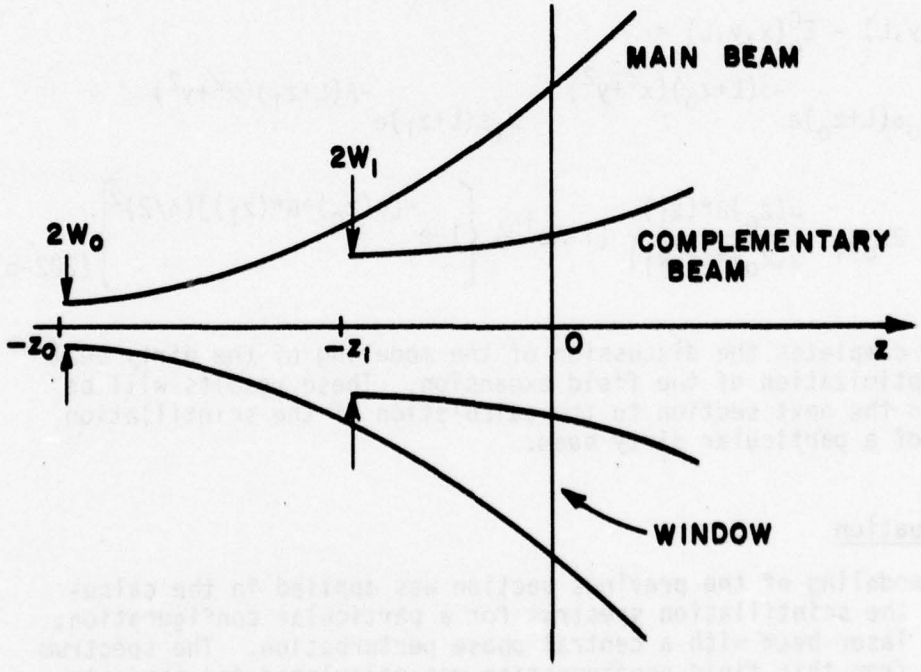

Figure 19--Sketch of transmitter plane fields.

With the beam waist locations and spotsizes for the main and complementary beams determined, the fields required (see Equation (202b)) in the calculation of the H function, and hence the spectrum, were specified. In calculating the H function (Equation (89b)) a point detector at a general location, $\underline{r}=\underline{r}_0$, was assumed.

A digital computer was employed in performing the path and frequency integrations of Equation (92). For the path integral a single eight or 32 point Gaussian quadrature [95,96,97] routine was used. Composite integration [98] using eight point Gaussian quadrature routines was used for the frequency integral. A listing and brief discussion of this program is contained in Appendix G.

Figure 20 shows the spectrum resulting from the dirty beam for an outer scale, L_0, of 100 meters and the detector positioned at $\underline{r}_0$ = (0,.88m). This spectrum is indistinguishable from the spectrum of a clean gaussian beam (see Figure 14 in Chapter III). Little effect of the beam being dirty was to be expected because of the extreme distance of the detector from the diffraction pattern of the phase obstacle ($r_0/W_1(L)$=1.4), and because the detector was still close to the axis of the main beam ($r_0/W_0(L)<<1$).

In Figure 21 we present the spectrum resulting from the same conditions as for Figure 20 except with the detector located at $\underline{r}_0$= (0,.44) ($r_0/W_1(L)$=.7). The low frequency behavior, which is characterized by the break point in the vicinity of $\omega/\omega_0 = 10^{-4}$, is the same as that shown in Chapter III for the off-axis detector. In this case however, the low frequency behavior was due to the detector being off-axis to the complementary beam, not the main beam.

The spectrum resulting from a different turbulence distribution is presented in Figure 22. In this case the outer scale was one meter and the detector location was the same as in Figure 21, however the turbulence structure parameter was specified as

$$C_n^2(z) = \left(\frac{L}{z_m}\right) C_n^2 \, e^{-z\left(\frac{L}{z_m}\right)} \quad , \; 0 \leq z \leq 1 \quad , \tag{203}$$

where z_m was 10 meters. This turbulence strength distribution would be appropriate for a situation in which all the turbulence was confined to a 10 meter thick region, i.e., boundary layer at the transmitter.

From the discussion in Chapter III of the spectrum differential path contribution we deduce that the complementary beam (because of the off-axis detector) interacts more strongly with the turbulence localized near the transmitter than does the main beam. This thought is reinforced by the order of magnitude difference between the low frequency portion of the spectrum in Figure 22 (due primarily to the

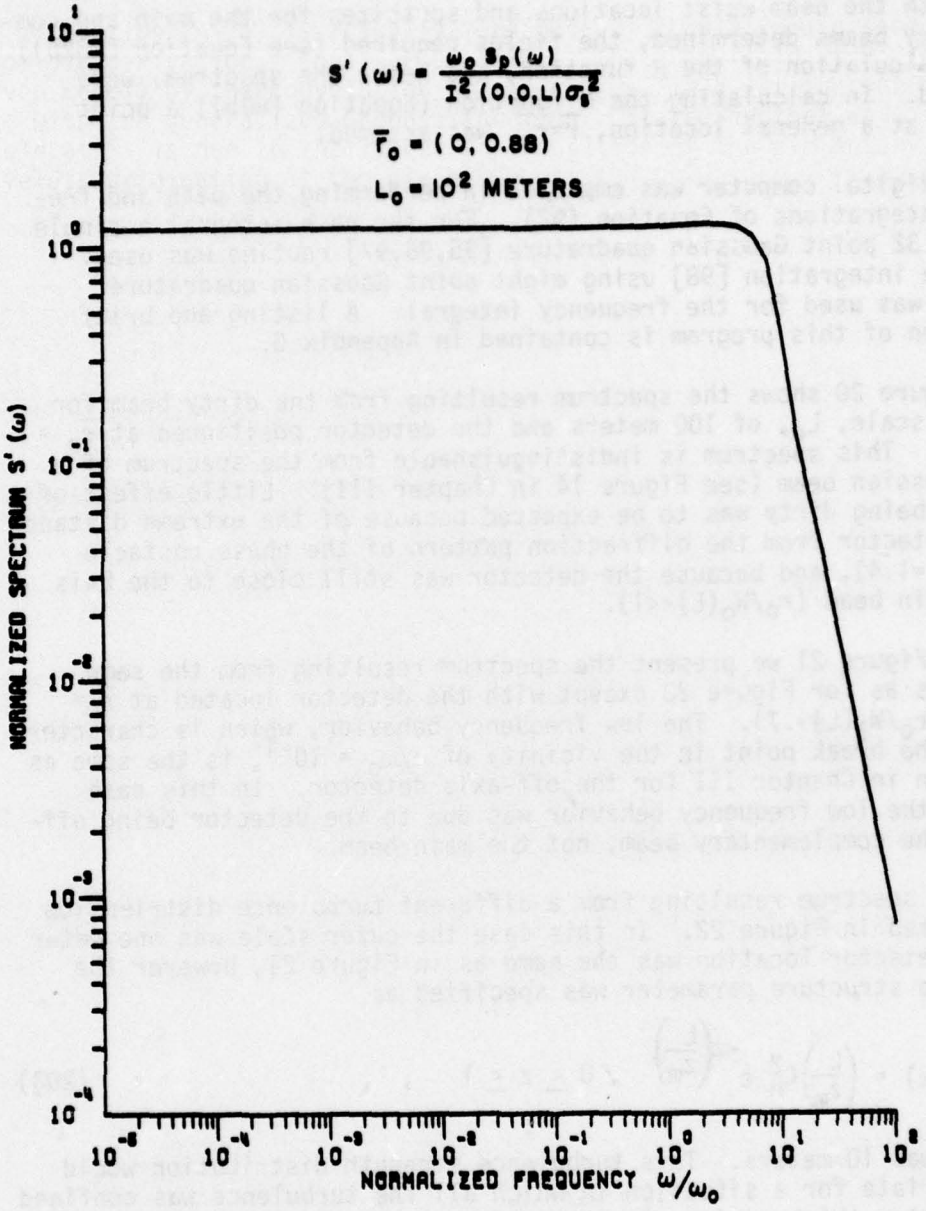

Figure 20--Spectrum for detector off-axis by a large distance.

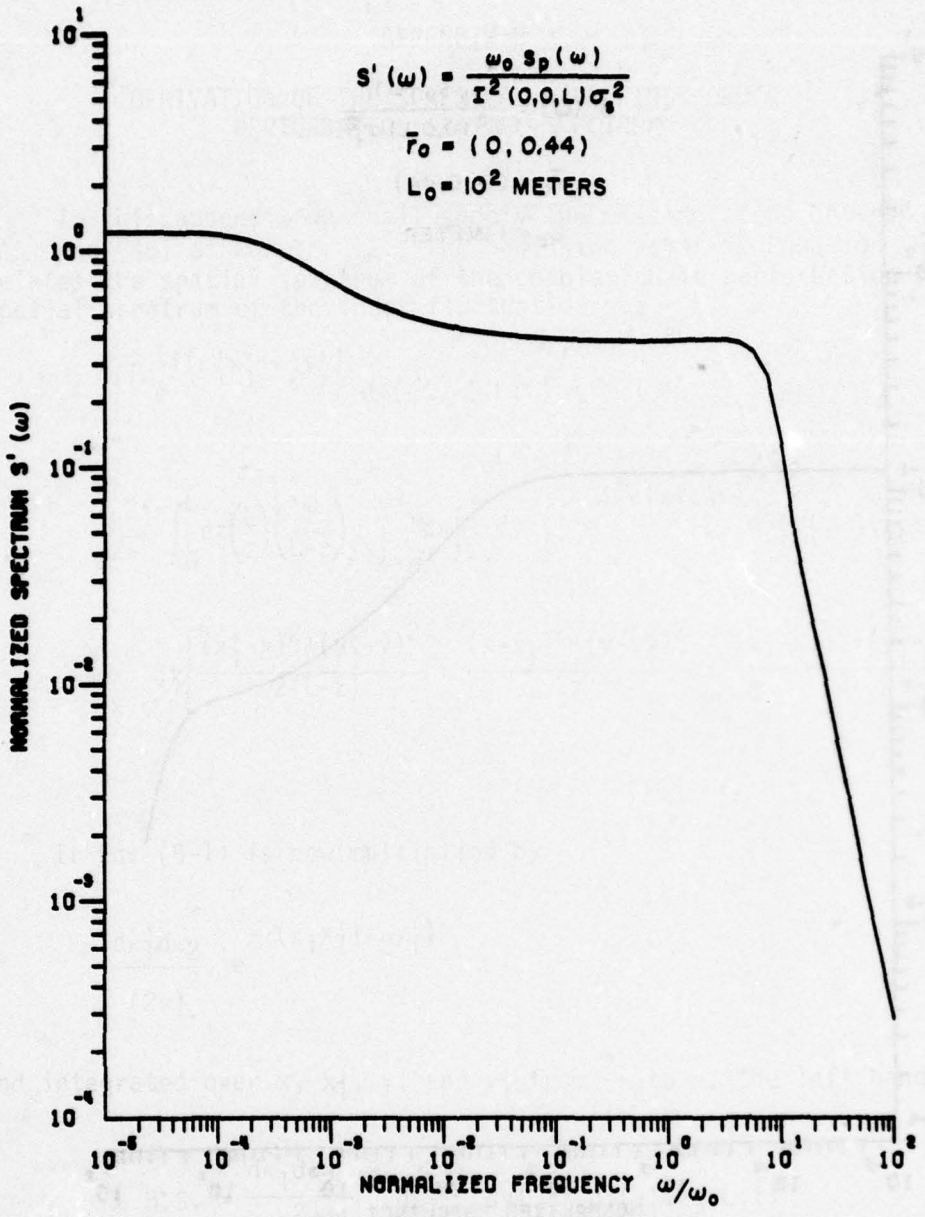

Figure 21--Spectrum for detector near diffraction pattern.

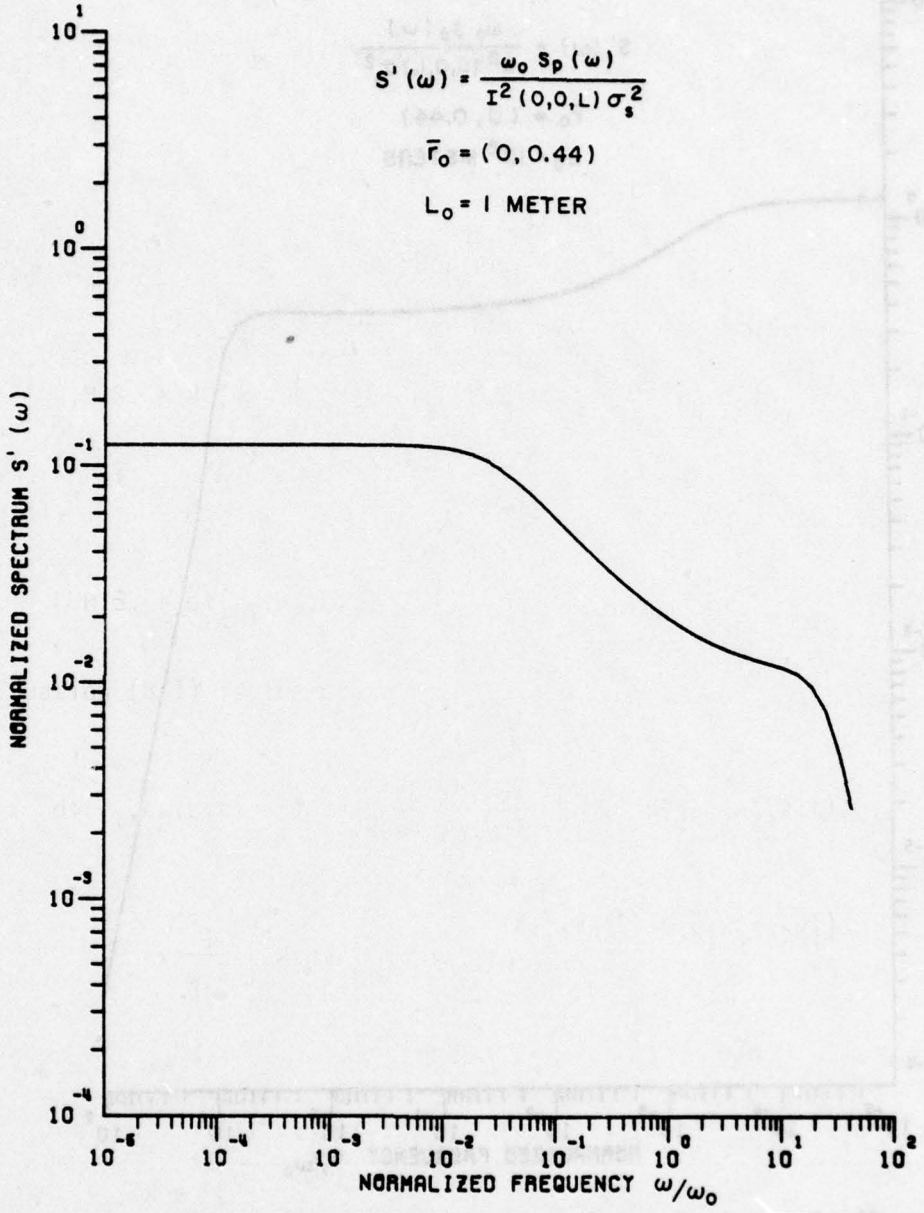

Figure 22--Spectrum for localized turbulence.

complementary beam) and the portion of the spectrum to the immediate left of the Fresnel breakpoint (due to the main beam).

A more realistic model of the turbulence field would contain homogeneous turbulence as well as a boundary layer at the transmitter. This would correspond to the situation in which the laser beam was being directed between two aircraft. In fact, to be totally realistic, we should include a boundary layer at the receiver. However, the differential path contribution plots of Chapter III have shown the insensitivity of the scintillation spectrum to such a turbulence distribution. Therefore the receiver plane boundary layer can be ignored.

Figure 23 shows the spectrum resulting from a combination of localized and distributed turbulence strengths. For this case the turbulence field model used was

$$\Phi_n(\kappa) = C_n^2 \left\{ \alpha\, e^{-z\left(\frac{L}{z_m}\right)} [\kappa^2 + (1.077/L_{01}')^2]^{-11/6} + \beta[\kappa^2 + (1.077/L_{02}')^2]^{-11/6} \right\} \quad , \; 0 \leq z \leq 1 \quad , \tag{204}$$

where the outer scales, L_{01} and L_{02}, were respectively one and 100 meters, the e^{-1} point of the localized turbulence was ten meters and the weights α and β were chosen subject to the restraint

$$\frac{1}{C_n^2 L} \int_0^L du\, C_n^2(u) = 1 \quad . \tag{205}$$

The restriction of Equation (205) was imposed merely to facilitate direct comparison of Figure 23 with the previous results of this chapter and Chapter III. It requires the path integral of the turbulence strength to be a constant. The turbulence model of Figure 22 also satisfies Equation (205). For the spectrum in Figure 23 we chose β=.05. Equation (205) then gave α=95, for a ratio of roughly three orders of magnitude between the turbulence strength in the boundary layer and that in the distributed turbulence. Also indicated in Figure 23 are the two outer scale and two Fresnel breakpoints which are due to the two turbulence strength distributions. This figure is illustrative of the increased sensitivity, of the dirty beam scintillation spectrum, to an inhomogeneous turbulence distribution.

Shown in Figure 24 is the spectrum resulting from a different combination of localized and distributed turbulence. For this case we used

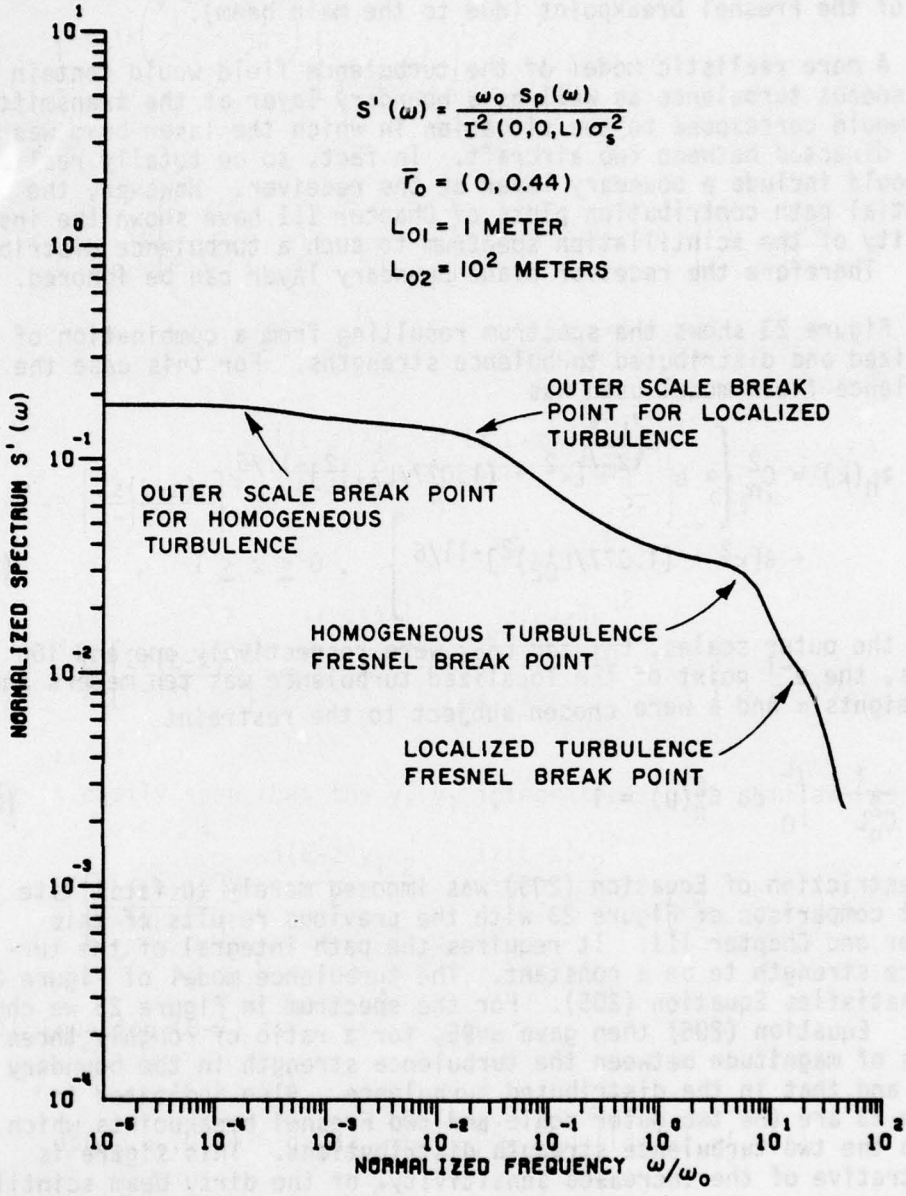

Figure 23--Spectrum for combination of localized and distributed turbulence.

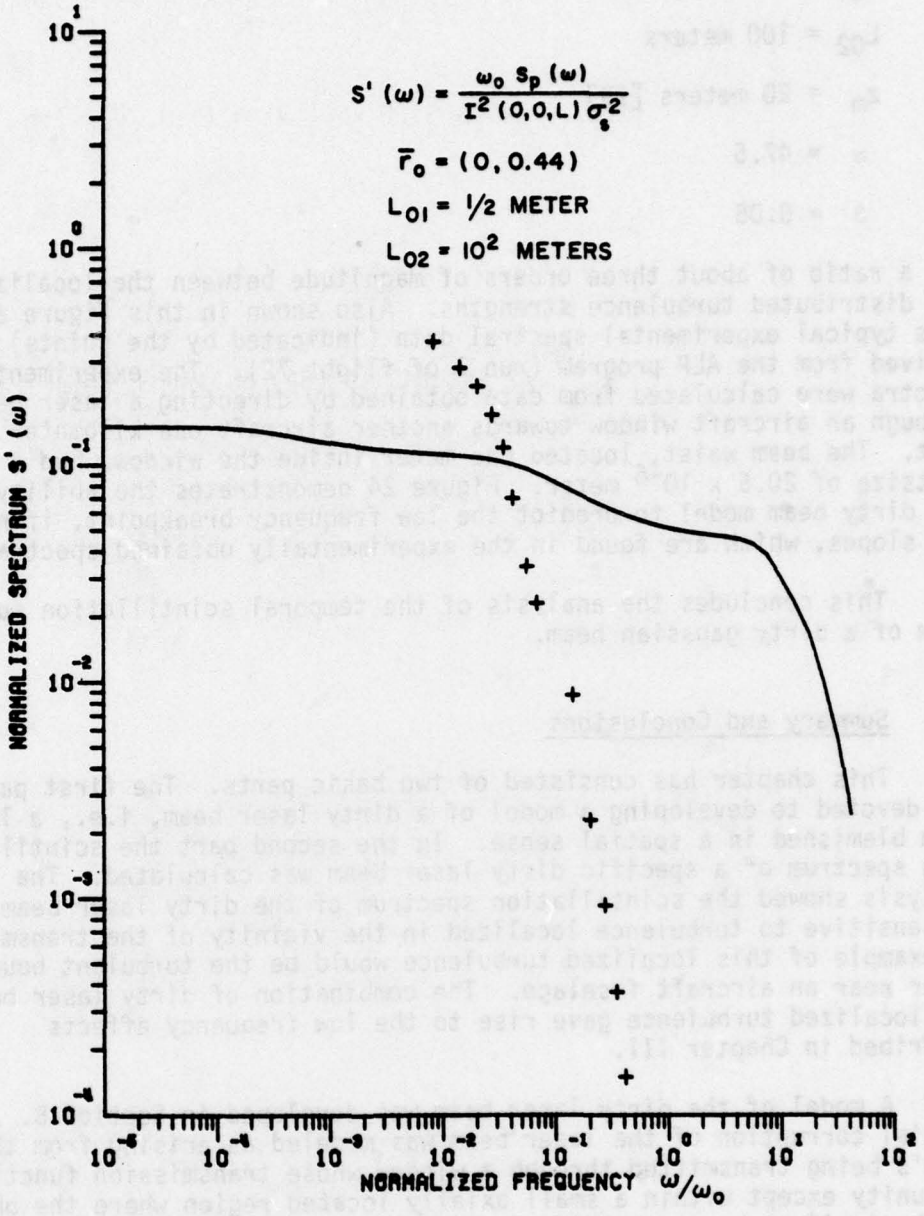

Figure 24--Comparison of experimental and theoretical spectra.

L_{01} = 1/2 meter [87]

L_{02} = 100 meters

z_m = 20 meters [99]

α = 47.5

β = 0.05

for a ratio of about three orders of magnitude between the localized and distributed turbulence strengths. Also shown in this figure are some typical experimental spectral data (indicated by the points) derived from the ALP program (run 7 of flight 72). The experimental spectra were calculated from data obtained by directing a laser beam through an aircraft window towards another aircraft one kilometer distant. The beam waist, located one meter inside the window, had a spotsize of 20.6×10^{-6} meter. Figure 24 demonstrates the ability of the dirty beam model to predict the low frequency breakpoint, if not the slopes, which are found in the experimentally obtained spectra.

This concludes the analysis of the temporal scintillation spectrum of a dirty gaussian beam.

D. Summary and Conclusions

This chapter has consisted of two basic parts. The first part was devoted to developing a model of a dirty laser beam, i.e., a laser beam blemished in a spatial sense. In the second part the scintillation spectrum of a specific dirty laser beam was calculated. The analysis showed the scintillation spectrum of the dirty laser beam to be sensitive to turbulence localized in the vicinity of the transmitter. An example of this localized turbulence would be the turbulent boundary layer near an aircraft fuselage. The combination of dirty laser beam and localized turbulence gave rise to the low frequency effects described in Chapter III.

A model of the dirty laser beam was developed in Section B. The spatial corruption of the laser beam was modeled as arising from the beam's being transmitted through a window whose transmission function was unity except within a small axially located region where the phase of the incident beam was shifted slightly. Using Babinet's Principle the equivalent fields were expanded, within the transmitter plane, in a series of eigen-modes of the free space wave operator. This expansion enabled the receiver plane fields to be written down immediately by inspection.

The phase and diameter of the phase obstacle were assumed to have been chosen a priori and an optimized expansion was developed which minimized the integral square error between the actual complementary field and its truncated series approximation. This optimization scheme was used to approximate the complementary field by its lowest order eigen mode so that, essentially the dirty beam consisted of the weighted sum of two gaussian beams.

Section C of this chapter dealt with a computer evaluation of the scintillation spectrum of a particular formulation of the dirty gaussian beam. Analyses were provided for three different index of refraction spatial spectra: 1) homogeneous turbulence with a large outer scale, 2) localized turbulence with a small outer scale, and 3) a combination of these two. The third turbulence distribution is appropriate when the laser beam originates from an aircraft. Experimental evidence [87] supports this assumption of a turbulent boundary layer typified by outer scales on the order of one meter or less. The results of the evaluation showed that the scintillation spectrum of a dirty beam displays behavior similar to that of a clean laser beam with an off-axis detector. In addition, it was demonstrated that the scintillation spectrum of a dirty beam can display increased sensitivity to inhomogeneous turbulence strengths.

This completes the analysis of the scintillation spectrum of a dirty gaussian beam. Although the model developed herein was a simple one, we have shown it to qualitatively describe a much broader class of situations. In practice, an actual laser beam may be expected to contain a much more complicated spatial noise component. However, we have demonstrated that the scintillation spectrum is largely independent of the actual structure of this spatial noise.

In the next chapter we shall summarize the work presented in this and the preceding chapters, and present additional discussion and comments.

CHAPTER V

SUMMARY AND DISCUSSION

A. Summary and Conclusions

The effort described herein was aimed at developing a simplified formula for temporal scintillation spectra and applying it to the analysis of the scintillation spectrum of a dirty, i.e., spatially corrupted, laser beam. The major accomplishments of this work were:

1) the derivation of a general but very compact expression for the temporal scintillation spectrum of an arbitrary extended source,

2) interpretation of the scintillation spectrum formula in terms of a phase grating model of the index of refraction field,

3) asymptotic and numerical calculation of spectra for a gaussian beam with an off-axis detector,

4) modeling of a spatially blemished laser beam, and

5) qualitative but not exact quantitative agreement between theoretically predicted and experimentally obtained scintillation spectra.

Use was made of the so-called Extended Huygens Fresnel integral to derive a formula for the temporal scintillation spectrum of an arbitrary source. This expression was in terms of the second order spatio-temporal statistical moments of spherical waves. Expressions for these statistical moments were derived by the method of smooth perturbations, the weak turbulence approximation was employed, and various observations made, to produce the final expression for the spectrum. This final formula for the scintillation spectrum was in terms of the free-space receiver plane fields of an unspecified extended source, and in terms of an extended receiver. A phase grating model of the atmospheric turbulence field provided an interpretation of this expression.

The general formula was used to derive an expression for the scintillation spectrum of a clean laser beam with an off-axis point detector. A thorough asymptotic evaluation of this expression, valid for arbitrary beam Fresnel number, was provided and numerical results were given from a computer evaluation for a typical gaussian beam.

As a result of the analysis it was shown that, by moving the detector off-axis to the beam, an additional breakpoint or peak (depending upon the relationship of the detector and beam axis with respect to the wind direction) was introduced in the spectrum at a frequency below the Fresnel breakpoint.

The dirty laser beam was envisioned as arising from the propagation of an initially clean gaussian beam through a window and then into the turbulent atmosphere. The window's transmission function was assumed to be unity except within a small axial region in which the incident field was shifted slightly in phase. Babinet's principle was used to calculate the equivalent transmitter plane field which was then expanded in a series of eigen modes of the free space wave operator. This expansion enabled the calculation of the free space receiver plane field, as required in the general formula, by inspection rather than by performing the diffraction integral over the transmitter plane field. The series approximation to the transmitter plane field was truncated. A procedure therefore was given which optimized the expansion.

This modeling procedure was applied to the description of a particular dirty beam and the resulting expression was evaluated numerically on a digital computer. The results showed the dirty beam scintillation spectrum to be sensitive to turbulence in the vicinity of the transmitter despite the fact that the beam Fresnel number was very large. Specifically, the spectrum displayed a low frequency outer scale dependent behavior like that of a clean gaussian beam with an off-axis detector. It was demonstrated that this particular model of a dirty laser beam qualitatively predicts the scintillation spectrum of a much more complicated dirty gaussian beam.

B. Discussion

The general formula for the temporal scintillation spectrum is of significant worth because of its simplicity, flexibility, and easy interpretation. Its principle utility is in predicting the spectrum for complicated extended source fields (for example the field of a laser with cassegrainian optics, or a spatially noisy laser beam) and for complicated receiver apertures. With this formula it is possible therefore to easily predict the scintillation spectrum under realistic conditions rather than the highly idealized situations which other analyses presume.

The major limitation of our formula is its restriction to the weak turbulence regime. Thus one of the suggestions for future analytic work concerns its generalization to the strong turbulence regime. There are two methods by which this problem may be attacked. First, expressions for the spherical wave statistical moments could be found which are valid within the multiple scattering domain.

Second, an heuristic derivation, in the manner of Section E, Chapter II, using a phase grating model of the turbulence field could be attempted.

Another topic of further analytical effort could be the consideration of the detector location as being a random function of time. This is equivalent to the laser pointing direction being a random variable. Under the assumption of an appropriate statistical behavior for the detector location, it should be possible to determine the effect upon the measured temporal scintillation spectrum.

Throughout this paper we have assumed the spatial noise structure of the initial laser beam to be non-periodic. Perhaps a more realistic model of a dirty laser beam should also contain a certain amount of periodic spatial noise. This situation would be encountered when the laser beam is passed through a window and is multiply reflected at the two surfaces.

For future experimental effort we have a number of suggestions.

The easiest experiment to perform would be aimed at verifying the predicted low frequency behavior of the spectrum due to an off-axis detector. This should be a simple method of determining the outer scale of turbulence.

In case the laser beam is being aimed by a pointer-tracker, it would be interesting to calculate the temporal power spectra of the servo system error signals.

Finally, we suggest a closely controlled experiment in which the source field is perturbed in a known manner. The resultant data should provide information on the routinely encountered problem of a dirty laser beam.

APPENDIX A

THE EXTENDED HUYGENS-FRESNEL INTEGRAL

This appendix is devoted to a discussion of the application of the Green's function technique to the problem of propagation within a randomly inhomogeneous medium. In the literature this generalized Green's function technique is commonly referred to as the Extended Huygens-Fresnel Principle.

It can be demonstrated [100] that at optical frequencies (wavelengths much shorter than the inner scale of turbulence) polarization effects are negligible. We are therefore justified in employing the scalar form of the wave equation.

$$[\nabla^2+k^2n^2(\overline{R})]E(\overline{R}) = 0, \tag{A-1}$$

where the index of refraction is a random function of position. We now propose the existence of a Green's function such that

$$[\nabla^2+k^2n^2(\overline{R})]G(\overline{R},\overline{R}') = -4\pi\delta(|\overline{R}-\overline{R}'|). \tag{A-2}$$

By left-multiplying Equation (A-1) by $G(\overline{R},\overline{R}')$ and Equation (A-2) by $E(\overline{R})$, subtracting the two resulting equations, and integrating over the scattering volume we obtain

$$\int_V d\overline{R}[G(\overline{R},\overline{R}')\nabla^2E(\overline{R})-E(\overline{R})\nabla^2G(\overline{R},\overline{R}')]$$

$$= 4\pi\int_V d\overline{R}\ E(\overline{R})\delta(|\overline{R}-\overline{R}'|) = 4\pi E(\overline{R}')\ . \tag{A-3}$$

Figure 1 illustrates the geometry of interest. Point P_o denotes the source point and P_1 the field point, Σ and Σ' the surfaces bounding the scattering volume v and $\hat{N}$ the outward directed unit normal to the surface.

If the first and second partial derivatives of G and E are single valued and continuous on Σ and Σ' we can make use of Green's second identity, which when applied to Equation (A-3) yields

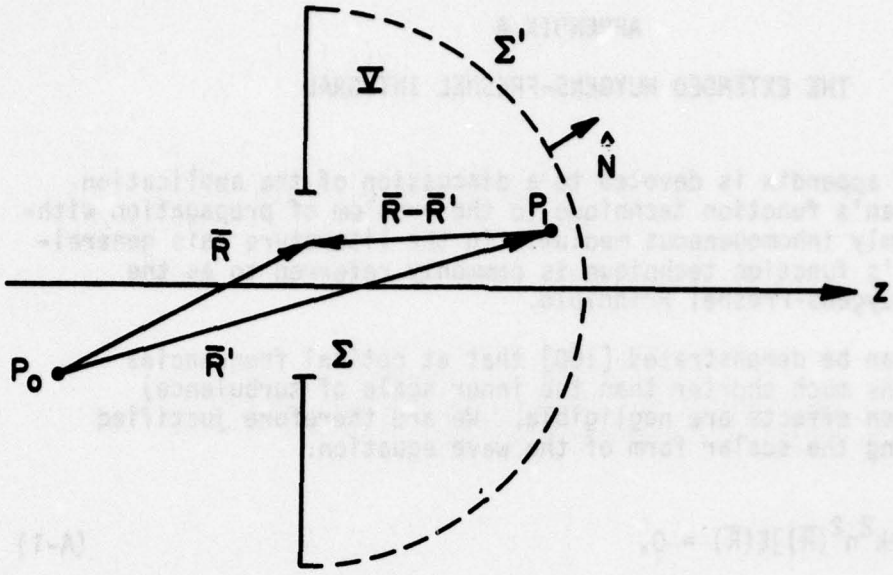

Figure A-1--Illustration of variables pertinent to Green's function technique.

$$E(\bar{R}') = \frac{1}{4\pi} \int_{\Sigma+\Sigma'} [G(\bar{R},\bar{R}')\nabla E(\bar{R}) - E(\bar{R})\nabla G(\bar{R},\bar{R})]\cdot\hat{N}\, dA. \qquad \text{(A-4)}$$

The component of the gradient operator in the direction normal to the surface we shall denote as

$$\nabla(\quad)\cdot\hat{N} = \frac{\partial(\quad)}{\partial N} \qquad \text{(A-5)}$$

so that Equation (A-4) may be written

$$E(\bar{R}') = \frac{1}{4\pi} \int_{\Sigma+\Sigma'} [G(\bar{R},\bar{R}') \frac{\partial}{\partial N} E(\bar{R}) - E(\bar{R}) \frac{\partial}{\partial N} G(\bar{R},\bar{R}')]dA \qquad \text{(A-6)}$$

Assuming that $E(\bar{R})$ satisfies the Sommerfeld Radiation condition [101], so that the integral along Σ' can be neglected Equation (A-6) becomes

$$E(\bar{R}') = \frac{1}{4\pi} \int_{\Sigma} \left(G \frac{\partial E}{\partial N} - E \frac{\partial G}{\partial N} \right) ds, \qquad \text{(A-7)}$$

where in the interest of notational simplicity we have dropped the explicit dependence of E and G upon $\bar{R}$ and $\bar{R}'$.

For the field of a point source

$$E(\bar{R}) = \frac{e^{ikR}}{R} \qquad \text{(A-8)}$$

the partial derivative normal to the surface Σ is

$$\frac{\partial E}{\partial N} = E\left(ik - \frac{1}{R}\right) \frac{\partial R}{\partial N} . \qquad \text{(A-9)}$$

If we assume $R >> 1/k$, i.e., the surface Σ is many wavelengths removed from the point source at p_o, then we have

$$\frac{\partial E}{\partial N} \approx ikE(\bar{R}) \frac{\partial R}{\partial N} . \qquad \text{(A-10)}$$

Using the notation

$$\frac{\partial R}{\partial N} = -\hat{R} \cdot \hat{z} , \qquad \text{(A-11)}$$

in which the circumflex accent denotes a unit vector, we have

$$\frac{\partial E}{\partial N} \approx -ikE(\bar{R})\hat{R} \cdot \hat{z} . \qquad \text{(A-12)}$$

We now claim [41] that the generalized Green's function can be expressed as

$$G(\bar{R},\bar{R}') = \frac{e^{ik|\bar{R}-\bar{R}'|+\psi(\bar{R},\bar{R}')}}{|\bar{R}-\bar{R}'|} \qquad \text{(A-13)}$$

where ψ is a complex function arising from propagation through the inhomogeneous medium. The perturbation, ψ, to the field of a spherical wave is obtained by solving the scalar wave equation (Equation (A-1)) for the Green's function, G, rather than for the field, E. However, for the purposes of this discussion, we need only to bound the magnitude of ψ. This task is easily accomplished by inspecting ψ within the geometrical optics domain ($\sqrt{\lambda L} < \ell_o$). Under this condition we find that [41]

$$\psi(\bar{R},\bar{R}') = ik \int n_1(s)ds \qquad \text{(A-14)}$$

where

$$s = |\bar{R}-\bar{R}'|$$

and we have used Reynold's convention [102] on the index field

$$n(\bar{R}) = n_1(\bar{R}) + < n(\bar{R}) > = n_1(\bar{R}) + 1.$$

The generalized Green's function as given by Equations (A-13) and (A-14) can be shown to satisfy the homogeneous wave equation (A-1) if the term proportional to ∇n_1 is neglected. (The polarization term [100] in the wave equation, which is a function of ∇n_1, was neglected in obtaining Equation (A-1).)

Now the partial derivative of the Green's function is given by

$$\frac{\partial G}{\partial N} = G\left[\left(ik - \frac{1}{s}\right)\frac{\partial s}{\partial N} + \frac{\partial \psi}{\partial N}\right] . \qquad \text{(A-15)}$$

For $s >> 1/k$ Equation (A-15) is

$$\frac{\partial G}{\partial N} \approx ikG\left[\frac{\partial s}{\partial N} + \frac{1}{ik}\frac{\partial \psi}{\partial N}\right] . \qquad \text{(A-16)}$$

Within the geometrical optics domain

$$\frac{1}{ik}\frac{\partial \psi}{\partial N} = \frac{\partial}{\partial N}\int n_1(s)ds = \frac{\partial s}{\partial N}\frac{\partial}{\partial s}\int n_1(s)ds$$

$$\frac{1}{ik}\frac{\partial \psi}{\partial N} = \frac{\partial s}{\partial N}\, n_1(s). \qquad \text{(A-17)}$$

Since

$$\left|\frac{1}{ik}\frac{\partial \psi}{\partial N}\right| \sim |n_1(s)| << 1, \qquad \text{(A-18)}$$

and $\frac{\partial s}{\partial N} \sim 1$, Equation (A-15) becomes

$$\frac{\partial G}{\partial N} = -ikG(\bar{R},\bar{R}')\,\hat{s}\cdot\hat{z}, \qquad \text{(A-19)}$$

where we have defined

$$\frac{\partial s}{\partial N} = -\hat{s} \cdot \hat{z} \ .$$

With Equations (A-12) and (A-19) the expression for the field at p_1 becomes

$$E(\overline{R}') = - \frac{ik}{4\pi} \int G(\overline{R},\overline{R}')E(\overline{R})(\hat{R}\cdot\hat{z} - \hat{s}\cdot\hat{z})dA. \qquad \text{(A-20)}$$

If we make the paraxial approximation, i.e., restrict our attention to small angles with respect to the axis of propagation, we can approximate the obliquity factor [103] and the Green's functions respectively by

$$\hat{R}\cdot\hat{z} - \hat{s}\cdot\hat{z} \approx 2$$

and

$$G(\overline{R},\overline{R}') \approx \frac{e^{ik|\overline{R}-\overline{R}'|+\psi(\overline{R},\overline{R}')}}{L} \ .$$

With these approximations Equation (A-20) becomes

$$E(\overline{R}') = \frac{-ik}{2\pi L} \int E(\overline{R})e^{ik|\overline{R}-\overline{R}'|+\psi(\overline{R},\overline{R}')} \, d\overline{R} \ . \qquad \text{(A-21)}$$

Equation (A-21) is the final result of this appendix.

Although in the preceding discussion we restricted our attention to the case in which ψ was purely imaginary, it is in general complex. This approximation was merely a device to enable the neglect of the term involving the partial derivative of ψ. The actual expression for ψ is obtained by solving the scalar wave equation for the generalized Green's function. This Green's function is simply the field (which has been perturbed in phase and magnitude due to propagation through the turbulent atmosphere) of a point source. An approximate expression for the complex phase perturbation, ψ, is derived by Tatarski [52].

Equation (A-21) is actually more general than it would seem from our derivation. This formula states that the field at $\bar{R}'$ is given merely by the convolution of the source field, at the surface $\bar{R}'$, with the generalized Green's function. Stated another way, the field at $\bar{R}'$ is due to the linear superposition of the elementary wavelets originating at the plane $\bar{R}$.

APPENDIX B

DERIVATION OF THE SPHERICAL WAVE FIRST ORDER PERTURBATION SPATIAL SPECTRUM

In this appendix we shall supply the missing steps between Equations (45) and (46) of Chapter II. The beginning point is Equation (45) which relates the spatial spectrum of the complex phase perturbation ψ to the spatial spectrum of the index fluctuations ν;

$$\iint_{-\infty}^{\infty} e^{i(\kappa_1' x_1' + \kappa_2' y_1')} \, d\Phi(\kappa_1', \kappa_2', L; t) =$$

$$\frac{k^2}{2\pi} \int_0^L dz \left(\frac{L}{z}\right)\left(\frac{1}{L-z}\right) \int_{-\infty}^{\infty} dx \int_{-\infty}^{\infty} dy \iint_{-\infty}^{\infty} e^{i(\kappa_1' x + \kappa_2' y)} \, d\nu(\kappa_1', \kappa_2', z; t)$$

$$\times \, e^{ik\left[\frac{(x_1'-x)^2+(y_1'-y)^2}{2(L-z)} + \frac{(x-x_i)^2+(y-y_i)^2}{2z} - \frac{(x_1'-x_i)^2+(y_1'-y_i)^2}{2L}\right]} . \tag{B-1}$$

If Eq. (B-1) is now multiplied by

$$\frac{d\kappa_1 d\kappa_2}{(2\pi)^2} \, e^{-i(\kappa_1 x_1' + \kappa_2 y_1')} \tag{B-2}$$

and integrated over x, x_1', y, and y_1' from $-\infty$ to ∞, the left hand side is

$$\text{L.H.S.} = \frac{d\kappa_1 d\kappa_2}{4\pi^2} \int_{-\infty}^{\infty} dx_1' \int_{-\infty}^{\infty} dy_1' \iint_{-\infty}^{\infty} d\Phi(\kappa_1', \kappa_2', L; t)$$

$$\times \, e^{i(\kappa_1' x_1' + \kappa_2' y_1') - i(\kappa_1 x_1' + \kappa_2 y_1')} . \tag{B-3}$$

Interchanging orders of integration gives

$$\text{L.H.S.} = d\kappa_1 d\kappa_2 \iint_{-\infty}^{\infty} d\Phi(\kappa_1', \kappa_2', L; t) \left\{ \frac{1}{2\pi} \int_{-\infty}^{\infty} dx_1' \, e^{ix_1'(\kappa_1' - \kappa_1)} \right\}$$

$$\times \left\{ \frac{1}{2\pi} \int_{-\infty}^{\infty} dy_1' \, e^{iy_1'(\kappa_2' - \kappa_2)} \right\} \qquad \text{(B-4)}$$

which is

$$\text{L.H.S.} = d\kappa_1 d\kappa_2 \iint_{-\infty}^{\infty} d\Phi(\kappa_1', \kappa_2', L; t) \delta(\kappa_1' - \kappa_1) \delta(\kappa_2' - \kappa_2) \qquad \text{(B-5)}$$

or finally

$$\text{L.H.S.} = d\Phi(\kappa_1, \kappa_2, L; t) \quad . \qquad \text{(B-6)}$$

Equation (B-1) is therefore

$$d\Phi(\kappa_1, \kappa_2, L; t) = d\kappa_1 d\kappa_2 \frac{k^2}{2\pi} \int_0^L \frac{dz}{L-z} \left(\frac{L}{z} \right) \iint_{-\infty}^{\infty} d\nu(\kappa_1', \kappa_2', z; t)$$

$$\times \frac{1}{4\pi^2} \iint_{-\infty}^{\infty} dx dy \iint_{-\infty}^{\infty} dx_1' dy_1' \, e^{i(\kappa_1' x + \kappa_2' y) - i(\kappa_1 x_1' + \kappa_2 y_1')}$$

$$\times e^{ik\left[\frac{(x_1' - x)^2 + (y_1' - y)^2}{2(L-z)} + \frac{(x - x_i)^2 + (y - y_i)^2}{2z} - \frac{(x_1' - x_i)^2 + (y_1' - y_i)^2}{2L} \right]}.$$

(B-7)

The x, x_1' integrals only are

$$\frac{1}{2\pi}\int_{-\infty}^{\infty}dx\int_{-\infty}^{\infty}dx_1' \; e^{i(\kappa_1' x-\kappa_1 x_1')} \; e^{ik\left[\frac{(x_1'-x)^2}{2(L-z)}+\frac{(x-x_i)^2}{2z}-\frac{(x_1'-x_i)^2}{2L}\right]}$$

$$=\frac{1}{2\pi}\int_{-\infty}^{\infty}dx\int_{-\infty}^{\infty}dx_1' \; e^{i(\kappa_1' x-\kappa_1 x_1')} \tag{B-8a}$$

$$\times\, e^{ik\left[\frac{x_1'^2-2x_1'x+x^2}{2(L-z)}+\frac{x^2-2xx_i+x_i^2}{2z}-\frac{x_1'^2-2x_1'x_i+x_i^2}{2L}\right]} \tag{B-8b}$$

$$=e^{ik\left(\frac{x_i^2}{2z}-\frac{x_i^2}{2L}\right)}\frac{1}{2\pi}\int_{-\infty}^{\infty}dx_1' \; e^{-i\kappa_1 x_1'} \; e^{ik\left[\frac{x_1'^2}{2(L-z)}-\frac{x_1'^2-2x_1'x_i}{2L}\right]} \tag{B-8c}$$

$$\times\int_{-\infty}^{\infty}dx\; e^{i\kappa_1' x} \; e^{ik\left[\frac{-2x_1'x+x^2}{2(L-z)}+\frac{x^2-2xx_i}{2z}\right]} \; .$$

The exponent of the x integrand only is

$$x^2\left[\frac{ik}{2z}+\frac{ik}{2(L-z)}\right]-2x\left[\frac{ikx_1'}{2(L-z)}-\frac{i\kappa_1'}{2}+\frac{ikx_i}{2z}\right] \; . \tag{B-9}$$

This is of the form Ax^2-2xB. Completing the square and performing the x integration gives the following:

$$\int_{-\infty}^{\infty}dx\; e^{Ax^2-2xB}=e^{-B^2/A}\int_{-\infty}^{\infty}dx\; e^{A(x-B/A)^2} \tag{B-10}$$

$$=\sqrt{\frac{\pi}{-A}}\; e^{-B^2/A} \; .$$

The x, x_1' integrals are then

$$\frac{1}{2\pi} e^{ik\left(\frac{x_i^2}{2z} - \frac{x_i^2}{2L}\right)} \left[\frac{2z(L-z)\pi}{-ikL}\right]^{\frac{1}{2}} \int_{-\infty}^{\infty} dx_1' \, e^{-i\kappa_1 x_1'}$$

$$e^{ik\left[\frac{x_1'^2}{2(L-z)} - \frac{x_1'^2 - 2x_1'x_i}{2L}\right]} \quad e^{\frac{-ikz(L-z)}{2L}\left[\frac{x_i}{z} + \frac{x_1'}{L-z} - \frac{\kappa_1'}{k}\right]^2} \tag{B-11a}$$

$$= \left[\frac{2z(L-z)\pi}{-ikL}\right]^{\frac{1}{2}} e^{\frac{i(L-z)x_i\kappa_1'}{L} - \frac{iz(L-z)\kappa_1'^2}{2kL}} \frac{1}{2\pi} \int_{-\infty}^{\infty} dx_1' \, e^{-ix_1'\left(\kappa_1 - \kappa_1'\frac{z}{L}\right)} \tag{B-11b}$$

$$= \frac{L}{z}\left[\frac{2z(L-z)\pi}{-ikL}\right]^{\frac{1}{2}} e^{\frac{i(L-z)x_i\kappa_1'}{L} - \frac{iz(L-z)\kappa_1'^2}{2kL}} \delta\left(\kappa_1' - \frac{L}{z}\kappa_1\right) . \tag{B-11c}$$

It is easily seen that the y, y_1' integrations give similar results;

$$\frac{L}{z}\left[\frac{2z(L-z)\pi}{-ikL}\right]^{\frac{1}{2}} e^{\frac{i(L-z)y_i\kappa_2'}{L} - \frac{iz(L-z)\kappa_2'^2}{2kL}} \delta\left(\kappa_2' - \frac{L}{z}\kappa_2\right) \tag{B-12}$$

so that Equation (B-7) is

$$d\Phi(\kappa_1,\kappa_2,L;t) = d\kappa_1 d\kappa_2 \frac{k^2}{2\pi} \int_0^L \frac{dz}{L-z}\left(\frac{L}{z}\right) \iint_{-\infty}^{\infty} d\nu(\kappa_1',\kappa_2',z;t)$$

$$\times \left(\frac{L}{z}\right)^2 \left[\frac{2z(L-z)\pi}{-ikL}\right] \delta\left(\kappa_1' - \frac{L}{z}\kappa_1\right) \delta\left(\kappa_2' - \frac{L}{z}\kappa_2\right)$$

$$\times e^{\frac{i(L-z)}{L}(x_i\kappa_1' + y_i\kappa_2') - \frac{iz(L-z)}{2kL}(\kappa_1'^2 + \kappa_2'^2)} \tag{B-13}$$

Performing the κ' integrations then gives the final answer;

$$d\phi(\kappa_1,\kappa_2,L;t) = ik \int_0^L dz\, d\nu\left(\frac{L}{z}\kappa_1, \frac{L}{z}\kappa_2, z; t\right)$$

$$\times\, e^{\frac{i(L-z)}{z}\bar{r}_i\cdot\bar{\kappa}}\; e^{\frac{-i(L-z)}{2k}\frac{L}{z}\kappa^2} \qquad \text{(B-14)}$$

which is simply Equation (46) of Chapter II.

APPENDIX C

THE WEAK TURBULENCE APPROXIMATION

This appendix is devoted to a description of the conditions under which we are justified in making the weak turbulence approximation as it is employed in Section D of Chapter II.

The weak turbulence approximation requires that

$$|\alpha|, |\beta| \ll 1 \quad , \tag{C-1}$$

where

$$\alpha = \frac{1}{2}\left[D_W(\bar{r}_1-\bar{r}_2;0;0) + D_W(\bar{r}_3-\bar{r}_4;0;0)\right] \tag{C-2}$$

and

$$\begin{aligned}\beta = -\frac{1}{2}\Big[&D_W(\bar{r}_1-\bar{r}_4;\bar{r}'_1-\bar{r}'_2;\tau) + D_W(\bar{r}_2-\bar{r}_3;\bar{r}'_1-\bar{r}'_2;\tau) \\ &- D_W(\bar{r}_1-\bar{r}_3;\bar{r}'_1-\bar{r}'_2;\tau) - D_W(\bar{r}_2-\bar{r}_4;\bar{r}'_1-\bar{r}'_2;\tau)\Big] \\ &+ 2\Big[C_\chi(\bar{r}_1-\bar{r}_3;\bar{r}'_1-\bar{r}'_2;\tau) + C_\chi(\bar{r}_2-\bar{r}_4;\bar{r}'_1-\bar{r}'_2;\tau) \\ &+ iC_{\chi S}(\bar{r}_1-\bar{r}_3;\bar{r}'_1-\bar{r}'_2;\tau) - iC_{\chi S}(\bar{r}_2-\bar{r}_4;\bar{r}'_1-\bar{r}'_2;\tau)\Big] \quad .\end{aligned} \tag{C-3}$$

DISCUSSION OF α

From the results of Chapter II, Section C, viz. Equation (76), we can express α as

$$\alpha = 2k^2L^2 \iint_{-\infty}^{\infty} d\bar{\kappa} \left\{\int_0^{1/2} dz \int_0^{2z} d\rho + \int_{1/2}^{1} dz \int_0^{2(1-z)} d\rho\right\}$$

$$\times F_n(\kappa_1,\kappa_2,\rho L)\left[1 - e^{i(1-z)\bar{\kappa}\cdot(\bar{r}_1-\bar{r}_2)} + 1 - e^{i(1-z)\bar{\kappa}\cdot(\bar{r}_3-\bar{r}_4)}\right] . \tag{C-4}$$

Since the ρ integrand is non-negative (F_n is a power spectrum) we have

$$\alpha < 2k^2L^2 \int_0^1 dz \iint_{-\infty}^{\infty} d\bar{\kappa} \left[1 - e^{i(1-z)\bar{\kappa}\cdot(\bar{r}_1-\bar{r}_2)} + 1 - e^{i(1-z)\bar{\kappa}\cdot(\bar{r}_3-\bar{r}_4)} \right]$$

$$x \int_0^{\infty} d\rho \; F_n(\kappa_1,\kappa_2,\rho L) \quad . \tag{C-5}$$

Using the relationship between the two and three dimensional index of refraction spectra,

$$\int_0^{\infty} d\rho \; F_n(\kappa_1,\kappa_2,\rho L) = \frac{\pi}{L} \Phi_n(\kappa_1,\kappa_2,0) \quad , \tag{C-6}$$

and making the change of variable

$$u = 1 - z \tag{C-7}$$

gives for Eq. (C-5)

$$\alpha < 2\pi k^2 L \iint_{-\infty}^{\infty} d\bar{\kappa} \; \Phi_n(\kappa_1,\kappa_2,0) \int_0^1 du$$

$$x \left[1 - e^{iu\bar{\kappa}\cdot(\bar{r}_1-\bar{r}_2)} + 1 - e^{iu\bar{\kappa}\cdot(\bar{r}_3-\bar{r}_4)} \right] \quad . \tag{C-8}$$

Changing the $\bar{\kappa}$ variable of integration to polar coordinates, assuming isotropic turbulence, and performing the angular integration yields

$$\alpha < 4\pi^2 k^2 L \int_0^{\infty} d\kappa \; \kappa \; \Phi_n(\kappa) \int_0^1 du$$

$$x \left[1 - J_0(u\kappa\rho_{12}) + 1 - J_0(u\kappa\rho_{34}) \right] \quad , \tag{C-9}$$

where

$$\rho_{12} = |\bar{r}_1 - \bar{r}_2|$$

and

$$\rho_{34} = |\bar{r}_3 - \bar{r}_4| \quad .$$

Now for the von Kármán form of the index of refraction spectrum,

$$\Phi_n(\kappa) = .033\, C_n^2[\kappa^2+(1.077/L_o)^2]^{-11/6} \quad , \qquad \text{(C-10)}$$

we have

$$\int_0^\infty d\kappa\, \kappa\, \Phi_n(\kappa)[1-J_o(u\kappa\rho_{12})] =$$

$$= .033\, C_n^2 \left\{\int_0^\infty d\kappa\, \kappa[\kappa^2+(1.077/L_o)^2]^{-11/6}\right.$$

$$\left. - \int_0^\infty d\kappa\, \kappa[\kappa^2+(1.077/L_o)^2]^{-11/6}\, J_o(u\kappa\rho_{12})\right\} \quad . \qquad \text{(C-11)}$$

The right hand side of this equation is easily put into the form

$$.033\, C_n^2 \left(\frac{1.077}{L_o}\right)^{-5/3} \left\{\int_0^\infty dx\, x(x^2+1)^{-11/6}\right.$$

$$\left. - y^{-1/2} \int_0^\infty dx\, x^{1/2}(x^2+1)^{-11/6}\, J_o(xy)\, \sqrt{xy}\right\} \quad , \qquad \text{(C-12a)}$$

where

$$y = 1.077\, \frac{u\rho_{12}}{L_o} \quad , \qquad \text{(C-12b)}$$

and we have made use of the change of variable $x = \kappa L_o/1.077$.

The first integral in the above expression yields a Beta function [73] and the second integral is a Hankel transform [104]. Performing these integrations results in

$$\int_0^\infty d\kappa\ \kappa\ \Phi_n(\kappa)[1-J_o(u\kappa\rho_{12})] =$$

$$.033\ C_n^2 \left(\frac{1.077}{L_o}\right)^{-5/3} \frac{\Gamma(5/6)}{2\Gamma(11/6)} \left[1 - 2\ \frac{y^{5/6}K_{5/6}(y)}{2^{5/6}\Gamma(5/6)}\right] \quad , \qquad \text{(C-13)}$$

where $K_{5/6}$ is the modified Bessel function of the second kind and order 5/6. We require the separation to be much smaller than the outer scale,

$$\rho_{12} << L_o \quad ,$$

so that the right hand side of Equation (C-13) can be approximated [105] as

$$.033\ C_n^2 \left(\frac{1.077}{L_o}\right)^{-5/3} \frac{\Gamma(5/6)}{2\Gamma(11/6)} \frac{\Gamma(1/6)}{\Gamma(11/6)} \left(\frac{y}{2}\right)^{5/3}$$

or

$$.033\ C_n^2\ \frac{3\Gamma(1/6)}{5\Gamma(11/6)} \left(\frac{u\rho_{12}}{2}\right)^{5/3} \quad . \qquad \text{(C-14)}$$

With these results, inequality (C-9) gives for α,

$$\alpha < 4\pi^2k^2L(.033)C_n^2\ \frac{3}{5}\frac{\Gamma(1/6)}{\Gamma(11/6)} \left[\left(\frac{\rho_{12}}{2}\right)^{5/3} + \left(\frac{\rho_{34}}{2}\right)^{5/3}\right]$$

$$x \int_0^1 du\ u^{5/3} \quad , \qquad \text{(C-15)}$$

or finally

$$\alpha < \frac{9}{10}\ (.033)C_n^2\ \pi^2k^2L\ \frac{\Gamma(1/6)}{\Gamma(11/6)} \left[\left(\frac{\rho_{12}}{2}\right)^{5/3} + \left(\frac{\rho_{34}}{2}\right)^{5/3}\right] \quad . \qquad \text{(C-16)}$$

The separations, ρ_{ij}, are bounded by

$$\rho_{ij} \ll \frac{\lambda L}{\ell_o}$$

where ℓ_o is the inner scale of turbulence. For a Helium-Neon laser ($\lambda = .6328 \times 10^{-6}$ meter), a one centimeter inner scale, and a one kilometer range we obtain

$$\alpha < 5.384 \times 10^{16}\, C_n^2 \left(\rho_{12}^{5/3} + \rho_{34}^{5/3}\right) \lesssim 10^{15}\, C_n^2 \quad . \tag{C-17}$$

Therefore for $10^{15}\, C_n^2 < 1$ we can employ the weak turbulence approximation.

DISCUSSION OF β

With Equations (72), (74) and (76) in the text, β is expressed as

$$\beta = 2k^2L^2 \iint_{-\infty}^{\infty} d\bar{\kappa} \left\{ \int_0^{1/2} dz \int_0^{2z} d\rho + \int_{1/2}^{1} dz \int_0^{2(1-z)} d\rho \right\} F_n(\kappa_1, \kappa_2, \rho L)$$

$$\times\, e^{i\kappa\cdot[z(\bar{r}_1'-\bar{r}_2')+\tau\bar{v}]} \left[e^{i(1-z)\bar{\kappa}\cdot(\bar{r}_1-\bar{r}_4)} + e^{i(1-z)\bar{\kappa}\cdot(\bar{r}_2-\bar{r}_3)} \right.$$

$$\left. - e^{i(1-z)\bar{\kappa}\cdot(\bar{r}_1-\bar{r}_3)-i2\gamma} - e^{i(1-z)\bar{\kappa}\cdot(\bar{r}_2-\bar{r}_4)+i2\gamma} \right] \quad , \tag{C-18a}$$

where

$$\gamma = (z-z^2-\rho^2/4)\ \frac{L\kappa^2}{2k} \quad . \tag{C-18b}$$

Now β is maximum for zero time lag(τ=0) and zero receiver plane separation ($\bar{r}_1'-\bar{r}_2'$=0) so that

$$\beta \leq 2k^2L^2 \iint_{-\infty}^{\infty} d\bar{\kappa} \left\{ \int_0^{1/2} dz \int_0^{2z} d\rho + \int_{1/2}^{1} dz \int_0^{2(1-z)} d\rho \right\} F_n(\kappa_1, \kappa_2, \rho L)$$

$$\times \left[e^{i(1-z)\bar{\kappa}\cdot\bar{r}_{14}} + e^{i(1-z)\bar{\kappa}\cdot\bar{r}_{23}} \right.$$

$$\left. - e^{i(1-z)\bar{\kappa}\cdot\bar{r}_{13}-i2\gamma} - e^{i(1-z)\bar{\kappa}\cdot\bar{r}_{24}+i2\gamma} \right] \quad , \tag{C-19}$$

where $\bar{r}_{ij} = \bar{r}_i - \bar{r}_j$.

Further, β is maximized by setting the separations $\bar{r}_{ij}$ equal to zero:

$$\beta \lesssim 4k^2L^2 \iint_{-\infty}^{\infty} d\bar{\kappa} \left\{ \int_0^{1/2} dz \int_0^{2z} d\rho + \int_{1/2}^{1} dz \int_0^{2(1-z)} d\rho \right\} F_n(\kappa_1, \kappa_2, \rho L)$$

$$\times \left\{ 1 - \cos\left[(z - z^2 - \rho^2/4) \frac{L\kappa^2}{k} \right] \right\} \quad . \tag{C-20}$$

Little error is incurred by dropping the ρ dependence of the cos function and extending the upper limits on the ρ integrals to infinity (see Appendix D) to obtain

$$\beta \lesssim 4\pi k^2 L \iint_{-\infty}^{\infty} d\bar{\kappa} \int_0^1 dz\, \Phi_n(\kappa_1, \kappa_2, 0) \left\{ 1 - \cos\left[\frac{z(1-z)L}{k} \kappa^2 \right] \right\} \quad . \tag{C-21}$$

Changing the $\bar{\kappa}$ variable to polar coordinates, assuming isotropic turbulence, and performing the angular integration gives

$$\beta \lesssim 8\pi^2 k^2 L \int_0^{\infty} d\kappa\, \kappa\, \Phi_n(\kappa) \int_0^1 dz \left\{ 1 - \cos\left[\frac{z(1-z)L}{k} \kappa^2 \right] \right\} \tag{C-22}$$

With the identity

$$1 - \cos x = x \int_0^1 du \sin ux \tag{C-23}$$

inequality (C-22) becomes

$$\beta \lesssim 8\pi^2 k^2 L \int_0^{\infty} d\kappa\, \kappa\, \Phi_n(\kappa) \int_0^1 dz \left[\frac{z(1-z)L}{k} \kappa^2 \right]$$

$$\times \int_0^1 du \sin\left[u \frac{z(1-z)L}{k} \kappa^2 \right] \quad , \tag{C-24}$$

or

$$\beta \lesssim 8\pi^2 k^2 L \int_0^1 dz \left[\frac{z(1-z)L}{k}\right] \int_0^1 du$$

$$\times \int_0^\infty d\kappa\, \kappa^3\, \Phi_n(\kappa) \sin\left[u\,\frac{z(1-z)L}{k}\,\kappa^2\right] \quad . \tag{C-25}$$

For the von Kármán index of refraction spectrum, as in Equation (C-10), we find

$$\beta \lesssim .033\, C_n^2\, 8\pi^2 k^2 L \int_0^1 dz \left[\frac{z(1-z)L}{k}\right] \int_0^1 du$$

$$\times \int_0^\infty d\kappa\, \kappa^3 [\kappa^2 + (1.077/L_o)]^{-11/6} \sin\left[u\,\frac{z(1-z)L}{k}\,\kappa^2\right] \quad . \tag{C-26}$$

A stronger inequality results if the outer scale is set to infinity $(1.077/L_o = 0)$;

$$\beta < .033\, C_n^2\, 8\pi^2 k^2 L \int_0^1 dz \left[\frac{z(1-z)L}{k}\right] \int_0^1 du$$

$$\times \int_0^\infty d\kappa\, \kappa^{-2/3} \sin\left[u\,\frac{z(1-z)L}{k}\,\kappa^2\right] \quad , \tag{C-27}$$

or

$$\beta < .033\, C_n^2\, 4\pi^2 k^2 L \int_0^1 dz \left[\frac{z(1-z)L}{k}\right] \int_0^1 du$$

$$\times \int_0^\infty dx\, x^{-5/6} \sin\left[u\,\frac{z(1-z)L}{k}\,x\right] \quad , \tag{C-28}$$

where we have made use of the change of variable

$$x = \kappa^2 \ .$$

Performing the x integration [106] yields

$$\beta < .033\ C_n^2\ 4\pi^2 k^2 L \int_0^1 dz \left[\frac{z(1-z)L}{k}\right] \int_0^1 du$$

$$\left[u\ \frac{z(1-z)L}{k}\right]^{\frac{5}{6}-1} \Gamma\left(1 - \frac{5}{6}\right) \cos\left(\frac{1}{2} \cdot \frac{5}{6}\ \pi\right) \quad , \tag{C-29}$$

or

$$\beta < .033\ C_n^2\ 4\pi^2 k^{7/6} L^{11/6}\ \Gamma(1/6)\ \cos\left(\frac{5\pi}{12}\right)$$

$$x \int_0^1 dz\ z^{5/6}(1-z)^{5/6} \int_0^1 du\ u^{-1/6} \quad . \tag{C-30}$$

The u integral gives the value 6/5 and the z integral is a Beta function [73]. Finally we have

$$\beta < .022\ C_n^2\ \pi^2 k^{7/6} L^{11/6}\ \frac{9}{5}\ \cos\frac{5\pi}{12}\ \frac{\Gamma(1/6)\Gamma^2(11/6)}{\Gamma(8/3)} \quad . \tag{C-31}$$

From Tatarski [21], the log-amplitude variance for a spherical wave with an infinite outer scale of turbulence is

$$\sigma_\chi^2 = .124\ C_n^2\ k^{7/6} L^{11/6} \tag{C-32}$$

so that

$$\beta < 4\sigma_\chi^2 \quad . \tag{C-33}$$

Inequalities (C-17) and (C-33) constitute the results of this appendix. These expressions state that we are justified in employing the weak turbulence approximation in the development of Chapter II if

$$5.384 \times 10^{13}\ C_n^2 L \left(\rho_{12}^{5/3} + \rho_{34}^{5/3}\right) << 1$$

and

$$4\sigma_\chi^2 << 1 \quad .$$

APPENDIX D

DEPENDENCE UPON LARGE OUTER SCALES

In this appendix we discuss the approximations involved in going from Equation (88) to Equation (89) in Chapter II.

The scintillation spectrum is expressed by Eq. (88).

$$S_p(\omega) = 2k^2L^2 \left\{ \int_0^{1/2} dz \int_0^{2z} d\rho + \int_{1/2}^{1} dz \int_0^{2(1-z)} d\rho \right\}$$

$$\times \int\int_{-\infty}^{\infty} d\bar{\kappa}\, F_n(\kappa_1, \kappa_2, \rho L)\, [2\pi\delta(\omega - \bar{\kappa}\cdot\bar{V})]$$

$$\times \left| H(z,\rho,\bar{\kappa},w) - H^*(z,\rho,-\bar{\kappa},w) \right|^2 \quad , \tag{D-1a}$$

where

$$H(z,\rho,\bar{\kappa},w) = \frac{-i(1-z-\rho^2/4)L\kappa^2}{2k} \int d\bar{r} w(\bar{r})\, e^{i\bar{\kappa}\cdot\bar{r}}\, E\left(\bar{r} - \frac{L(1-z)\bar{\kappa}}{k}\right) E^*(\bar{r}) \quad . \tag{D-1b}$$

We will show that under a reasonable set of circumstances, the ρ dependence of the H function can be suppressed and the limits on the ρ integrations extended to infinity. First we shall demonstrate the approximations for high spatial frequencies and then for low spatial frequencies.

To simplify the discussion which follows, we adopt the following notation:

$$H_+ \equiv H(z,\rho,\bar{\kappa},w) \tag{D-2a}$$

$$H_- \equiv H(z,\rho,-\bar{\kappa},w) \quad . \tag{D-2b}$$

The square modulus term in Equation (D-1a) is then given by

$$|H_+ - H_-^*|^2 = \left|\int d\bar{r} w(\bar{r}) e^{i\bar{\kappa}\cdot\bar{r}} E\left(\bar{r} - \frac{L(1-z)}{k}\kappa\right) E^*(\bar{r})\right|^2$$

$$+ \left|\int d\bar{r} w(\bar{r}) e^{i\bar{\kappa}\cdot\bar{r}} E(\bar{r}) E^*\left(\bar{r} + \frac{L(1-z)}{k}\bar{\kappa}\right)\right|^2$$

$$- e^{-i(1-z-\rho^2/4)\frac{L\kappa^2}{k}} \left[\int d\bar{r} w(\bar{r}) e^{i\bar{\kappa}\cdot\bar{r}} E\left(\bar{r} - \frac{L(1-z)}{k}\bar{\kappa}\right) E^*(\bar{r})\right]$$

$$\times \left[\int d\bar{r} w(\bar{r}) e^{-i\bar{\kappa}\cdot\bar{r}} E^*(\bar{r}) E\left(\bar{r} + \frac{L(1-z)}{k}\bar{\kappa}\right)\right]$$

$$- e^{i(1-z-\rho^2/4)\frac{L\kappa^2}{k}} \left[\int d\bar{r} w(\bar{r}) e^{-i\bar{\kappa}\cdot\bar{r}} E^*\left(\bar{r} - \frac{L(1-z)}{k}\bar{\kappa}\right) E(\bar{r})\right]$$

$$\times \left[\int d\bar{r} w(\bar{r}) e^{i\bar{\kappa}\cdot\bar{r}} E(\bar{r}) E^*\left(\bar{r} + \frac{L(1-z)}{k}\bar{\kappa}\right)\right] \quad . \qquad \text{(D-3)}$$

For high spatial frequencies ($\kappa >> 2\pi/\sqrt{\lambda L}$) the exponential terms involving ρ oscillate so rapidly with respect to the other terms in the expression that we may replace them by their average integral value, zero. Within the high frequency region then

$$|H_+ - H_-^*|^2 = |H_+|^2 + |H_-|^2 \quad , \qquad \text{(D-4)}$$

and the dependence upon ρ disappears from this term. The onset of this region is at roughly

$$\frac{L\kappa^2}{k} \sim 2\pi \quad ,$$

that is

$$\kappa \sim 2\pi/\sqrt{\lambda L} \quad . \qquad \text{(D-5)}$$

However, under the assumption of isotropic turbulence, the two dimensional index of refraction spectrum has a breakpoint[57] at

$$\kappa\rho L \sim 2\pi \tag{D-6}$$

beyond which the spectrum decreases rapidly. So, for high spatial frequencies, F_n is very small beyond the point

$$\frac{2\pi}{\sqrt{\lambda L}}\rho L \sim 2\pi$$

or

$$\rho \sim \sqrt{\frac{\lambda}{L}} <<< 1 \quad . \tag{D-7}$$

Therefore we may, with little error, extend the upper limit on the ρ integrals to infinity to obtain

$$\left\{\int_0^{1/2} dz \int_0^{2z} d\rho + \int_{1/2}^{1} dz \int_0^{2(1-z)} d\rho\right\} F_n(\kappa_1,\kappa_2,\rho L)$$

$$\times \left|H(z,0,\bar{\kappa},w)-H^*(z,0,-\bar{\kappa},w)\right|^2$$

$$= \frac{\pi}{L}\Phi_n(\kappa_1,\kappa_2,0)\int_0^1 dz \left|H(z,0,\bar{\kappa},w)-H^*(z,0,-\bar{\kappa},w)\right|^2 \quad , \tag{D-8}$$

where we have made use of the relationship between the two and three dimensional index of refraction spectra;

$$\int_0^\infty d\rho\ F_n(\kappa_1,\kappa_2,\rho L) = \frac{\pi}{L}\ \Phi_n(\kappa_1,\kappa_2,0) \quad . \tag{D-9}$$

Equation (D-8) is the desired result of this appendix. We have justified this approximation for high spatial frequencies ($\kappa >> 2\pi/\sqrt{\lambda L}$). It will now be demonstrated that Equation (D-8) is valid at low frequencies as well.

Now recall that the two dimensional index of refraction spectrum, F_n, is small beyond the point $\kappa\rho L \sim 2\pi$. Therefore the frequencies for which F_n is significant are given by

$$\kappa\rho L \lesssim 2\pi \quad , \tag{D-10}$$

or

$$(\kappa\rho L)^2 \lesssim (2\pi)^2$$

or

$$\frac{(\kappa\rho)^2 L}{8k} \lesssim \frac{\pi}{4}\frac{\lambda}{L} << \pi \quad . \tag{D-11}$$

The left-most term in Inequality (D-11) is merely the ρ dependence of the *H function* (*Equation* (D-1b)). Since the ρ dependent term of the *H* functions is much less than π within the region where F_n is significant, i.e., low spatial frequencies, we can drop this term altogether. The *H* function therefore becomes

$$H(z,\bar{\kappa},w) = e^{\frac{-i(1-z)L\kappa^2}{2k}} \int d\bar{r} w(\bar{r})\, e^{i\bar{\kappa}\cdot\bar{r}}\, E\left(\bar{r} - \frac{L(1-z)\bar{\kappa}}{k}\right) E^*(\bar{r}) \quad . \tag{D-12}$$

For low spatial frequencies such that

$$\kappa << 2\pi/\sqrt{\lambda L}$$

the field translation term in the expression for the *H* function is bounded in the following manner:

$$\frac{L(1-z)\kappa}{k} << \frac{L}{k}\frac{2\pi}{\sqrt{\lambda L}} = \sqrt{\lambda L} \quad . \tag{D-13}$$

For well behaved (free space) receiver plane fields, i.e., those varying slowly over a lateral distance on the order of a fraction of the Fresnel zone, $\sqrt{\lambda L}$, the square modulus term in Equation (D-1a) can be written

$$|H_+ - H_-^*|^2 \approx 4C^2 \sin^2\left[(1-z)\frac{L\kappa^2}{2k}\right] \tag{D-14a}$$

or further

$$|H_+ - H_-^*|^2 \approx 4C^2 \left[(1-z)\frac{L}{2k}\right]^2 \kappa^4 \quad , \tag{D-14b}$$

where

$$C = \int d\bar{r}\, e^{i\bar{r}\cdot\bar{\kappa}}\, w(\bar{r})\, |E(\bar{r})|^2 \quad . \qquad \text{(D-15)}$$

Under most cases of interest (receiver pupil, w, smaller than a Fresnel zone, $\sqrt{\lambda L}$) the C function is a very weak function of κ for $\kappa < 2\pi/\sqrt{\lambda L}$. Hence the low frequency dependence of the modulus squared term is κ^4. This fourth power dependence upon spatial frequency strongly suppresses any contribution to the scintillation spectrum due to low spatial frequency atmospheric inhomogenieties. For the Kolmogorov (infinite outer scale) model of the index of refraction field the low frequency dependence of F_n is $\kappa^{-8/3}$. Even for this model the κ^4 dependence of the square modulus term will cause the scintillation spectrum to be highly insensitive to low spatial frequency index of refraction inhomogenieties.

With the foregoing arguments the scintillation spectrum is expressed as

$$S_p(\omega) = 4\pi^2 k^2 L \int_{-\infty}^{\infty}\int d\bar{\kappa}\, \Phi_n(\kappa_1,\kappa_2,0)\,\delta(\omega-\bar{\kappa}\cdot\bar{v})$$

$$\times \int_0^1 dz\, |H(z,\bar{\kappa},w)-H^*(z,-\bar{\kappa},w)|^2 \quad , \qquad \text{(D-16a)}$$

where

$$H(z,\bar{\kappa},w) =$$

$$e^{\frac{-i(1-z)L}{2k}\kappa^2} \int d\bar{r} w(\bar{r}) e^{i\bar{\kappa}\cdot\bar{r}}\, E\left(\bar{r} - \frac{L(1-z)}{k}\,\bar{\kappa}\right) E^*(\bar{r}) \quad . \qquad \text{(D-16b)}$$

These expressions are identical to Equations (89-a) and (89-b).

Q.E.D.

APPENDIX E

DIFFRACTION OF AN ARBITRARY FIELD BY A PHASE GRATING

Within this appendix we develop a mathematical description of the fields diffracted by a weak phase grating.

We assume the same geometry as in Figure 8 of Chapter II; a phase grating of period $2\pi/|\bar{\kappa}|$ and orientation $\bar{\kappa}/|\bar{\kappa}|$ located in some plane z such that $0<z<L$. The weak phase grating is defined in terms of its transmission function

$$T(\bar{\kappa},\bar{r}) = e^{i\varepsilon\cos(\bar{\kappa}\cdot\bar{r})}, \tag{E-1}$$

where $|\varepsilon|<<1$.

Keeping only the first two terms in the series expansion of Equation (E-1) yields

$$T(\bar{\kappa},\bar{r}) \approx 1 + i\varepsilon\cos(\bar{\kappa}\cdot\bar{r}) = 1 + i\frac{\varepsilon}{2}e^{i\bar{\kappa}\cdot\bar{r}} + i\frac{\varepsilon}{2}e^{-i\bar{\kappa}\cdot\bar{r}} \tag{E-2}$$

Now assume an arbitrary field to be incident upon the grating from the left. At $z=z^-$ the field is

$$E(\bar{r})\Big|_{z^-}, \tag{E-3}$$

and at $z=z^+$ the field is

$$E(\bar{r})\Big|_{z^+} = \sum_{n=-1}^{1} C_n\, E(\bar{r})\Big|_{z^-} e^{in\bar{\kappa}\cdot\bar{r}} \tag{E-4}$$

where

$$C_n = (i\,\varepsilon/2)^{|n|} \tag{E-5}$$

The receiver plane field is determined by performing the Fresnel diffraction integral over the field within the plane $z=z^+$;

$$E(\bar{r}')\Big|_L = e^{ik(L-z)}\left[\frac{-ik}{2\pi(L-z)}\right]\int d\bar{r}\, E(\bar{r})\Big|_{z^+} e^{\frac{ik}{2(L-z)}(r^2-2\bar{r}\cdot\bar{r}'+r'^2)} \tag{E-6}$$

Combining Equations (E-4) and (E-6) yields

$$E(\bar{r}')\Big|_L = e^{ik(L-z)}\left[\frac{-ik}{2\pi(L-z)}\right] e^{\frac{ikr'^2}{2(L-z)}} \sum_{n=-1}^{1} C_n \int d\bar{r}\, E(\bar{r})\Big|_{z^-} \tag{E-7}$$

$$\times\, e^{\frac{ik}{2(L-z)}\left\{r^2 - 2\bar{r}\cdot\left[\bar{r} - \frac{n(L-z)}{k}\,\bar{\kappa}\right]\right\}}.$$

Symbolically performing the integration gives the receiver plane fields

$$e^{ik(L-z)} \sum_{n=-1}^{n} e^{in\bar{\kappa}\cdot\bar{r}'}\, e^{\frac{-in^2(L-z)}{2k}\kappa^2}\, E\left(\bar{r}' - \frac{n(L-z)}{k}\,\bar{\kappa}\right). \tag{E-8}$$

This expression for the principal diffracted fields (minus one, zeroth, and plus one) of a weak phase grating is the result of this appendix.

APPENDIX F

DETAILS OF THE DIRTY BEAM MODEL

The objectives of this appendix are twofold. First we shall demonstrate that, with little loss of generality, we can assume the phase obstacle to be axially located within the beam. Then we present an outline of the optimization of the eigen-mode expansion of the complementary field.

We restrict our attention to the situation in which the receiver is in the far-field of the main laser beam, (Fresnel number much larger than unity) and the detector is near the beam axis ($r_0 << w(L)$). Under these conditions the scintillation spectrum of the main beam alone is that of a spherical wave and is therefore insensitive to the detector location. Now consider the case in which the receiver plane field consists of the field of the main beam plus the diffraction pattern of the phase obstacle. As long as the detector is near the axis of the main beam the scintillation spectrum (of the dirty beam) will be dependent only upon the relative positions of the detector and the phase spot diffraction pattern. Therefore we can assume, without loss of generality, that the phase obstacle (and hence its diffraction pattern) are axially located with respect to the main beam.

Now in performing the actual eigen mode expansion of the complementary field, there are two points with which we must concern ourselves: 1) The phase curvatures (within the z=0 plane) of the main and complementary fields must be identical (so that the mode expansion will indeed converge to the actual complementary field). 2) Since we wish to approximate the complementary field by only a finite number of terms, we must insure a close approximation to the actual field, i.e., optimize the expansion.

The phase curvature of the complementary field is contained in the weighting function of the eigen mode expansion, (see Equations (200))

$$e^{-\frac{kM/2L}{1+iM(z+z_1)/L}(x^2+y^2)} \quad . \tag{F-1}$$

Comparison of this weighting function with that of Equation (194) shows that for equal phase curvatures (at the plane z=0) we must have

$$\mathrm{Im}\{\alpha(z_0)\} = \mathrm{Im}\{\beta(z_1)\} \quad ,$$

that is

$$\frac{z_0(N/L)^2}{1+(z_0N/L)^2} = \frac{z_1(M/L)^2}{1+(z_1M/L)^2} \quad . \tag{F-2}$$

Our optimization procedure is based on the minimization of the integral square error between the complementary field and its truncated series approximation. The error is defined as

$$\varepsilon_L \equiv \iint_{-\infty}^{\infty} |E^C(x,y,0)-E_L^C(x,y,0)|^2 \, dxdy \quad , \tag{F-3}$$

where

$$E_L^C(x,y,z) = \sum_{m=0}^{L}\sum_{n=0}^{L} \gamma_{mn}\, g_m(x,z+z_1)g_n(y,z+z_1) \quad . \tag{F-4}$$

By making use of the orthonormality of the mode functions and Equation (198) for the complementary field we find that Equation (F-3) can be expressed as

$$\varepsilon_L = \iint_{-\infty}^{\infty} dxdy \, |D'_\delta(x-x_s,y-y_s)E(x,y,0)|^2 - \sum_{m=0}^{L}\sum_{n=0}^{L} |\gamma_{mn}|^2 \quad . \tag{F-5}$$

The error is then minimized by taking the partial derivative of ε_L with respect to the complementary beam Fresnel number:

$$\frac{\partial}{\partial M} \sum_{m=0}^{L}\sum_{n=0}^{L} |\gamma_{mn}|^2 = 0 \quad . \tag{F-6}$$

The entire problem now reduces to that of solving two simultaneous equations (Equations (F-2) and (F-6)) for the complementary beam waist spot-size W_1 and locations z_1.

We now proceed with an example of the use of the foregoing complementary field expansion. In the interest of mathematical simplicity the complementary field is approximated by only its lowest order eigenmode. The expansion coefficient of this mode is given by

$$\gamma_{00} = \iint_{-\infty}^{\infty} dxdy\ E^C(x,y,0)\ g_0^*(x,z_1)g_0^*(y,z_1) \quad . \tag{F-7}$$

As has been justified previously, without loss if generality we can assume the phase object, described by D_δ, to be axially located. That is

$$D_\delta(x,y) = \begin{cases} A\ e^{i\mu} & ;\ \sqrt{x^2+y^2} \leq \delta/2 \\ 1 & ;\ \text{elsewhere} \end{cases} \quad . \tag{F-8}$$

Employing Equations (194), (198), (200), (F-7), and (F-8) we obtain

$$\gamma_{00} = \pi\sqrt{\frac{2}{\pi}}\, W_0 W_1 [1-A\ e^{i\mu}]\ \frac{\alpha(z_0)\beta^*(z_1)}{\alpha(z_0)+\beta^*(z_1)}$$

$$x \left\{ 1 - e^{-[\alpha(z_0)+\beta^*(z_1)](\delta/2)^2} \right\} \quad . \tag{F-9}$$

Application of Equation (F-6) to γ_{00} yields, after some lengthy algebraic manipulations

$$x = \frac{1}{y}\, \ell n \left[1-2xy\left(\frac{1+x}{1-x}\right) \right] - 1 \quad , \tag{F-10a}$$

where we have defined

$$x = \frac{\beta_r(z_1)}{\alpha_r(z_0)} \tag{F-10b}$$

and

$$y = \alpha_r(z_0) \left(\frac{\delta}{2}\right)^2 \quad . \tag{F-10c}$$

In Equations (F-10) x is seen to be the square of the ratio of the main beam to complementary beam spotsizes (at z=0) and y the square of the ratio of the spot radius to the main beam spotsize. Solution of Equation (F-10a), which at first glance appears a formidable task, is easily accomplished by an iterative technique;

$$x_{n+1} = \frac{1}{y} \ln \left[1-2yx_n\left(\frac{1+x_n}{1-x_n}\right)\right] - 1 \quad , \tag{F-11a}$$

in which we let

$$x_0 = y^{-1} \quad . \tag{F-11b}$$

Equation (F-11b) for the initial guess for x states simply that (at z=0) the complementary beam spotsize will be on the order of the radius of the phase obstacle.

From Equation (D-10b) we see that

$$\beta_r(z_1) = x\, \alpha_r(z_0) \tag{F-12}$$

and from Equation (D-2)

$$\beta_i(z_1) = \alpha_i(z_0) \quad . \tag{F-13}$$

Since x is known (from the solution of Equation (F-10a)) and $\alpha(z_0)$ is known, we have two simultaneous equations in the two unknowns, w_1 and z_1. At this point the complementary beam (including the mode coefficient, γ_{00}) is completely specified. Within the transmitter plane the total field is

$$E(x,y,0) = E_0^c(x,y,0) \tag{F-14}$$

and at the receiver the field is

$$E(x,y,L) - E_0^C(x,y,L) \quad . \tag{F-15}$$

This concludes the appendix.

APPENDIX G

COMPUTER PROGRAM LISTINGS

This appendix contains listings and brief discussions of the computer programs used to evaluate the temporal scintillation spectrum for the clean gaussian beam (Chapter III) and the dirty gaussian beam (Chapter IV) for homogeneous and/or localized turbulence. These programs are designed to evaluate the expression

$$\frac{\omega_0 S_p(\omega)}{I^2(0,0,L)\sigma_s^2} = \frac{C}{I^2(0,0,L)} \int_0^1 dz \int_{-\infty}^{\infty} d\kappa \; f(z)[\omega/\omega_0)^2 + \kappa^2$$

$$+ (1.077/L_0')^2]^{-11/6} \times \left| H\left(z, \frac{\omega}{\omega_0}, \kappa, W\right) - H^*\left(z, -\frac{\omega}{\omega_0}, -\kappa, W\right)\right|^2, \quad \text{(G-1a)}$$

where

$$H\left(z, \frac{\omega}{\omega_0}, \kappa, W\right) = e^{-i\frac{(1-z)}{4\pi}\left[\left(\frac{\omega}{\omega_0}\right)^2 + \kappa^2\right]} e^{i\left(\frac{\omega}{\omega_0}\frac{x_0}{\sqrt{\lambda L}} + \kappa\frac{y_0}{\sqrt{\lambda L}}\right)}$$

$$\times E\left(x_0 - \frac{\sqrt{\lambda L}(1-z)\omega/\omega_0}{2\pi}, y_0 - \frac{\sqrt{\lambda L}(1-z)\kappa}{2\pi}\right) E^*(x_0, y_0), \quad \text{(G-1b)}$$

C is a constant defined as

$$C = \frac{256\sqrt{2}\Gamma(4/3)}{3\pi^{2/3}}\left(-\cos\frac{11}{12}\pi\right) = 48.527, \quad \text{(G-1c)}$$

and f(z) is a longitudinal turbulence strength distribution function. For homogeneous turbulence, as in program one,

$$f(z) = 1. \quad \text{(G-2)}$$

In program two we used

$$f(z) = 100\, e^{-100z}. \quad \text{(G-3)}$$

Equation (G-1b) was obtained from Equation (89b) in the text by assuming a point detector,

$$w(\bar{r}) = \delta(|\bar{r}-\bar{r}_0|) \quad .$$

For the clean gaussian beam the field, E, in Equation (G-1b) was given by Equation (194) in the text. The field of the dirty gaussian beam was given by Equation (202b).

To simplify the programming, use was made of the change of variable

$$\kappa^2 \longleftarrow \kappa$$

so that the expression for the spectrum was given by

$$\frac{\omega_0 S_D(\omega)}{I^2(0,0,L)\sigma_s^2} = \frac{C}{2I^2(0,0,L)} \int_0^1 dz f(z) \int_0^\infty d\kappa\, \kappa^{-1/2}$$

$$\times \left[\left(\frac{\omega}{\omega_0}\right)^2 + \kappa + (1.077/L_0')^2\right]^{-11/6}$$

$$\times \left[\left|H\left(z,\frac{\omega}{\omega_0},\sqrt{\kappa},W\right) - H^*\left(z,-\frac{\omega}{\omega_0},-\sqrt{\kappa},W\right)\right|^2\right.$$

$$\left. + \left|H\left(z,\frac{\omega}{\omega_0},-\sqrt{\kappa},W\right) - H^*\left(z,-\frac{\omega}{\omega_0},\sqrt{\kappa},W\right)\right|^2\right] \quad , \qquad \text{(G-4a)}$$

where

$$H\left(z,\frac{\omega}{\omega_0},\sqrt{\kappa},W\right) = e^{-i\frac{(1-z)}{4\pi}\left[\left(\frac{\omega}{\omega_0}\right)^2+\kappa\right]} e^{i\left(\frac{\omega}{\omega_0}\frac{x_0}{\sqrt{\lambda L}} + \sqrt{\kappa}\frac{y_0}{\sqrt{\lambda L}}\right)}$$

$$\times E\left(x_0 - \frac{\sqrt{\lambda L}(1-z)\omega/\omega_0}{2\pi}, y_0 - \frac{\sqrt{\lambda L}(1-z)\sqrt{\kappa}}{2\pi}\right) E^*(x_0,y_0) \quad . \qquad \text{(G-4b)}$$

The numerical algorithm employed in approximating the integrals in Equation (G-4) was Gaussian quadrature [95,96,97]. This technique basically involves fitting a Hermite polynomial to the function to be integrated and integrating the polynomial over the desired limits. To approximate the integration over the range variable z, a single 32 point Gaussian quadrature routine was used. The 32 point routine as opposed to a higher order quadrature formula was deemed adequate because the z integrand was slowly varying. The κ integration was approximated by breaking the range into segments thus

$$\int_0^\infty d\kappa\, F(\kappa) \approx \sum_{i=1}^{M} \int_{(i-1)\Delta}^{i\Delta} d\kappa\, F(\kappa) \quad , \tag{G-5}$$

and employing an eight point Gaussian quadrature routine on each segment. In Equation (G-5) the width, Δ, of the segments was chosen such that

$$\Delta = \begin{cases} \left(\frac{\omega}{\omega_0}\right)^2 + \left(\frac{1.077}{L_0'}\right)^2 & ; \ \left(\frac{\omega}{\omega_0}\right) < 1 \\ 1/(\omega/\omega_0) & ; \ \left(\frac{\omega}{\omega_0}\right) > 1 \end{cases} \tag{G-6}$$

and the upper limit, M, on the sum was such that the last segment integrated made a negligible contribution to the integral, i.e.,

$$\frac{\int_{(M-1)\Delta}^{M\Delta} d\kappa F(\kappa)}{\sum_{i=1}^{M-1} \int_{(i-1)\Delta}^{i\Delta} d\kappa F(\kappa) + \int_{(M-1)\Delta}^{M\Delta} d\kappa F(\kappa)} < 10^{-5} \quad . \tag{G-7}$$

This method of breaking a large integration range into smaller pieces is commonly called composite or compound integration [98]. The advantages of this technique are a smaller error and the ability to approximate integrations over infinite or semi-infinite ranges [98].

Listings of the programs used in Chapters III and IV follow. Also included are listings for the eight and 32 point Gaussian quadrature subroutines. The notation used in programs one and two is consistent with that of the text and of this appendix.

Program one calculates the dirty beam scintillation spectrum for homogeneous turbulence. To obtain the scintillation spectrum of a clean beam from this program, the complex variable C2 is set to zero. The dirty beam spectrum for localized turbulence is calculated by program two. A linear combination of the results of these two programs yields the dirty beam spectrum for the combination of homogeneous and localized turbulence.

PROGRAM ONE

```
C SCINTILLATION SPECTRUM FOR DIRTY BEAM (PHASE OBJECT)
C WITH OFF-AXIS POINT DETECTOR AND LOCALIZED TURBULENCE.
C ZERO-ZERO ORDER APPROXIMATION TO DIRT SPOT
      OPTIONS DP
      INCLUDE DQG8B:DOH8B
      EXTERNAL ZINT,EFIELD
      REAL IOSO
      COMPLEX A,B,BC,AL,BL,C1,C2,EFO,EFIELD
      COMMON AL,BL,C1,C2,OMEG,FOMEG1,FOMEG2,F1Z,F2Z,EFO,EKSO,WYEO
     1,PI,FRES
      CALL ASSIGN(6HTMPOUT,0.,6)
      CALL FERR(0)
      CALL DEASSN
      PI=4.*ATAN(1.)
C POSITION OF POINT DETECTOR
      EKSO=0.
      WYEO=SQRT(.2)
C DIAMETER AND PHASE OF DIRT SPOT
      DEL=.917E-3
      PHI=5.333580778
C WAIST SPOTSIZES AND LOCATIONS FOR MAIN AND COMPLEMENTARY BEAMS
      WO=20.2E-6
      W1=3.146345943E-4
      ZO=1.
      Z1=.4080236159
C RANGE, OUTER SCALE, AND WAVELENGTH
      EL=1.E3
      ELO=1.
      ALAM=.6328E-6
      FRES=SQRT(ALAM*EL)
      FELOP=1.077/(ELO/FRES)
C AA=M/L
      AA=ALAM/(PI*WO*WO)
C BB=M/L
      BB=ALAM/(PI*W1*W1)
C A=ALPHA(ZO)
      A=WO*WO*CMPLX(1.,AA*ZO)
      A=1./A
C B=BETA(Z1)
      B=W1*W1*CMPLX(1.,BB*Z1)
      B=1./B
      BC=CONJG(B)
C AL=ALPHA(L+ZO)
      AL=WO*WO*CMPLX(1.,AA*(ZO+EL))
      AL=1./AL
C C1=ALPHA(L+O)*WO
      C1=WO*AL
C IOSQ=I(O,O,L)**2
      IOSO=REAL(C1*CONJG(C1))**2
C BL=BETA(L+Z1)
      BL=W1*W1*CMPLX(1.,BB*(Z1+EL))
      BL=1./BL
C C2=BETA(L+Z1)*GAMMA00*W1
      C2=(1.-CEXP(-(A+BC)*(DEL/2.)**2))*(1.-CEXP(CMPLX(0.,PHI)))
      C2=C2*A*BC/(A+BC)
      C2=2.*W1*WO*C2
      C2=C2*BL*W1
      EFO=EFIELD(EKSO,WYEO)
C OMEG=OMEGA/OMEGAO
      OMEG=1.E-5
      FRINC=10.**(1./8.)
      CONST=48.52728232
      DO 50 I=1,57
      FOMEG1=(OMEG)**2
      FOMEG2=FOMEG1+FELOP**2
```

```
      CALL DQG32(0.,1.,ZINT,ANS)
      ANS=.5*ANS*CONST/IOSQ
      WRITE(6,-)OMEG,ANS
50    OMEG=OMEG*FRINC
      CALL EXIT
      END
C
C THIS IS THE INTEGRAND FOR THE PATH INTEGRATION
      FUNCTION ZINT(Z)
      EXTERNAL AKINT
      COMPLEX AL,BL,C1,C2,EF0
      COMMON AL,BL,C1,C2,OMEG,FOMEG1,FOMEG2,F1Z,F2Z,EF0,EKS0,WYE0
     1,PI,FRES
      F1Z=(1.-Z)/(2.*PI)
      F2Z=F1Z*FRES
      AUPR=FOMEG2
      IF(FOMEG1.GE.1.)AUPR=1./SQRT(FOMEG1)
      ZINT=0.
      ALWR=0.
5     CALL DQG8(ALWR,AUPR,AKINT,ANS)
      ZINT=ZINT+ANS
      ALWR=AUPR
      AUPR=2.*AUPR
      IF(ANS.LT.1.E-5*ZINT)RETURN
      GOTO5
      END
C
C THIS IS THE KAPPA INTEGRAND
      FUNCTION AKINT(AKP)
      COMPLEX AL,BL,C1,C2,EF0,FCN,EFIELD,F6,F7
      COMMON AL,BL,C1,C2,OMEG,FOMEG1,FOMEG2,F1Z,F2Z,EF0,EKS0,WYE0
      F1=AKP+FOMEG1
      F2=AKP+FOMEG2
      F3=F1Z*F1*.5
      F4=F2Z*SQRT(AKP)
      F5=F2Z*OMEG
      F6=EF0*CEXP(CMPLX(0.,F3))
      F7=CONJG(F6)
      FCN=EFIELD(EKS0-F5,WYE0-F4)*F7
      FCN=FCN-CONJG(EFIELD(EKS0+F5,WYE0+F4))*F6
      AKINT=REAL(FCN*CONJG(FCN))
      FCN=EFIELD(EKS0-F5,WYE0+F4)*F7
      FCN=FCN-CONJG(EFIELD(EKS0+F5,WYE0-F4))*F6
      AKINT=AKINT+REAL(FCN*CONJG(FCN))
      AKINT=AKINT*F2**(-1.83333333333)*AKP**(-.5)
      RETURN
      END
C
C THIS FUNCTION CALCULATES THE EFIELD AT THE RECEIVER PLANE.
      COMPLEX FUNCTION EFIELD(X,Y)
      COMPLEX AL,BL,C1,C2
      COMMON AL,BL,C1,C2
      RSQ=X*X+Y*Y
      EFIELD=C1*CEXP(-AL*RSQ)-C2*CEXP(-BL*RSQ)
      RETURN
      END
**
```

PROGRAM TWO

```
C SCINTILLATION SPECTRUM FOR DIRTY BEAM (PHASE OBJECT)
C WITH OFF-AXIS POINT DETECTOR.
C ZERO-ZERO ORDER APPROXIMATION TO DIRT SPOT
      OPTIONS DP
      INCLUDE DQG8E:DQG32B
      EXTERNAL ZINT,EFIELD
      REAL IOSQ
      COMPLEX A,B,BC,AL,BL,C1,C2,EFO,EFIELD
      COMMON AL,BL,C1,C2,OMEG,FOMEG1,FOMEG2,F1Z,F2Z,EFO,EKSO,WYEO
     1,PI,FRES
      CALL ASSIGN(6HTMPOUT,0.,6)
      CALL DEASSN
      CALL FERR(0)
      PI=4.*ATAN(1.)
C POSITION OF POINT DETECTOR
      EKSO=0.
      WYEO=SQRT(.4)
C DIAMETER AND PHASE OF DIRT SPOT
      DEL=.917E-3
      PHI=5.333580778
C WAIST SPOTSIZES AND LOCATIONS FOR MAIN AND COMPLEMENTARY BEAMS
      WO=20.2E-6
      W1=3.146345943E-4
      ZO=1.
      Z1=.4080236159
C RANGE, OUTER SCALE, AND WAVELENGTH
      EL=1.E3
      ELO=1.E2
      ALAM=.6328E-6
      FRES=SQRT(ALAM*EL)
      FELOP=1.077/(ELO/FRES)
C AA=M/L
      AA=ALAM/(PI*WO*WO)
C BB=M/L
      BB=ALAM/(PI*W1*W1)
C A=ALPHA(ZO)
      A=WO*WO*CMPLX(1.,AA*ZO)
      A=1./A
C B=BETA(ZO)
      B=W1*W1*CMPLX(1.,BB*Z1)
      B=1./B
      BC=CONJG(B)
C AL=ALPHA(L+ZO)
      AL=WO*WO*CMPLX(1.,AA*(ZO+EL))
      AL=1./AL
C C1=ALPHA(L+ZO)*WO
      C1=WO*AL
C IOSQ=I(0,0,L)**2
      IOSQ=REAL(C1*CONJG(C1))**2
C BL=BETA(L+Z1)
      BL=W1*W1*CMPLX(1.,BB*(Z1+EL))
      BL=1./BL
C C2=BETA(L+Z1)*GAMMA00*W1
      C2=(1.-CEXP(-(A+BC)*(DEL/2.)**2))*(1.-CEXP(CMPLX(0.,PHI)))
      C2=C2*A*BC/(A+BC)
      C2=2.*W1*WO*C2
      C2=C2*BL*W1
      EFO=EFIELD(EKSO,WYEO)
C OMEG=OMEGA/OMEGA0
      OMEG=1.E-5
      FRINC=10.**(1./8.)
      CONST=48.52728232
      DO 50 I=1,57
      FOMEG1=(OMEG)**2
      FOMEG2=FOMEG1+FELOP**2
```

```
      CALL DQH8(0.,.2,ZINT,ANS)
      ANS=.5*ANS*CONST/IOSQ
      ANS=ANS*EL/10.
      WRITE(6,-)OMEG,ANS
50    OMEG=OMEG*FRINC
      CALL EXIT
      END
C
C THIS IS THE INTEGRAND FOR THE PATH INTEGRATION
      FUNCTION ZINT(Z)
      EXTERNAL AKINT
      COMPLEX AL,BL,C1,C2,EFO
      COMMON AL,BL,C1,C2,OMEG,FOMEG1,FOMEG2,F1Z,F2Z,EFO,EKSO,WYEO
     1,PI,FRES
      F1Z=(1.-Z)/(2.*PI)
      F2Z=F1Z*FRES
      AUPR=FOMEG2
      IF(FOMEG1.GE.1.)AUPR=1./SQRT(FOMEG1)
      ZINT=0.
      ALWR=0.
5     CALL DQG8(ALWR,AUPR,AKINT,ANS)
      ZINT=ZINT+ANS
      ALWR=AUPR
      AUPR=2.*AUPR
      IF(ANS.LT.1.E-5*ZINT)GOTO10
      GOTO5
10    ZINT=ZINT*EXP(-Z*100.)
      RETURN
      END
C
C THIS IS THE KAPPA INTEGRAND
      FUNCTION AKINT(AKP)
      COMPLEX AL,BL,C1,C2,EFO,FCN,EFIELD,F6,F7
      COMMON AL,BL,C1,C2,OMEG,FOMEG1,FOMEG2,F1Z,F2Z,EFO,EKSO,WYEO
      F1=AKP+FOMEG1
      F2=AKP+FOMEG2
      F3=F1Z*F1*.5
      F4=F2Z*SQRT(AKP)
      F5=F2Z*OMEG
      F6=EFO*CEXP(CMPLX(0.,F3))
      F7=CONJG(F6)
      FCN=EFIELD(EKSO-F5,WYEO-F4)*F7
      FCN=FCN-CONJG(EFIELD(EKSO+F5,WYEO+F4))*F6
      AKINT=REAL(FCN*CONJG(FCN))
      FCN=EFIELD(EKSO-F5,WYEO+F4)*F7
      FCN=FCN-CONJG(EFIELD(EKSO+F5,WYEO-F4))*F6
      AKINT=AKINT+REAL(FCN*CONJG(FCN))
      AKINT=AKINT*F2**(-1.83333333333)*AKP**(-.5)
      RETURN
      END
C
C THIS FUNCTION CALCULATES THE EFIELD AT THE RECEIVER PLANE.
      COMPLEX FUNCTION EFIELD(X,Y)
      COMPLEX AL,BL,C1,C2
      COMMON AL,BL,C1,C2
      RSQ=X*X+Y*Y
      EFIELD=C1*CEXP(-AL*RSQ)-C2*CEXP(-BL*RSQ)
      RETURN
      END
$$
```

EIGHT POINT GAUSSIAN QUADRATURE SUBROUTINE

```
C                                                                       12
C     SUBROUTINE DQG8                                                   13
C                                                                       14
C     PURPOSE                                                           15
C        TO COMPUTE INTEGRAL(FCT(X), SUMMED OVER X FROM XL TO XU)       16
C                                                                       17
C     USAGE                                                             18
C        CALL DQG8  (XL,XU,FCT,Y)                                       19
C        PARAMETER FCT REQUIRES AN EXTERNAL STATEMENT                   20
C                                                                       21
C     DESCRIPTION OF PARAMETERS                                         22
C        XL      -DOUBLE PRECISION LOWER BOUND OF THE INTERVAL.         23
C        XU      -DOUBLE PRECISION UPPER BOUND OF THE INTERVAL.         24
C        FCT     -THE NAME OF AN EXTERNAL DOUBLE PRECISION FUNCTION     25
C                 SUBPROGRAM USED.                                      26
C        Y       -THE RESULTING DOUBLE PRECISION INTEGRAL VALUE.        27
C                                                                       28
C     REMARKS                                                           29
C        NONE                                                           30
C                                                                       31
C     SUBROUTINES AND FUNCTION SUBPROGRAMS REQUIRED                     32
C        THE EXTERNAL DOUBLE PRECISION FUNCTION SUBPROGRAM FCT(X)       33
C        MUST BE FURNISHED BY THE USER.                                 34
C                                                                       35
C        METHOD                                                         36
C        EVALUATION IS DONE BY MEANS OF  8-POINT GAUSS QUADRATURE       37
C        FORMULA, WHICH INTEGRATES POLYNOMIALS UP TO DEGREE 15          38
C        EXACTLY. FOR REFERENCE, SEE                                    39
C     HANDBOOK OF MATHEMATICAL FUNCTIONS WITH FORMULAS, GRAPHS, AND     40
C        MATHEMATICAL TABLES,EDITED BY M. ABRAMOWITZ AND I. A. STEGUN
C        U.S. GOVERNMENT PRINTING OFFICE, WASHINGTON D.C.               42
C        PAGES 887,888,919                                              43
C                                                                       44
C                                                                       46
C                                                                       47
      SUBROUTINE DQG8 (XL,XU,FCT,Y)                                     48
C                                                                       49
C                                                                       50
      DOUBLE PRECISION XL, XU, Y, A, B, C, FCT                          51
C                                                                       52
      A=.5D0*(XU+XL)                                                    53
      B=XU-XL                                                           54
      C=.48014492824876D0*B                                             55
      Y=.5061426814518 8D-1*(FCT(A+C)+FCT(A-C))                         56
      C=.39833323870681*B                                               57
      Y=Y+.11119051722668D0*(FCT(A+C)+FCT(A-C))                         58
      C=.2627662049 5816*B                                              59
      Y=Y+.15685332293894D0*(FCT(A+C)+FCT(A-C))                         60
      C=.9171732124782D-1*B                                             61
      Y=B*(Y+.18134189168918D0*(FCT(A+C)+FCT(A-C)))                     62
      RETURN                                                            63
      END                                                               64
$$
```

THIRTY-TWO POINT GAUSSIAN QUADRATURE SUBROUTINE

```
C      SUBROUTINE DQG32                                                    14
C                                                                          15
C      PURPOSE                                                             16
C         TO COMPUTE INTEGRAL(FCT(X), SUMMED OVER X FROM XL TO XU)         17
C                                                                          18
C      USAGE                                                               19
C         CALL DQG32 (XL,XU,FCT,Y)                                         20
C         PARAMETER FCT REQUIRES AN EXTERNAL STATEMENT                     21
C                                                                          22
C      DESCRIPTION OF PARAMETERS                                           23
C         XL      -DOUBLE PRECISION LOWER BOUND OF THE INTERVAL.           24
C         XU      -DOUBLE PRECISION UPPER BOUND OF THE INTERVAL.           25
C         FCT     -THE NAME OF AN EXTERNAL DOUBLE PRECISION FUNCTION       26
C                  SUBPROGRAM USED.                                        27
C         Y       -THE RESULTING DOUBLE PRECISION INTEGRAL VALUE.          28
C                                                                          29
C      REMARKS                                                             30
C         NONE                                                             31
C                                                                          32
C      SUBROUTINES AND FUNCTION SUBPROGRAMS REQUIRED                       33
C         THE EXTERNAL DOUBLE PRECISION FUNCTION SUBPROGRAM FCT(X)         34
C         MUST BE FURNISHED BY THE USER.                                   35
C                                                                          36
C         METHOD                                                           37
C         EVALUATION IS DONE BY MEANS OF 32-POINT GAUSS QUADRATURE         38
C         FORMULA, WHICH INTEGRATES POLYNOMIALS UP TO DEGREE 63            39
C         EXACTLY. FOR REFERENCE, SEE                                      40
C      HANDBOOK OF MATHEMATICAL FUNCTIONS WITH FORMULAS, GRAPHS, AND
C         MATHEMATICAL TABLES,EDITED BY M. ABRAMOWITZ AND I. A. STEGUN     42
C         U.S. GOVERNMENT PRINTING OFFICE, WASHINGTON D.C.                 43
C         PAGES 887,888,919                                                44
C                                                                          46
C                                                                          47
      SUBROUTINE DQG32(XL,XU,FCT,Y)                                        48
C                                                                          49
C                                                                          50
      DOUBLE PRECISION XL, XU, Y, A, B, C, FCT                             51
C                                                                          52
      A=.5D0*(XU+XL)                                                       53
      B=XU-XL                                                              54
      C=.4986319309247 4D0*B                                               55
      Y=.3509305004735 0D-2*(FCT(A+C)+FCT(A-C))                            56
      C=.4928057557726 3D0*B                                               57
      Y=Y+.8137197365452D-2*(FCT(A+C)+FCT(A-C))                            58
      C=.4823811277937 5D0*B                                               59
      Y=Y+.1269603265463 1D-1*(FCT(A+C)+FCT(A-C))                          60
      C=.4674530379688 6D0*B                                               61
      Y=Y+.1713693145651 0D-1*(FCT(A+C)+FCT(A-C))                          62
      C=.4481605778830 2D0*B                                               63
      Y=Y+.2141794901111 3D-1*(FCT(A+C)+FCT(A-C))                          64
      C=.4246838068662 8D0*B                                               65
      Y=Y+.2549902963118 8D-1*(FCT(A+C)+FCT(A-C))                          66
      C=.3972418979839 7D0*B                                               67
      Y=Y+.2934204673926 7D-1*(FCT(A+C)+FCT(A-C))                          68
      C=.3660910593701 4D0*B                                               69
      Y=Y+.3291111138818 0D-1*(FCT(A+C)+FCT(A-C))                          70
      C=.3315221334651 0D0*B                                               71
      Y=Y+.3617289705442 4D-1*(FCT(A+C)+FCT(A-C))                          72
      C=.2938578786203 8D0*B                                               73
      Y=Y+.3909694789353 5D-1*(FCT(A+C)+FCT(A-C))                          74
      C=.2534499544661 1D0*B                                               75
      Y=Y+.4165596211347 3D-1*(FCT(A+C)+FCT(A-C))                          76
      C=.2106756380653 1D0*B                                               77
      Y=Y+.4382604650220 1D-1*(FCT(A+C)+FCT(A-C))                          78
```

```
C=.16593430114106D0*B                                                    79
Y=Y+.4558693947881D-1*(FCT(A+C)+FCT(A-C))                                80
C=.11964368112606D0*B                                                    81
Y=Y+.46922199540402D-1*(FCT(A+C)+FCT(A-C))                               82
C=.7223598079139D-1*B                                                    83
Y=Y+.47819360039637D-1*(FCT(A+C)+FCT(A-C))                               84
C=.24153832843869D-1*B                                                   85
Y=B*(Y+.48270044257363D-1*(FCT(A+C)+FCT(A-C)))                           86
RETURN                                                                   87
END                                                                      88
```

BIBLIOGRAPHY

1. Fraser, A.B. and W.H. Mach, "Mirages," Scientific American, Vol. 234, No. 1, (January 1976), pp. 102-111.

2. Tatarski, V.I., The Effects of the Turbulent Atmosphere on Wave Propagation, National Technical Information Service, U.S. Department of Commerce, Springfield, Va., (1971), p. 284.

3. Meyer-Arendt, J.R. and C.B. Emmanuel, "Optical Scintillation: A Survey of the Literature," N.B.S. Tech. Note, (April 1965).

4. Clifford, S.F., Ochs, G.R. and R.S. Lawrence, "Saturation of Optical Scintillation by Strong Turbulence," J.O.S.A., Vol. 64, No. 2, (February 1974), pp. 148-154.

5. Yura, H.T., "Physical Model for Strong Optical-Amplitude Fluctuations in a Turbulent Medium," J.O.S.A., Vol. 64, No. 1, (January 1974), pp. 59-67.

6. deWolf, D.A., "Strong Irradiance Fluctuations in Turbulent Air, III. Diffraction Cutoff," J.O.S.A., Vol. 64, No. 3, (March 1974), pp. 360-365.

7. Lord Rayleigh (J.W. Strutt), Scientific Papers, Vols. 1-6, Cambridge, England: University Press, (1899-1920), (Reprinted, New York: Dover, 1964), Vol. IV [203] "On the Theory of Stellar Scintillation," Phil. Mag., 36, (1893), p. 129.

8. Salpeter, E.E., "Interplanetary Scintillations. I. Theory," Astrophysical Journal, (1967), pp. 433-448.

9. Cohen, M.H., E.J. Gundermann, H.E. Hardebeck and L.E. Sharp, "Interplanetary Scintillations. II. Observations," Astrophysical Journal, (1967), pp. 449-466.

10. Mitra, S.N., "A Radio Method of Measuring Winds in the Ionosphere," Proc. IEE, Vol. 96, Part 3, (1949), pp. 441-446.

11. Briggs, B.H. and M. Spencer, "Horizontal Movements in the Ionosphere," Reports on Progress in Physics, Vol. XVII, (1954), pp. 245-280.

12. Ochs, G.R., G.F. Miller and E.J. Goldenstein, "The NOAA Passive Optical Crosswind Monitor," NOAA Technical Memo ERL WPL-11,

U.S. Dept. of Commerce, NOAA Environmental Research Labs, Wave Propagation Lab, Boulder, Colorado, (September 1974).

13. Fried, D.L., "Optical Heterodyne Detection of an Atmospherically Distorted Signal Wavefront," Proc. IEEE, Vol. 55, No. 1, (January 1967), pp. 57-67.

14. Kennedy, Robert, "On the Atmosphere as an Optical Communication Channel," Massachusetts Institute of Technology, Lecture Series Notes, Ohio State University, (August 1967).

15. Lawrence, R.S., G.R. Ochs and S.F. Clifford, "Use of Scintillations to Measure Average Wind Across a Light Beam," Appl. Opt., Vol. 11, No. 2, (February 1972), pp. 239-243.

16. Kjelaas, A.G. and G.R. Ochs, "Study of Divergence in the Boundary Layer Using Optical Propagation Techniques," Journal of Applied Meteorology, Vol. 13, No. 2, (March 1974), pp. 242-248.

17. Wang, T., S.F. Clifford and G.R. Ochs, "Wind and Refractive-Turbulence Sensing Using Crossed Laser Beams," Appl. Opt., Vol. 13, No. 11, (November 1974), pp. 2602-2608.

18. Pearson, J.E., "Comparison of Scintillometer and Microthermometer Measurements of C_N^2," J.O.S.A., Vol. 65, No. 8, (August 1975), pp. 938-941.

19. Lawrence, R.S., "Remote Atmospheric Probing by Ground-to-Ground Line-of-Sight Optical Methods," ESSA Research Labs, Boulder, Colorado.

20. Tatarski, V.I., "The Effects of the Turbulent Atmosphere on Wave Propagation, op. cit., p. 218.

21. Ibid., p. 253.

22. Carlson, F.P., "Propagation in Stationary and Locally Stationary Random Media," Ph.D. Dissertation, (1967).

23. Carlson, F.P. and A. Ishimaru, "Propagation of Spherical Waves in Locally Homogeneous Random Media," J.O.S.A., Vol. 59, No. 3, (March 1969), pp. 319-327.

24. Schmeltzer, R.A., "Means, Variances, and Covariances for Laser Beam Propagation Through a Random Medium," Quart. Applied Math, Vol. XXIV, No. 4, (1967), pp. 339-354.

25. Fried, D.L. and J.B. Seidman, "Laser-Beam Scintillation in the Atmosphere," J.O.S.A., Vol. 57, No. 2, (February 1967), pp. 181-185.

26. Tatarski, V.I., "The Effects of the Turbulent Atmosphere on Wave Propagation," op. cit., p. 231.

27. Lutomirski, R.F., R.E. Huschke, W.C. Meecham and H.T. Yura, "Degradation of Laser Systems by Atmospheric Turbulence," Rand Corporation Report R-1171-ARPA/RC, (June 1973); prepared for Defense Advanced Research Projects Agency, pp. 75-86.

28. deWolf, D.A., "Angle-of-Arrival Difference Spectrum of a Simple Interferometer in Turbulent Air," J.O.S.A., Vol. 63, No. 6, (June 1973), pp. 657-660.

29. Collins, S.A., Jr. and Y.J. Liu, "Slewed Source Angle-of-Arrival With a Centroid Detector," Paper MF18 1976 Annual Meeting Optical Society of America. To be published.

30. Tatarski, V.I., "The Effects of the Turbulent Atmosphere on Wave Propagation," op. cit., p. 268.

31. Reinhardt, G.W. and S.A. Collins, Jr., "Outer-Scale Effects in Turbulence-Degraded Light-Beam Spectra," J.O.S.A., Vol. 62, No. 4, (December 1972), pp. 1526-1528 (Letter).

32. Collins, S.A., Jr. and D.D. Duncan, "Computer Simulation of Random Atmospherically Degraded Optical Beams," Report 3862-2, August 1975, The Ohio State University ElectroScience Laboratory, Department of Electrical Engineering; prepared under Contract F30602-74-C-0130 for Rome Air Development Center. (RADC-TR-75-222) (AD/A 016 772)

33. Tatarski, V.I., "The Effects of the Turbulent Atmosphere on Wave Propagation," op. cit., p. 269.

34. Clifford, S.F., G.M.B. Bouricious, G.R. Ochs and Margot H. Ackley, "Phase Variations in Atmospheric Optical Propagation," J.O.S.A., Vol. 61, No. 10, (October 1971), pp. 1279-1284.

35. Clifford, S.F., "Temporal-Frequency Spectra for a Spherical Wave Propagating Through Atmospheric Turbulence," J.O.S.A., Vol. 61, No. 10, (October 1971), pp. 1285-1292.

36. Tatarski, V.I., "The Effects of the Turbulent Atmosphere on Wave Propagation," op. cit., p. 277.

37. Mironov, V.L. and L.I. Shchavlev, "Spectra of Amplitude Fluctuations of Optical Beams in a Turbulent Atmosphere," Radiotekhnika I Electronica, (1974), pp. 131-133.

38. Ishimaru, A., "Temporal Frequency Spectra of Multifrequency Waves in Turbulent Atmosphere," IEEE Trans. on Antennas and Propagation, Vol. AP-20, No. 1, (January 1972), pp. 10-19.

39. Ishimaru, A., "Fluctuation of a Focused Beam Wave for Atmospheric Turbulence Probing," Proc. IEEE, Vol. 57, No. 4, (April 1969), pp. 407-414.

40. Kon, A. and V. Feizulin, Radiophys. Quantum Electron, 13 (1970), pp. 51-53.

41. Lutomirski, R.F. and H.T. Yura, "Propagation of a Finite Optical Beam in an Inhomogeneous Medium," Appl. Opt., Vol. 10, No. 7, (July 1971), pp. 1652-1658.

42. Born, M. and E. Wolf, Principles of Optics, Pergamon Press, Fourth Edition, (1970), pp. XXIV-XXV,

43. Fried, D.L., "Aperture Averaging of Scintillation," J.O.S.A., Vol. 57, No. 2, (1967), pp. 169-175.

44. Homstad, G.E., J.W. Strohbehn, R.H. Berger and J.M. Heneghan, "Aperture-Averaging Effects for Weak Scintillations," J.O.S.A., Vol. 64, No. 2, (February 1974), pp. 162-165.

45. Dunphy, J.R. and J.R. Kerr, "Experimental Effect of Finite Transmitter Apertures on Scintillations," J.O.S.A., Vol. 63, No.1., (January 1973), pp. 1-8.

46. Lutomirski, R.F., R.E. Huschke, W.C. Meecham and H.T. Yura, "Degradation of Laser Systems by Atmospheric Turbulence," op. cit., pp. 43-47.

47. Hogg, R.V. and A.T. Craig, Introduction to Mathematical Statistics, 3rd Edition, The MacMillan Company, (1965), pp. 105-106.

48. Fried, D.L., "Optical Resolution Through a Randomly Inhomogeneous Medium for Very Long and Very Short Exposures," J.O.S.A., Vol. 56, No. 10, (October 1966), pp. 1372-1379.

49. Lee, M.H., R.A. Elliott, J.F. Holmes and J.R. Kerr, "Variance of Irradiance for Saturated Scintillations," J.O.S.A., Vol. 66, No. 12, (December 1976), pp. 1389-1392.

50. Gebhardt, F.G., "The Log-Amplitude Mean Value for Laser-Beam Propagation in the Atmosphere, With Applications for Optical Communications," Report 2156-8, 16 May 1968, The Ohio State University ElectroScience Laboratory, Department of Electrical

Engineering; prepared under Contract AF 33(615)-3419 for Air Force Avionics Laboratory, Wright-Patterson Air Force Base, Ohio. (AD 832 645), pp. 225-237.

51. Brown, W.P., "Validity of the Rytov Approximation," J.O.S.A., Vol. 57, No. 12, (December 1967), pp. 1539-1543.

52. Tatarski, V.I., "The Effects of the Turbulent Atmosphere on Wave Propagation," op. cit., p. 223.

53. Yaglom, A.M., An Introduction to the Theory of Stationary Random Functions, Prentice-Hall, Inc., Englewood Cliffs, New Jersey, (1962).

54. Papoulis, A., The Fourier Integral and Its Applications, McGraw-Hill Book Company, Inc., (1962), p. 11.

55. Tatarksi, V.I., "The Effects of the Turbulent Atmosphere on Wave Propagation," op. cit., p. 88.

56. Carlson, F.P., "Propagation in Stationary and Locally Stationary Random Media," op. cit., p. 23.

57. Tatarski, V.I., "The Effects of the Turbulent Atmosphere on Wave Propagation," op. cit., p. 230.

58. Fante, R.L., "Two Source Spherical-Wave Structure Functions in Atmospheric Turbulence," J.O.S.A., Vol. 66, No. 1, (January 1976) p. 74.

59. Wang, T., S.F. Clifford and G.R. Ochs, "Wind and Refractive-Turbulence Sensing Using Crossed Laser Beams," Appl. Opt., Vol. 13, No. 11, (November 1974), pp. 2602-2608.

60. Lutomirski, R.F. and G.R. Buser, "Mutual Coherence Function of a Finite Optical Beam and Application to Coherent Detection," Applied Optics, Vol. 12, (September 1973), pp. 2153-2160.

61. Kinoshita, Y., T. Asakura and M. Suzuki, "Autocorrelation of Gaussian-Beam Fluctuation Caused by a Random Medium," J.O.S.A., Vol. 58, No. 8, (August 1968), pp. 1040-1047.

62. Lawrence, R.S. and J.W. Strohbehn, "A Survey of Clear-Air Propagation Effects Relevant to Optical Communications," Proc. IEEE, Vol. 58, No. 10, (October 1970), pp. 1523-1545.

63. Collins, S.A., Jr., "A Model for Visualizing Atmospheric Turbulence," presented at April Meeting of Optical Society of America, (1967)

64. Born, M. and E. Wolf, Principles of Optics, op. cit. pp. 401-414.

65. Wylie, C.R., Jr., Advanced Engineering Mathematics, McGraw-Hill Book Company, (1960), pp. 317-318.

66. Ralson, A., A First Course in Numerical Analysis, McGraw-Hill Book Company, (1965), p. 27.

67. Tatarski, V.I., "The Effects of the Turbulent Atmosphere on Wave Propagation," op. cit., p. 228.

68. Ibid., p. 229.

69. Fried, D.L., "Statistics of Laser Beam Fade Induced by Pointing Jitter," Appl. Opt., Vol. 12, No. 2, (February 1973), pp. 422-423.

70. Tatarski, V.I., "The Effects of the Turbulent Atmosphere on Wave Propagation," op. cit., Sections 45 and 46.

71. Ibid., p. 202.

72. Ibid., pp. 250-253.

73. Abramowitz, Milton and Irene A. Stegun, Handbook of Mathematical Functions with Formulas, Graphs, and Mathematical Tables, U.S. Department of Commerce, National Bureau of Standards, Applied Mathematics series, (June 1964), p. 258.

74. Bateman, H., Tables of Integral Transforms, Vol. I, McGraw-Hill Book Company, (1954), Formula 22, p. 139.

75. Ibid., p. 386.

76. Abramowitz, Milton and Irene A. Stegun, Handbook of Mathematical Functions with Formulas, Graphs, and Mathematical Tables, op. cit., pp. 504-505.

77. Bateman, H., Tables of Integral Transforms, Vol. I, op. cit., Formula 3, p. 137.

78. Gradshteyn, I.S. and I.M. Ryzhik, Tables of Integrals Series and Products, Fourth Edition, Academic Press, New York and London, (1965), p. 940.

79. Kreyszig, E., Advanced Engineering Mathematics, Third Edition, John Wiley and Sons, Inc., (1972), p. 584.

80. Ibid., p. 108.

81. Ibid., pp. 584-586.

82. Gradshteyn, I.S. and I.M. Ryzhik, Tables of Integrals Series and Products, op. cit., Formula 3.381-1, p. 317.

83. Ibid., Formula 3.194-1, p. 284.

84. Ibid., p. 1039.

85. Esposito, R., "Power Scintillations Due to the Wandering of the Laser Beam," Proc. IEEE, (August 1967), pp. 1533-1534, (Letter).

86. Cook, R.J., "Beam Wander in a Turbulent Medium: An Application of Ehrenfest's Theorem," J.O.S.A., Vol. 65, No. 8, (August 1975), pp. 942-948.

87. Collins, S.A., Jr., and Y.J. Liu, Private Communication, to be published.

88. Gradshteyn, I.S. and I.M. Ryzhik, Tables of Integrals Series and Products, op. cit., Formula 6.574-2, p. 692.

89. Tennekes, H. and J.L. Lumley, A First Course in Turbulence, MIT Press, Cambridge, Massachusetts, (1972).

90. Kogelnik, H. and T. Li, "Eigenmodes of Stable Optical Resonators," Proc. IEEE, Vol. 54, (1966), p. 1312. Also Appl. Opt., Vol. 5, (1966), p. 1550.

91. Siegman, A.E. and E.A. Sziklas, "Mode Calculations in Unstable Resonators with Flowing Saturable Gain. 1: Hermite-Gaussian Expansion," Appl. Opt., Vol. 13, No. 12, (December 1974), pp. 2775-2792.

92. Jenkins, F.A. and H.E. White, Fundamentals of Optics, McGraw-Hill Book Company, Third Edition, (1957), p. 377.

93. Sansone, G., Orthogonal Functions, Interscience Publishers, Inc., Chapter IV: "Expansions in Laguerre and Hermite Series," (1959).

94. Gradshteyn, I.S. and I.M. Ryzhik, Tables of Integrals Series and Products, op. cit., Formula 7.374-1, p. 837.

95. Abramowitz, Milton and Irene A. Stegun, Handbook of Mathematical Functions with Formulas, Graphs, and Mathematical Tables, op. cit., pp. 887-888; 816-817.

96. Gerald, C.F., Applied Numerical Analysis, Addison-Wesley Publishing Company, (1973), p. 70.

97. Ralston, A., A First Course in Numerical Analysis, op. cit., pp. 87-103.

98. Ibid., pp. 111-114.

99. The estimated wing length of a K-135 aircraft is 20 meters.

100. Tatarski, V.I., "The Effects of the Turbulent Atmosphere on Wave Propagation," op. cit., pp. 103-106.

101. Stratton, J.A., Electromagnetic Theory, McGraw-Hill Book Company, (1941), pp. 485-486.

102. Tennekes, H. and J.L. Lumley, A First Course in Turbulence, op. cit., p. 28.

103. Goodman, J.W., Introduction to Fourier Optics, McGraw-Hill Physical and Quantum Electronics Series, McGraw-Hill Book Company, (1968), pp. 37-46.

104. Bateman, H., Tables of Integral Transforms, Vol. II, McGraw-Hill Book Company, (1954), Formula 20, p. 24.

105. Abramowitz, Milton and Irene A. Stegun, Handbook of Mathematical Functions with Formulas, Graphs, and Mathematical Tables, op. cit., p. 375.

106. Bateman, H., Tables of Integral Transforms, op. cit., Formula 1, p. 68.